博士論文

Investigation on base catalytic properties of nitrogen sites in nitrogen-containing porous materials

（窒素含有多孔質材料における窒素種の塩基触媒特性に関する研究）

Aisa Kawano

河野　愛紗

Supervisor Professor
Masaru Ogura

Department of Chemical System Engineering
The University of Tokyo

March 2022

Table of Contents

Chapter 1. General Introduction

1.1. Solid base catalyst

1.1.1 Homogeneous and heterogeneous catalyst

Catalytic processes can be divided into two categories: homogeneous and heterogeneous.

Processes in which the catalyst and reactant are both gases (e.g., decomposition of ozone by chlorine) or liquids (e.g., carbonization of methanol to acetic acid by $[Rh(CO)_2I_2]$-complex) are called homogeneous catalytic processes. Metal complexes that are soluble in solvent and ions in aqueous solution are used as homogeneous catalysts.

Processes in which the catalytic phase and the reaction phase are different are called heterogeneous catalytic processes. If the catalyst is a solid, the reaction takes place on the surface of the solid. For this reason, porous materials with large surface areas are often used.

Advantages of heterogeneous catalysts in industrial use are as follows:[1]

1. In order to recover homogeneous catalysts, it is necessary to precipitate the catalyst using reagents. On the other hand, since heterogeneous catalysts are mainly solid, they can be easily recovered by filtration and other operations, are easy to reuse. Therefore, heterogeneous catalysts are environmentally friendly.
2. In the homogeneous system, the solvent used for the reaction must be one that can dissolve both the catalyst and the reactants. For this reason, methyl chloride (CH_3Cl) and dimethyl sulfoxide (DMSO) are often used as solvents, but these substances are toxic and must be handled with care. In addition, the reaction temperature is limited below boiling temperature of the solvent. On the other hand, in a heterogeneous system, all that is needed is a solvent that dissolves the reactants. Therefore, there is a wide range of solvents to choose from.

Characteristics of both systems are shown in Table 1-1.

Table 1-1 General characteristics of homogeneous and heterogeneous system.

	Homogeneous	Heterogeneous
Separation of catalyst and product	1. Precipitation by reagent 2. Filtration	Filtration
Recycle of catalyst	Difficult, high cost	Easy
Stability	Low	High (high thermal stability)
Reaction temperature	Low (< 200 °C)	Low and high
Selectivity	High	Low
Diffusion	Easy	Difficult

1.1.2 Typical solid base catalysts

Many types of materials can act as solid base catalysts. Typical solid base catalysts are listed in Table 1-2. In this section, alkaline earth metal oxides and alkali cation-exchanged zeolites are discussed as typical solid base catalysts.

Table 1-2 Classification of solid base catalysts.[2]

Metal oxides	MgO, CaO, Al_2O_3, ZrO_2, La_2O_3, Rb_2O
Mixed oxides	SiO_2-MgO, SiO_2-CaO, MgO-La_2O_3, MgO-Al_2O_3 (calcined hydrotalcite)
Alkali or alkaline earth oxides on support	Na_2O/SiO_2, MgO/SiO_2, Cs oxides supported on zeolites
Metal oxynitrides and metal nitrides	AlPON, partially nitrided zeolites and mesoporous silica
Alkali compounds on support	KF/Al_2O_3, K_2CO_3/Al_2O_3, KNO_3/Al_2O_3, $NaOH/Al_2O_3$, KOH/Al_2O_3
Amides, imines on support	KNH_2/Al_2O_3, K, Y, Eu supported on zeolites from the ammoniacal solution
Alkali metals on support	Na/Al_2O_3, K/Al_2O_3, K/MgO, Na/zeolite
Anion exchangers	Anion exchange resins Hydrotalcite and modified hydrotalcite
Zeolites	K, Rb, Cs-exchanged X, Y-zeolites, ETS-10
Clays	Sepiolite, Talc
Phosphates	Hydroxyapatite, metal phosphates, natural phosphates
Amines or ammonium ions tethered to a support	Aminopropyl group /silica, MCM-41, SBA-15 Alkylammonium group/MCM-41

1.1.2.1. Alkaline earth metal oxide

Alkaline earth metal oxides such as MgO, CaO, SrO, and BaO are representative of solid base catalysts and have been studied for a long time. The base strength of the surface is considered to be in the order of MgO < CaO < SrO < BaO.[2] In general, alkaline earth metal oxides are obtained by thermal decomposition of hydroxides. The surface structural model of MgO is shown in Figure 1-1.[3] Although there are several types of Mg and O ions with different coordination numbers, the combination of 3-coordinated Mg^{2+} and 3-coordinated O^{2-} (Mg^{2+}_{3C}-O^{2-}_{3C}) is reported to be the most active and adsorbs carbon dioxide and water easily. Alkali metal earth oxides have been reported to catalyze a variety of reactions, such as Henry reaction[4] and Michael reaction.[5]

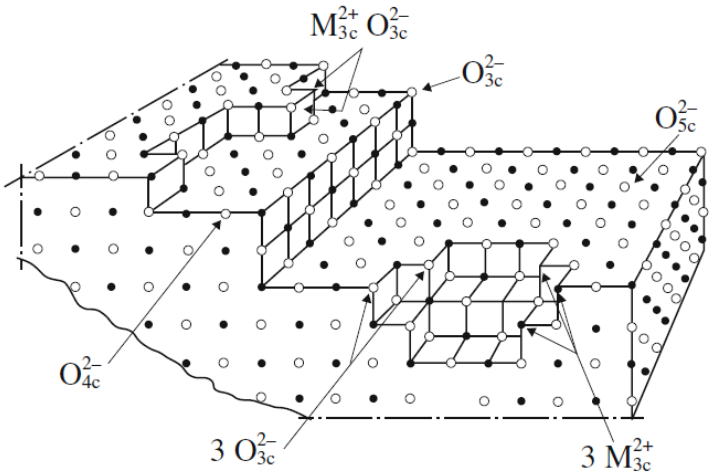

Figure 1-1 The surface structural model of MgO.[3]

1.1.2.2. Alkali cation-exchanged zeolite[6]

Zeolites exchanged with alkali metal cations exhibit basic properties. The alkali cation exchange of faujasite (X-type zeolite and Y-type zeolite) has been studied mainly for the dehydrogenation reactions of alcohols.[7] The catalytic properties of alkali cation-exchanged zeolites in dehydrogenation reactions show the following features:

1) The activity order is Cs-Y>Rb-Y>K-Y>Na-Y>Li-Y.

2) Na-X is more active than Na-Y.

3) H-Y is not active.

The activity of alkali cation-exchanged zeolites with the same structure tends to be higher with larger radius of the exchanged cation and lower electronegativity. A similar feature has been observed in the alkylation of toluene with methanol and formaldehyde[7] and the reaction of γ-thiolactone formation from γ-butyrolactone and hydrogen sulfide.[8]

1.1.3 Industrial use of solid base catalyst

Many research has been done on solid acid catalysts due to their demand in the petrochemical (oil refining and oil reforming) field. On the other hand, solid base catalysts have not been studied as much as solid acid catalysts. One possible reason for this is the poisoning of solid base catalysts. Water and carbon dioxide in the air adsorb onto the solid base catalyst, causing it to become inactive. Therefore, they need to be pre-treated at high temperature before use, but there is a risk of sintering and deactivation of the catalyst during the high temperature treatment. Thus, solid base catalysts are more difficult to handle than solid acid catalysts.

The industrial processes in which solid base catalysts are used are shown in Table 1-3.[1] In the future, it will be necessary to shift from homogeneous to heterogeneous base catalysts in terms of

environmental burden and cost.

Table 1-3 Industrial processes in which solid base catalysts are used.[1]

Reaction	Catalyst	Year
Alkylation		
Alkylation of phenol with methanol	MgO	1970, 1985
Alkylation of xylene with butadiene	Na/K_2CO_3	1995
Alkylation of cumene with ethylene	$Na/KOH/Al_2O_3$	1988
Isomerization		
Isomerization of safrole to isosafrole	$Na/NaOH/Al_2O_3$	1988
Isomerization of 2,3-dimethyl-1-butene	$Na/NaOH/Al_2O_3$	1988
Isomerization of 3,5-vinylbicyclo[2,2,1]heptane	$Na/NaOH/Al2O_3$	1988
Isomerization of 1,2-propadine to propyne	K_2O/Al_2O_3	1996
Dehydration/condensation		
Dehydration of 1-cyclohexylethanol	ZrO_2	1986
Dehydration of propylamine-2-ol	ZrO_2/KOH	1992
Isobutyraldehyde to diisopropyl ketone	ZrO_2	1973
Dehydrotrimerization of isobutyraldehyde	BaO–CaO	1998
Esterification		
Esterification of ethylene oxide	Hydrotalcite	1994
Transesterification of triglycerides	$ZnO–Al_2O_3$	2006
Miscellaneous		
Carboxylic acids to aldehydes	$ZrO_2–Cr_2O_3$	1988
Thiols from alcohols with hydrogen sulfide	$Alkali/Al_2O_3$	1988
Cyclization of imine with sulfur dioxide	Cs-zeolite	1995

1.2 Nitrided silica

By substituting nitrogen atoms for oxygen atoms in the silica framework (nitridation), the Lewis base property appears in the non-covalent electron pair of the nitrogen atom, which has a weaker electron affinity than the oxygen atom, and acts as a base point (Figure 1-2). Many types of nitrided silica materials, such as amorphous silica[9], zeolite (FAU[10-14], MFI[11, 15-21], BEA[22], FER[23], LTA[24], MWW[21, 25]), zeolite analogue ($AlPO_4$[11, 26], SAPO-34[27, 28]), mesoporous silica (MCM-41[29-33], MCM-48[33-35], SBA-15[30, 33, 36-42], FSM-16[43], IUMUV-6[44]), and fibrous silica (KCC-1[30, 45, 46]) has been reported.

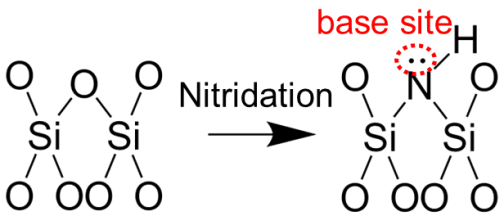

Figure 1-2 Base site of nitrided silica.

1.2.1 Preparation of nitrided silica

In 1968, Kerr *et al.* reported about HY zeolite treated with ammonia at 773 K.[10] Since then, nitridation of various silica materials has been studied. A typical nitridation experimental setup is shown in Figure 1-3. First, a ceramic boat loaded with silica material is placed in a quartz tube. The sample is heated in a temperature programmable furnace under N_2 gas flow. When the temperature reaches above 643K, the N_2 gas is switched to ammonia gas. When the sample has reached the desired temperature and held for several hours, the material is cooled. When the temperature reaches below 643K, the ammonia gas is switched to N_2 gas. The sample should be removed when it reaches room temperature.

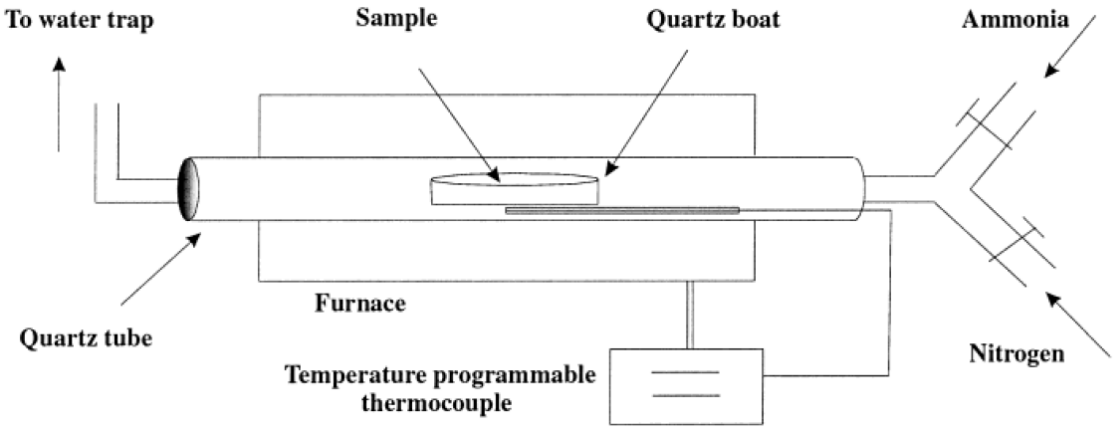

Figure 1-3 Nitridation experimental setup.[29]

The relationship between nitridation conditions (e.g., time, temperature, ammonia flow rate) and the properties of the nitrided materials (e.g., nitrogen content, crystallinity, nitrogen species, basicity, acidity) has been investigated in various silica materials.

First, the nitridation of zeolite is discussed. In 2004, Zhang *et al.* reported the nitrided ZSM-5 with bimodal pores.[15] The commercial ZSM-5 heated in air at 1273 K for 2.5 h and heated in ammonia flow (500 mL·min^{-1}) at 1323 or 1373 K for 4.5, 8, or 10 h. N_2 adsorption shows ZSM-5 nitrided at 1323 K was slightly destroyed and ZSM-5 nitrided at 1373 K was dramatically damaged (Table 1-4). XRD measurement and SEM also proved that nitridation at 1323 K leaded slight destruction of

zeolite structure. The nitrogen content of nitrided ZSM-5 measured by CHN analysis increased with nitridation time and temperature (7.2-15.6 wt%). ^{29}Si MAS NMR showed that the $SiNO_3$ phase formed and that the SiO_3-OH phase disappeared in ZSM-5 nitrided at 1323 K. TG-MS and CO_2-TPD indicated that stronger basic sites were existed in nitrided ZSM-5. Furthermore, TG-MS and NH_3-TPD indicated that small quantity of acid sites was still existed after nitridation.

Table 1-4 Textual properties of ZSM-5 before and after nitridation.[15]

Samples	*N* (wt.%)	BET surface area (m^2/g)	Micropore surface area (m^2/g)	Micropore volume (cm^3/g)	BJH desorption (1.7–300 nm)	
					Pore volume (cm^3/g)	Surface area (m^2/g)
ZSM-5	–	346.3	261.6	0.120	0.036	38.0
ZSM-5-1323-4.5N	7.2	283.5	152.6	0.077	0.117	174.2
ZSM-5-1323-8N	10.4	280.8	172.5	0.089	0.104	140.3
ZSM-5-1373K-10N	15.6	155.5	128.2	0.060	0.053	46.2

Nitrided HZSM-5 was reported by Guan *et al.* in 2006.[17] The nitridation temperature was 1073 K and the nitridation time was 5, 10, and 15 h. XRD measurement, N_2 adsorption, and SEM showed the structure of HZSM-5 had no great change after nitridation. The nitrogen content measured by alkaline digestion increased with increasing nitridation time (0.82-1.24 wt%). NH_3-TPD showed that nitridation reduced the strong acid sites and did not affect the weak sites (Figure 1-4). Therefore, the acid strength distribution of HZSM-5 was more homogeneous after nitridation. Pyridine-IR measurement showed that Brönsted acid sites decreased sharply and Lewis acid sites decreased slightly after nitridation. TG analysis showed that nitridation leaded less deposition of coke probably due to weaker acidity.

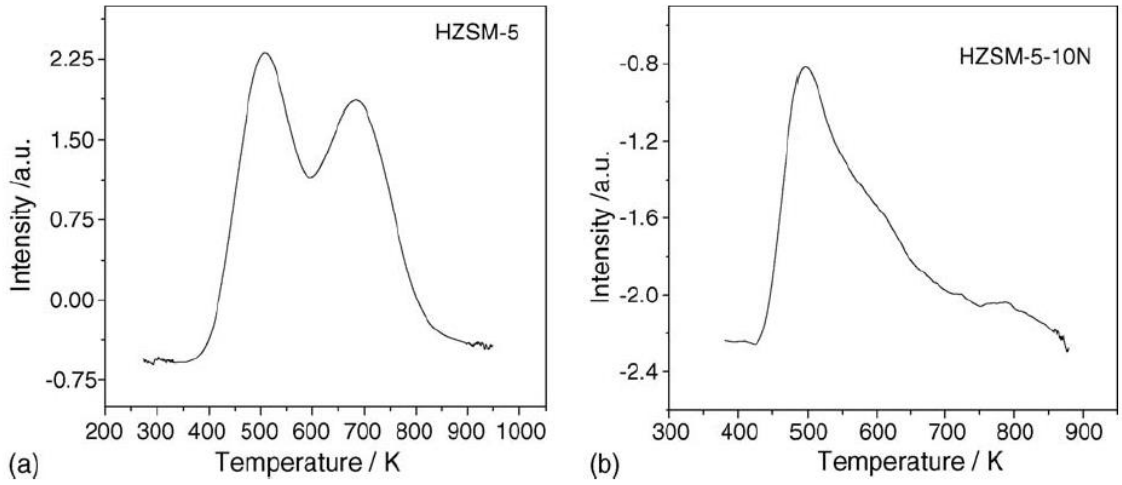

Figure 1-4 The patterns of NH_3-TPD of (a) HZSM-5 and (b) HZSM-5-10N.[17]

Narasimharao *et al.* attempted to prepare basic zeolite by low temperature nitridation.[22] They

selected zeolite beta as parent material due to their large concentrations of defect sites. Synthesized zeolite bate was heated in ammonia flow (60 mL min^{-1}) between 573 and 1073 K for 24 or 48 h. XRD measurement showed that the crystallinities of nitrided zeolite gradually decreased with increasing nitridation temperature and time. The nitrogen content measured by alkaline digestion increased with increasing nitridation temperature and time (1.25-10.85 wt%). When zeolite beta was heated in air at 1073 K for 24 h, the resulting material was amorphous. This suggested that the ammonia atmosphere probably contributed to preserving the zeolite framework. The result of N_2 adsorption measurement corresponded with XRD result. The nitrogen content of nitrided zeolite beta increased with nitridation time and temperature. Compared with NaY and ZSM-5, the nitrogen incorporation capacity of zeolite beta was higher at the same temperature probably due to their large concentrations of defect sites, which may promote a formation of terminal $–NH_2$ groups. FTIR measurement showed that the intensity of bands attributed to silanol groups decreased with increasing nitridation temperature and that both basic sites and acid sites were present in zeolite nitrided at temperatures below 973 K. From this result, the following nitridation mechanism was suggested. At lower temperatures, Si-NH_2 species were generated from silanol groups (Eqs. (1) and (2)). At higher temperatures, Si-NH-Si or Si-NH-Al species were generated (Eqs. (3)-(5)).

$$\equiv Si - OH + NH_3 \rightarrow \equiv Si - NH_2 + H_2O \quad (1)$$

$$\equiv Si - O - Si\equiv + NH_3 \rightarrow \equiv Si - NH_2 + \equiv Si - OH \quad (2)$$

$$\equiv Si\text{-}NH_2 + \equiv Si\text{-}OH \longrightarrow \equiv Si\text{-}\overset{H}{N}\text{-}Si + H_2O \quad (3)$$

$$\equiv Si\text{-}NH_2 + \equiv H_2N\text{-}Si \longrightarrow \equiv Si\text{-}\overset{H}{N}\text{-}Si + NH_3 \quad (4)$$

$$\equiv Si\text{-}\overset{H}{O}\text{-}Al\equiv + NH_3 \longrightarrow \equiv Si\text{-}NH_2\text{-}Al + H_2O \quad (5)$$

Scheme 1-1 The mechanism of nitridation in nitrided zeolite.[22]

Dogan *et al.* examined the effect of Si/Al ratio, charge-compensating cation, and treatment temperature on reactivity, degree of nitrogen substitution, and framework stability of nitrided zeolite.[12] Commercial HY (Si/Al = 15), NH_4Y (Si/Al = 2.55), NaY (Si/Al = 2.55), and HY (Si/Al = 2.55) were used as starting materials. The zeolite was heated in ammonia flow (approximately 2000 $cm^3 \cdot min^{-1}$) at 1023-1123 K in 24 or 48 h. XRD measurement and N_2 adsorption showed HY (Si/Al = 15 and 2.55) and NaY maintained their structure during nitridation (Figure 1-5 a, b, and c). However, the crystallinity of NH_4Y decreased after nitridation (Figure 1-5 d) due to dihydroxylation of the Si-O(H)-Al linkages Elemental analysis (5.4-13.9 wt%) and EDX analysis (5.6-34.7 wt%) showed that the nitrogen content increased with increasing nitridation time and temperature in all sample.

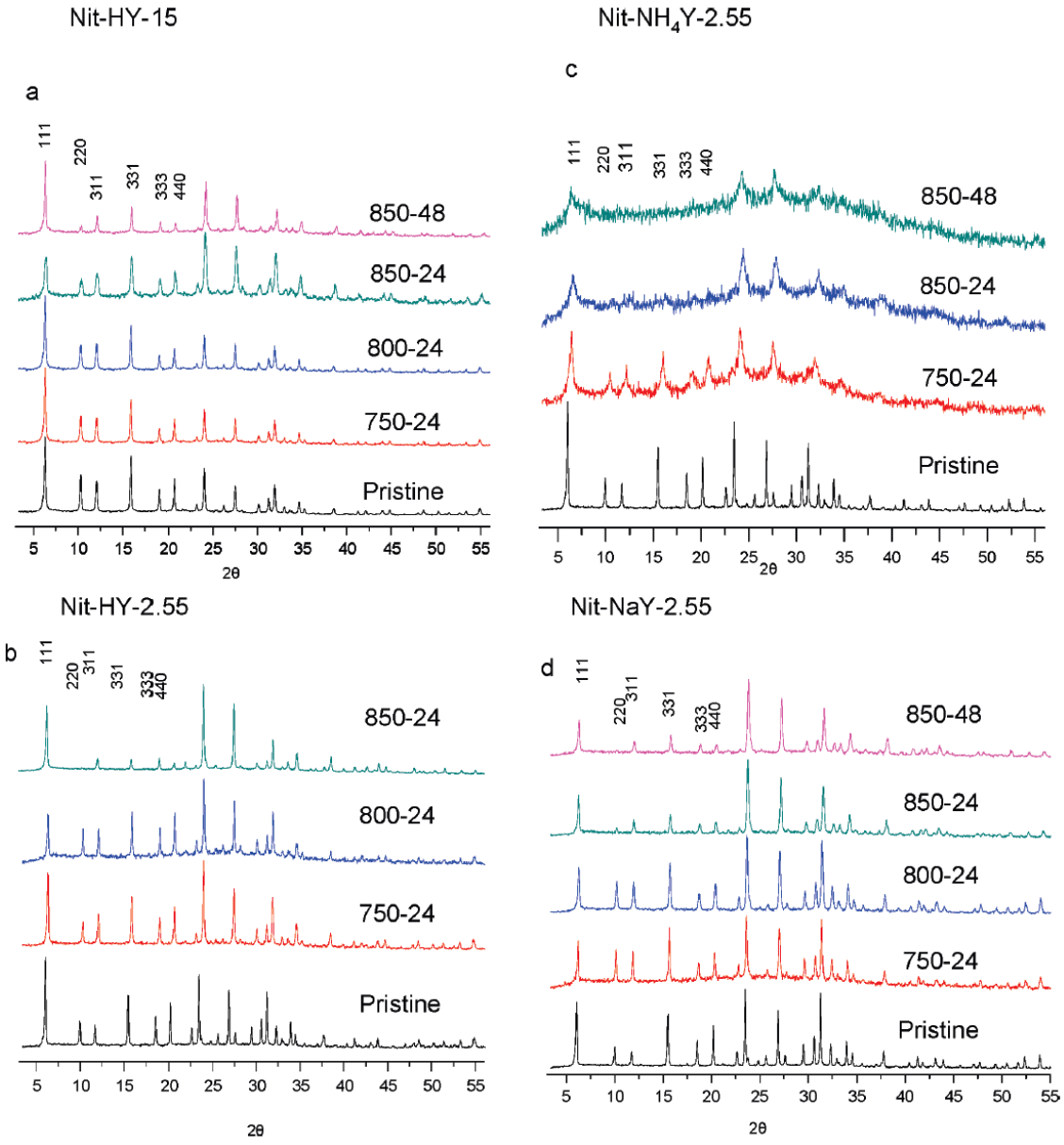

Figure 1-5 Powder XRD pattern for nitrided zeolite Y. The first six reflections of the faujasite cell are indexed.[12]

Srasra *et al.* reported the effect of nitridation temperature on nitrogen amount and species of nitrided zeolite.[47, 48] Y zeolite (Si/Al = 2.6) and ultrastable Y zeolites (Si/Al =13 and 37) were heated in ammonia flow (60 mL min^{-1}) for 48 h at 1023-1123 K. XRD and N_2 adsorption results showed that nitridation caused a decrease of crystallinity of the samples. The crystallinity of 2.6Y and 37USY decreased more rapidly than that of 13USY. The content of total nitrogen was determined by the Grekov method and the content of surface nitrogen was determined by XPS analysis (Table 1-5). Both content increased with nitridation temperature in all samples. The content

of total nitrogen and that of surface nitrogen were similar. Therefore, the nitridation of the external and internal surfaces might proceed at the same rate. At the same nitridation temperature, all samples showed comparable nitrogen contents only excepted for samples nitrided at 1123 K. XPS analysis showed not only the quantity of nitrogen but also the chemical environment of nitrogen. Nitrided zeolites had some nitrogen species and nitrogen species appeared in the following order of increasing temperature: NH_4^+, NH_3 adsorbed on Lewis acid sites, $-NH_2$, -NH- and >N- (Figure 1-6). The nitridation temperature affected their relative concentration. The result of DRIFTS corresponded with XPS result.

Table 1-5 Total and surface nitrogen contents of the parent and nitrided zeolites.[47]

Samples	N_T (wt %)	N_S (wt %)[a]
2.6Y	3.3	2.9
2.6Y600N	1.2	1.2
2.6Y800N	6.8	7.6
2.6Y900N	16.3	18.4
13USY	–	0.6
13USY600N	1.3	0.7
13USY800N	6.0	6.0
13USY900N	10.0	10.7
37USY	–	0.2
37USY600N	2.2	1.2
37USY800N	7.0	4.9
37USY900N	15.6	14.8

[a] Deduced from XPS analysis

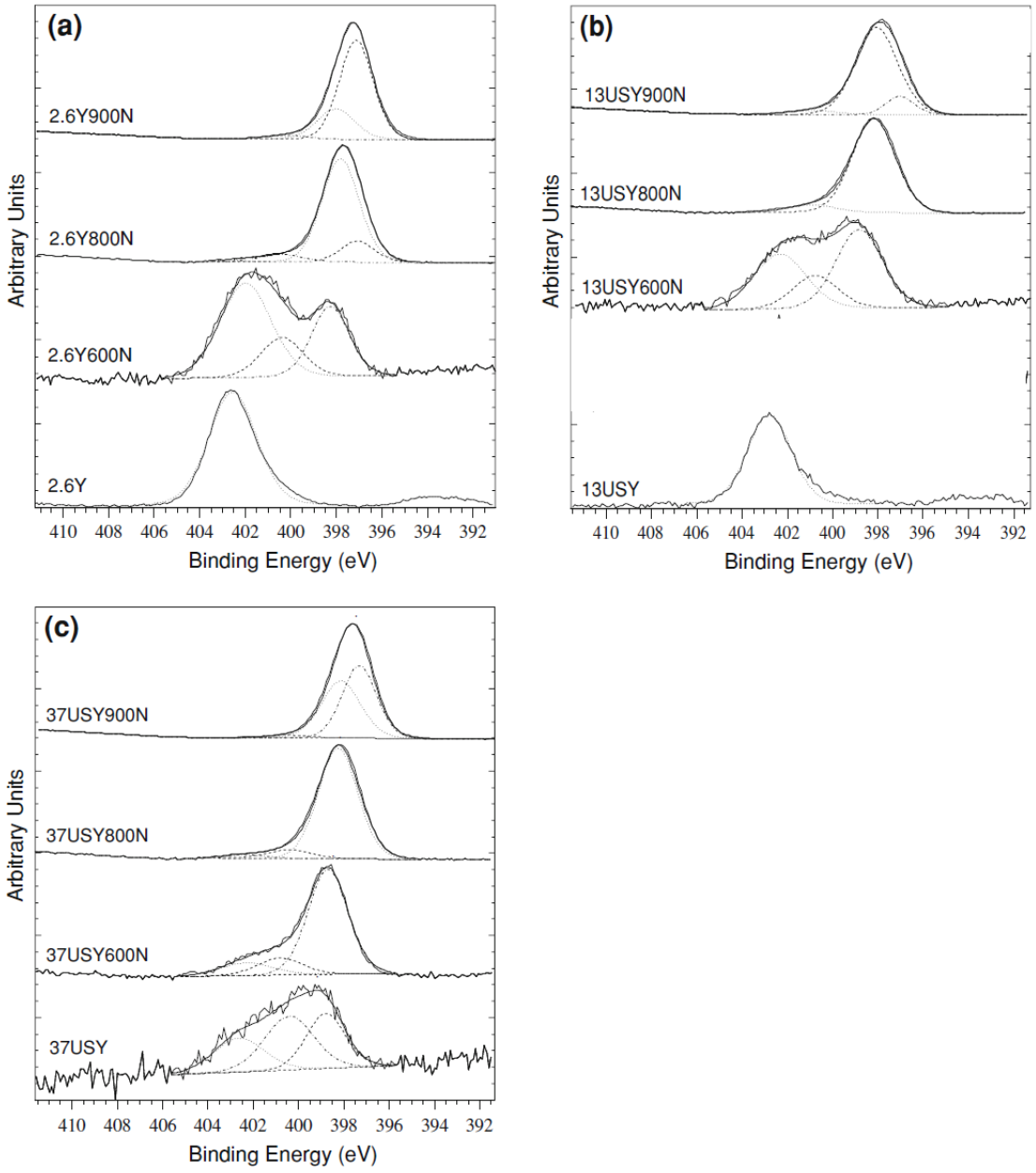

Figure 1-6 N1s XPS spectra of parent and nitrided zeolites. The relative intensities of each spectrum have been normalized. The deconvoluted peaks are assigned to NH_4^+, ammonia adsorbed on Lewis acid sites, $-NH_2$ and -NH- groups, and >N- groups with the binding energy of 402, 400, 398 and 397 eV, respectively. [47]

Wu *et al.* remarked nitrogen species of nitrided zeolites.[18] ZSM-5 (Si/Al > 300) was heated in ammonia flow (60 mL·min^{-1}) at 973-1173 K for 8 h. XRD measurement, N_2 adsorption, and SEM characterization indicated that the crystallinity of zeolite was well-preserved after nitridation. CHN analysis indicated that nitrogen content of nitrided zeolite increased with nitridation temperature

(1.10-1.49 wt%). The result of FTIR and ^{29}Si MAS NMR indicated that nitrogen atoms were introduced into the framework of ZSM-5 and Si-NH-Si group and/or Si-NH_2 group were formed. Si-NH-Si groups are formed when nitridation temperature above 1073 K (Figure 1-7). In this report, the band assigned to Si-NH_2 groups is not observed probably due to instability of Si-NH_2 groups.

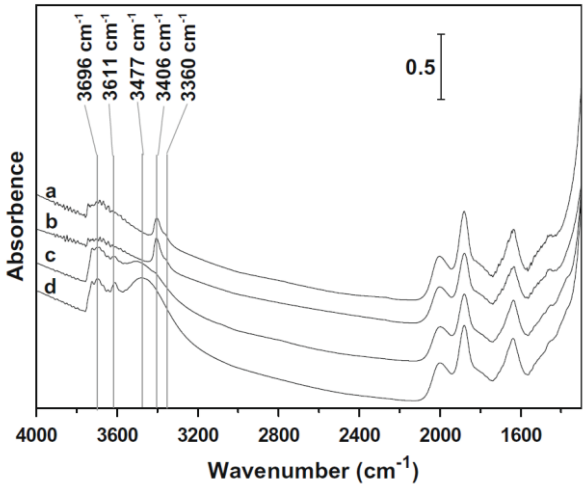

Figure 1-7 FTIR spectra of nitrided samples treated under vacuum at 673 K for 1 h before IR measurements. (a) NZ-1173, (b) NZ-1073, (c) NZ-973, and (d) parent ZSM-5. The bands are assigned to Si-OH groups, Si-OH-Al groups, adsorbed water, Si-NH-Si groups, and Si-NH-Al groups with the wavenumber of 3696, 3611, 3477, 3406, and3360 cm^{-1} respectively.[18]

Hammond *et al.* investigated the effect of nitridation conditions, such as the ammonia introduction temperature/time, the ammonia treatment temperature/time, and the ammonia flow rate.[49] And they proposed recommended conditions. HY zeolite (Si/Al ≈ 20 estimated by ^{29}Si MAS NMR) was heated in ammonia flow (70-2000 $cm^3 \cdot min^{-1}$) at 823-1123 K for 8-48 h. The ammonia introduction temperature was 673-1123 K. The nitrided zeolite was characterized by XRD, ^{29}Si MAS NMR, N_2 adsorption, and FT-IR spectroscopy. When the ammonia was introduced before the furnace reached the reaction temperature, the zeolite contained fewer defects after nitridation than the temperature was reaction temperature. That might be because that high temperature treatment without ammonia gas causes dealumination and/or structural distortion. It was also revealed that the higher ammonia flow rate leaded the higher degree of nitrogen substitution due to higher ammonia concentration and lower H_2O concentration. Longer nitridation time and higher nitridation temperature leaded more nitrogen substitution and partial collapse of the zeolite structure. Consequently, the condition; nitridation time = 8 h, nitridation temperature = 1023 K, ammonia flow started at 400 °C, ammonia flow rate = 600 $cm^3 \cdot min^{-1}$ was recommended for zeolite Y.

Not only aluminosilicates but also silicoaluminophosphates (SAPO-34) were nitrided. Nitrided SAPO-34 was firstly reported by Guan *et al.* in 2006.[28] Synthesized SAPO-34 was heated in dry ammonia flow at 973, 1073, and 1173 K. In this material, the nitrogen content increased and subsequently decreased with the increase of nitridation temperature because of partial destruction of the framework and elimination of some nitrogen species during nitridation. XRD measurement confirmed the destruction of the framework in SAPO-34 nitrided at 1173 K. DRIFTS of CO_2 adsorption and CO_2-TPD measurement showed that basic sites existed on the surface of nitrided SAPO-34.

Titanosilicates were also nitrided. Nitrided titanosilicates were reported by Zhang *et al.* in 2012.[50] Synthesized Ti-MWW, TS-1, and Ti-Beta were used as starting materials. The zeolites were heated in ammonia flow (100 $cm^3 \cdot min^{-1}$) at 473-1173 K in 5 min-5 h. At lower temperature (under 873 K), the nitrogen content of nitrided Ti-MWW measured by CHNS analyzer slightly increased with increasing nitridation temperature (Figure 1-8). At higher temperature (over 1073 K), the nitrogen content increased obviously. That was because that the ammonia molecules might be adsorbed on the surface of titanosilicates at lower temperature and nitrogen could be incorporated titanosilicate framework only at higher temperature. XRD measurement showed high temperature nitridation caused structural degradation probably due to nitrogen incorporation. XRD measurement and N_2 adsorption showed that the structures of Ti-MWW, TS-1, and Ti-Beta were preserved during nitridation under 873 K. UV-Vis spectra did not change after nitridation. Therefore, nitridation had no effect on the state of Ti species.

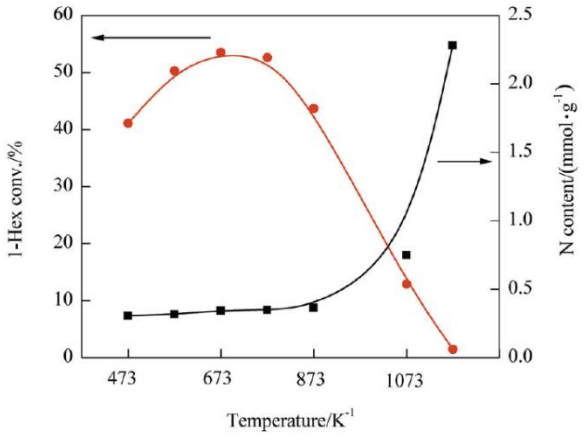

Figure 1-8 Dependence of the N content and the activity of nitrided-Ti-MWW on nitridation temperature.[50]

The mechanism of nitridation of mesoporous silica is shown in Scheme 1-2. First, the silanol groups on the surface are replaced by primary amine groups (1), and the water desorbs from the two

silanol groups to form the monoradical ≡ Si-O· (non bridging oxygen hole center, NBOHC) (2). This NBOHC produces ·NH_2 from ammonia molecules (3). The reaction between radicals also generates primary amine groups (4). Primary amine groups are also generated in reactions such as (5). Furthermore, at high temperatures (above 973 K), primary amine groups condense to form cross-linked secondary amine groups (Si-NH-Si), as in (7). Therefore, nitration at low temperature (~873 K) results in more primary amine groups, while nitration at high temperature results in more bridged amine groups.

$$\equiv Si\text{–}OH + NH_3 \rightarrow \equiv Si\text{–}NH_2 + H_2O \quad (1)$$
$$\equiv Si\text{–}OH + \equiv Si\text{–}OH \rightarrow \equiv Si\text{–}O^{\bullet} + \equiv Si^{\bullet} \quad (2)$$
$$\equiv Si\text{–}O^{\bullet} + NH_3 \rightarrow \equiv Si\text{–}OH + {}^{\bullet}NH_2 \quad (3)$$
$$\equiv Si^{\bullet} + {}^{\bullet}NH_2 \rightarrow \equiv Si\text{–}NH_2 \quad (4)$$
$$\equiv Si^{\bullet} + NH_3 \rightarrow \equiv Si\text{–}NH_2 + H^{\bullet} \quad (5)$$
$$\equiv Si\text{–}O^{\bullet} + H^{\bullet} \rightarrow \equiv Si\text{–}OH \quad (6)$$
$$\equiv Si\text{–}NH_2 + \equiv Si\text{–}NH_2 \rightarrow \equiv Si\text{–}NH\text{–}Si\equiv + NH_3 \quad (7)$$

Scheme 1-2 The mechanism of nitridation in nitrided mesoporous silica.[37]

1.2.2 Characterization of nitrided silica

XRD measurements are widely used to investigate the structural changes before and after nitridation. The higher the nitridation temperature, the larger the decrease in peak intensity.[12, 22, 47, 49] For zeolites, the peak position hardly changes[11, 12, 17, 22, 49], but for mesoporous silica, the peak position shifts to a higher angle as it is nitrided at higher temperatures.[31, 34, 40, 42, 51]

Many researchers used N_2 adsorption measurement in order to investigate textual properties of nitrided silica materials. In general, the higher the nitridation temperature, the lower the surface area and pore volume. In nitrided mesoporous silica, the higher the nitridation temperature, the thinner the wall thickness.[40, 42] Hammond proposed avoiding discussions of BET surface area of zeolites and instead concentrating on high-resolution adsorption or micropore volumes determined from the *t*-plots or α_s-plots.[49]

Combustion method, EDX measurement, alkaline digestion, titration method, and XPS measurement were often used for investigation on nitrogen content of nitrided materials. Combustion method (elemental analysis) shows lower nitrogen contents than EDX because of an incompletely combustion and a possible adsorption of water in zeolite.[12]

XPS analysis can investigate not only the quantity of nitrogen but also the chemical environment of nitrogen. However, there are few studies of XPS analysis on nitrided zeolites. Srasra *et al.* summarized N1s binding energy attribution of nitrided compounds (Table 1-6).[48] Figure 1-6 shows XPS peak spectra of N1s levels for parent and nitrided zeolite.[48] It suggests that amines were formed when the nitridation temperature was above 800 °C. Figure 1-9 shows XPS peak spectra of N1s levels for nitrided SBA-15.[42] It suggests that the higher the nitridation temperature,

the higher the series number of amines is formed. Similar results have been reported for nitrided KCC-1.[45]

Table 1-6 N1s binding energy attribution from the literature of some nitrided compounds.[48]

Nitrogen species	Assignment	BE N_{1s} / eV	Reference
>N–	SiN, SiN_xH_y	397.1–397.7	[52-56]
	AlN	396.4–396.8	[57-59]
	TiN	396.8–397.2	[60-63]
	AlPON	397.4	[64]
	ZrPON	397.0–397.7	[65]
$–NH_2$	SiN	398.6–399.4	[52]
	AlN	399.3	[57, 59]
	AlPON	399.0	[64]
–NH–	SiN, SiN_xH_y	398.0–399.6	[52]
	AlN	398.1	[57, 59]
$–NH_2$ and –NH– groups	AlPON, ZrPON	398.8–399.6	[66]
NH_3	NH_3–Y	400.4	[67]
	NH_3–Al_2O_3	400.8	[57, 60]
NH_4^+	NH_4^+–mordenite	403	[68]
	NH_4^+–ZSM-5	402.4–402.6	[67]

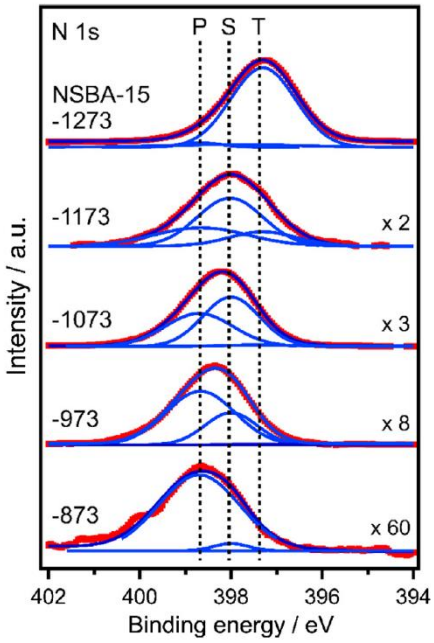

Figure 1-9 XPS spectra of N1s levels for nitrided SBA-15 with nitridation temperature of 873–1273

K. Red dots and blue carves are measured data and fitting curves, respectively. The deconvoluted peaks are assigned to primary (P), secondary (S), and tertiary (T) silanamine with the binding energy of 398.7, 398.0, and 397.3 eV, respectively.[42]

IR measurement was widely used to distinguish between different nitrogen species. Typical FT-IR peak assignments of nitrided SBA-15 are shown in Table 1-7[42] and those of nitrided zeolite are shown in Table 1-8.[48] FT-IR spectra of nitrided zeolites tend to be more complicated than those of nitrided mesoporous silica due to the presence of Al atoms.

Table 1-7 Peak assignments of FT-IR spectra of nitrided SBA-15.[42]

Wave number / cm^{-1}	Assignment	Reference
3536	$\nu_{NH\ asymmetric}$ (Si-NH_2)	[39]
3530	$\nu_{NH\ asymmetric}$ (Si-NH_2)	[37]
3516	$\nu_{NH\ asymmetric}$ (Si-NH_2)	[45]
3515	$\nu_{NH\ asymmetric}$ (Si-NH_2)	[42]
3505	ν_{NH} (Si-NH_2)	[69]
3452	$\nu_{NH\ symmetric}$ (Si-NH_2)	[39]
3452	$\nu_{NH\ symmetric}$ (Si-NH_2)	[37]
3444	$\nu_{NH\ symmetric}$ (Si-NH_2)	[45]
3405 (broad peak)	ν_{NH} (Si-NH-Si)	[69]
3403	ν_{NH} (Si-NH-Si)	[70]
3396 (broad peak)	ν_{NH} (Si-NH-Si)	[37]
3396	ν_{NH} (Si-NH-Si)	[34]
3388 (broad peak)	ν_{NH} (Si-NH-Si)	[31]
3368	ν_{NH} (Si-NH-Si)	[70]
3390–3350 (broad peak)	ν_{NH} (Si-NH-Si)	[42]
1555	δ_{NH} (Si-NH_2)	[69]
1555	δ_{NH} (Si-NH_2)	[31]
1552	δ_{NH} (Si-NH_2)	[45]
1551–1550	δ_{NH} (Si-NH_2)	[70]
1550	δ_{NH} (Si-NH_2)	[39]
1548	δ_{NH} (Si-NH_2)	[42]
1547	δ_{NH} (Si-NH_2)	[40]

Table 1-8 Peak assignments of FT-IR spectra of nitrided zeolite.[48]

species	assignments	band positions (cm^{-1})
NH_4^+	ν_s (NH)	3050−3200
Si-NH_2	ν_s (NH)	3430−45
	ν_{as} (NH)	3500−20
Al-NH_2	ν_s (NH)	3440
	ν_{as} (NH)	3500
Si-NH_2···Al	ν_s (NH)	3280−85
	ν_{as} (NH)	3330−35
Si-NH-Si	ν (NH)	3390−3405
Si-NH-Al	ν (NH)	3360−70
LF[a](OH) β cages	ν (OH)	3545−65
LF(OH) β cages with interaction with EXF[c]	ν (OH)	3520−30
HF(OH) α cages	ν (OH)	3622−40
HF[b](OH) α cages with interaction with EXF	ν (OH)	3603−14
Al−OH EXFAl species	ν (OH)	3600
Si−OH at defect sites or EXFAl species	ν (OH)	3650−74
Si−OH terminal silanols	ν (OH)	3734−49

[a] LF: low frequency. [b] HF: high frequency. [c] EXF: extra-framework.

^{29}Si MAS NMR is used to study the environment of Si atoms in nitrided silica materials. Dogan *et al.* calculated chemical shifts of ^{29}Si MAS NMR for nitrided HY and NaY.[12] Figure 1-10 shows Si MAS NMR spectra of parent and nitrided ZSM-5.[15] The sharp and strong peak near −112 ppm is derived from SiO_4, and the shoulder near −100 ppm is derived from SiO_3-OH, indicating the presence of silanol groups in the ZSM-5. After nitridation, the peak around −92 ppm derived from $SiNO_3$ appears and the peak at −110 ppm disappears. It suggests that $SiNO_3$ phase (nitrogen inside the ZSM-5 framework) had formed, and SiO_3-OH phase had disappeared (Si–OH + NH_3 → Si–NH_2 + H_2O). Similar results have been reported for nitrided KCC-1.[45]

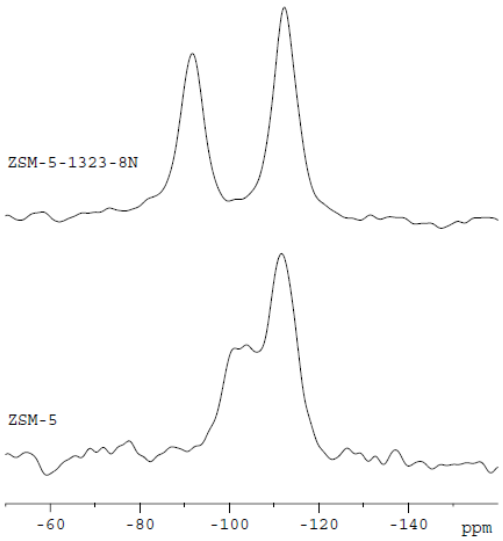

Figure 1-10 Si MAS NMR spectra of parent and nitrided ZSM-5 with nitridation temperature of 1323 K.[15]

1.2.3 Applications

1.2.3.1 Solid base catalyst

Nitrided zeolites have been attracted attention as solid catalysts due to their high crystallinity, porosity, and thermal stability. Knoevenagel condensation was widely used to investigate the base catalytic property of nitrided silica.

Climent *et al.* reported the base catalytic activity of nitrided amorphous aluminophosphates (ALPONs).[26] ALPONs with different nitrogen content were prepared by controlling the nitridation time. The basicity of ALPONs was investigated by carrying out the Knoevenagel condensation with reactants possessing different pK_a value, ethyl cyanoacetate and malononitrile. The activity of ALPON increased with nitrogen content. In the reaction with malononitrile, the nitrogen content and the activity showed a reasonable linear correlation. Thus, all the basic sites were enough and equally active for this reaction. However, in the case of ethyl cyanoacetate, not all the basic sites were equivalent b. The also compared the basicity of ALPONs was compared with other solid base catalysts. The basicity of ALPONs was stronger than that on alkaline ion (Cs) exchanged X zeolites and weaker than that on MgO and Mg-Al hydrotalcites.

Ernst *et al.* reported the catalytic activity of nitrided NaY in Knoevenagel condensation of benzaldehyde with malononitrile.[11] The catalysts were by nitridation at 800–900 °C to investigate the effect of nitridation temperature. NaY nitrided at 850 or 875 °C showed high yield of the aimed product, i.e. high catalytic activity. A leaching test and a recycle test clarified that the activity was not derived from dissolved ammonia. However, untreated NaY and NaY nitrided at 800 °C showed low activity. NaY nitrided above 900 °C also showed low activity due to their low crystallinity and fewer accessible base sites. They also compared the catalytic activity of nitrided NaY, NaX (FAU), ZSM-5, Silicalite-1 (MFI), $AlPO_4$-5, and amorphous AlPO in the same reaction. The catalysts were prepared by nitridation at 850 or 875 °C in order to investigate the effect of zeolite type. The catalytic activity increased with nitridation temperature. In FAU and MFI type zeolite, the activity increased with decreasing aluminum content. Nitrided $AlPO_4$-5 showed lower activity than nitrided amorphous AlPO because the latter contained stronger base sites, bridging P-NH-Al groups. On the other hand, a microporous catalyst like nitrided $AlPO_4$-5 could show higher selectivity than an amorphous one.

ZSM-5 nitrided at 1323 K catalyzed the Knoevenagel condensation of benzaldehyde with malononitrile.[15] The catalytic activity increased with nitridation time. However, ZSM-5 nitrided at 1373 K showed low catalytic activity, though its nitrogen content was higher. It was due to low crystallinity.

Y zeolite and USY zeolite nitrided at 1023-1123 K catalyzed the Knoevenagel condensation between benzaldehyde and malononitrile.[47] When nitrogen content was too high, in other words, nitridation temperature was high (1173 K) the catalyst was deactivated because of the lack of

crystallinity.

High Si ZSM-5 nitrided at 973-1173 K catalyzed the Knoevenagel condensation between benzaldehyde and malononitrile.[18] The selectivity of the objective product was almost 100% for all catalysts. The initial activity of ZSM-5 nitrided at 1073 K was higher than ZSM-5 nitrided at 973 K, however, the activity was lower after reaction for 6 h. It was because that not only nitrogen content but also nitrogen species affect the base catalytic activity.

Xia *et al.* reported that when nitrided MCM-48 was removed out from the reaction solution during Knoevenagel condensation between benzaldehyde and malononitrile, the reaction did not proceed further (Figure 1-11).[34] Therefore, the nitrogen in nitrided silica is not considered to be leached.

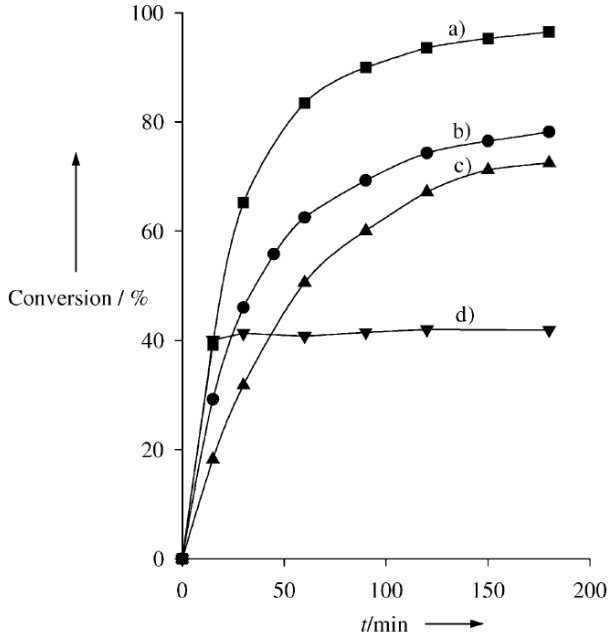

Figure 1-11 Conversion as a function of time in the Knoevenagel condensation between benzaldehyde and malononitrile at 60 °C in toluene solution catalyzed by: (a) N-MCM-48B, (b) N-MCM-48A, (c) MgO and conversion as a function of time (d) after removal of the catalyst (N-MCM-48B) by filtration of reaction mixture. The reaction had previously been allowed to proceed for 15 min in the presence of the NMCM-48B catalysts during which a conversion of 40% was attained.[34]

Methylation of nitrided mesoporous silica improves its basicity (Figure 1-12). Methylated nitrided mesoporous silica can catalyze the Knoevenagel condensation of benzaldehyde and diethyl malonate, which is not possible with conventional nitrided mesoporous silica.[71] Methylated nitrided mesoporous silica also can catalyze the carbonate synthesis from carbon dioxide and cyclic

ethers[72] and that from carbon dioxide and cyclic ethers.[73]

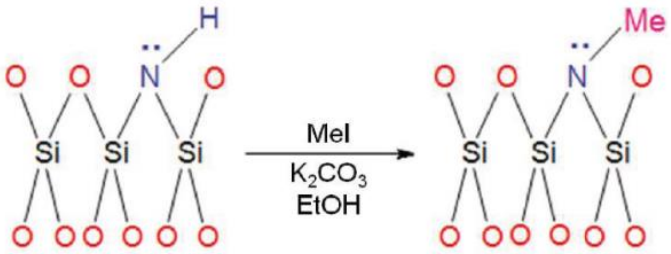

Figure 1-12 Methylation of nitrided mesoporous silica.[71]

1.2.3.2 Solid acid catalyst

Recently, nitrided zeolites for solid acid catalysts have been studied. Nitridation of H-form zeolite could decrease their Brönsted acid sites, but some acid sites existed after nitridation.[15] Therefore, nitridation suppress the formation of byproduct in acid catalysis.

In 2006, Guan *et al.* proposed the controlling zeolite acidity by nitridation for the first time.[17] They treated H-form ZSM-5 with ammonia at 1073 K for 5–15 h. The selectivity to para-diethylbenzene increased with nitridation time in the ethylation of ethylbenzene with ethanol due to decrease of Brönsted acid sites. Moreover, nitridation suppressed coke deposition.

In 2017, Lyu *et al.* reported nitrided hierarchical porous ZSM-5.[19] In benzene alkylation with methanol, nitrided hierarchical porous ZSM-5 suppressed the formation of byproduct like ethylbenzene. It was because that the Brönsted acid sites, Si-OH-Al species decreased during nitridation.

Chen *et al.* controlled the acidity of silica pillared MFI zeolite nanosheet via nitridation. Lewis acid sites were more influenced by nitridation than Brönsted acid sites in MFI nanosheet, therefore nitridation changed the Brönsted/Lewis acid site ratio. In benzylation of mesitylene and benzyl alcohol, nitrided zeolite improve the selectivity of 2-benzyl-1,3,5-trimethyl benzene.

Metal-loaded nitrided zeolite was reported by Zhang *et al.* in 2020 for the first time.[20] Metal-loaded nitrided zeolite (M/N-HZSM-5, M = Mg, Fe, Co, Cu, Ni, or Zn) was prepared by immersing in the aqueous solution, ultrasonic stirring, and calcination. The catalytic activities of M/N-ZSM-5 on preparation of 1-hydroxy-3,6-dioxabicyclo[3.2.1]octan-2-one by pyrolysis of cellulose were compared (Figure 1-13). Mg/N-HZSM-5 showed higher yield and higher selectivity probably due to their low Brönsted/Lewis acid ratio.

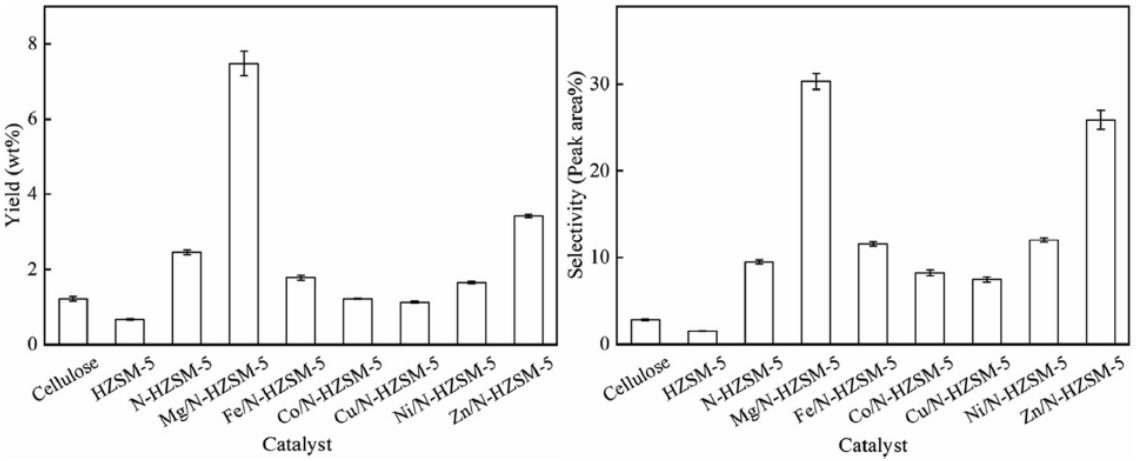

Figure 1-13 Catalytic effect on preparation of 1-hydroxy-3,6-dioxabicyclo[3.2.1]octan-2-one over different metal-loaded nitrided zeolite catalysts.[20]

1.2.3.3 Oxidation catalyst

Titanosilicates are considered as a promising catalyst for alkene epoxidation. Zhang *et al.* prepared nitrided Ti-MWW, TS-1, and Ti-Beta (N-Ti-MWW, N-TS-1, N-Ti-Beta) in order to enhance their catalytic activity.[50] The catalytic properties were evaluated by the epoxidation of 1-hexane with H_2O_2. In all topology, conversion of 1-hexane and epoxide selectivity increased after nitridation. Effect of nitridation condition on N-Ti-MWW was further investigated. At lower temperature (673 K), the conversion increased with nitridation time due to higher nitrogen content. At lower temperature (under 873 K), the conversion increased with nitridation temperature due to higher nitrogen content. At higher temperature (over 1073 K), the conversion decreased sharply due to partial collapse of the titanosilicate structure. The change with time of the activity, Ti-MWW was deactivated earlier than N-Ti-MWW. It would be because that ammonia molecules adsorbed on titanosilicate surface suppressed the epoxide hydrolysis and coke formation.

1.2.3.4. CO_2 adsorbent

Nitrided silica is expected to be an adsorbent for CO_2. Amine-functionalized silica materials have been used as CO_2 adsorbents, but they have various disadvantages such as leaching, structural degradation, using toxic solvent, and low thermal stability. Patil *et al.* prepared nitrided KCC-1, SBA-15, and MCM-41.[30] These materials have a high CO_2 adsorption capacity comparable to that of amine-functionalized mesoporous silica. The fact that the structure was maintained even after CO_2 adsorption/desorption indicates that these materials have high mechanical strength. Furthermore, TG analysis revealed that it possesses high thermal stability.

1.3 Porous carbon nitride

Porous carbon nitrides are expected to be used in various fields due to their large surface area, semiconductivity, basicity, intercalating and adsorption properties, and excellent physicochemical properties (Figure 1-14).[74] These materials are obtained by polymerization of precursors containing carbon and/or nitrogen. The structure of carbon nitride is showed in Figure 1-15.

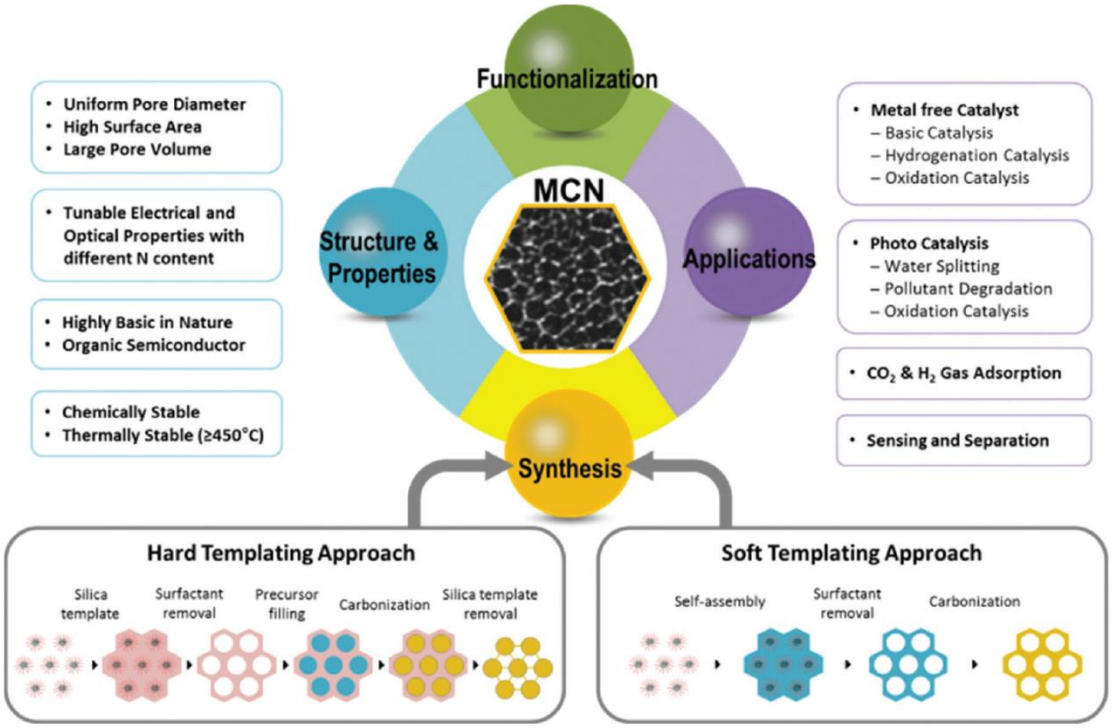

Figure 1-14 Overall scheme for the synthesis, functionalization, and applications of the mesoporous carbon nitride (MCN).[74]

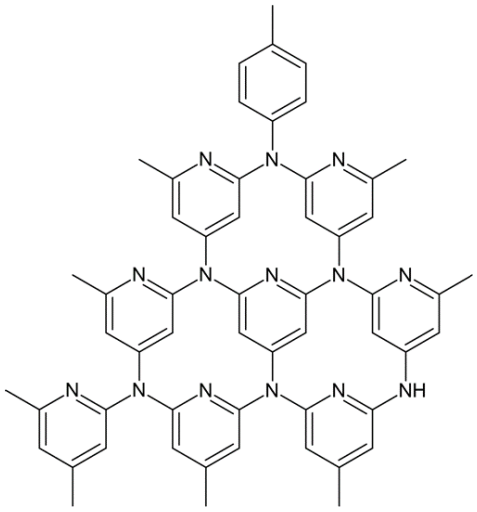

Figure 1-15 Structure of carbon nitride.[75]

1.3.1 Preparation of carbon nitride

There are two known methods for the preparation of porous carbon nitrides: the hard template method and the soft template method.[74] In the hard template method, mesoporous silica such as SBA-15 and KIT-6 is used as a template.[76, 77] The raw material is introduced into the template pores and carbonized by high temperature treatment. Then, the silica template is removed using hydrofluoric acid or sodium hydroxide solution to obtain porous carbon nitride. On the other hand, the soft template method uses a liquid template such as surfactant or ionic liquid.[78, 79] Unlike the hard template method, the soft template method requires only high temperature treatment to remove the template. However, since template removal and carbonization occur simultaneously, the structure is destroyed, and the specific surface area tends to become smaller. The textural parameters and the C/N ratio of porous carbon nitride prepared from both soft and hard template method are summarized in Table 1-9.

Table 1-9 Summary of the textural parameters and the C/N ratio of MCNs prepared from both soft and hard templating approaches.[74]

Name	Template	Precursor	C/N ratio	Structure & morphology	D_{pore} (nm)	S_{BET} ($m^2 g^{-1}$)	V_{Total} ($cm^3 g^{-1}$)	Key feature & application
MCN-1	SBA-15	• Carbon tetrachloride • Ethylenediamine	3.3–4.5	• 2D hexagonal • *p6mm* symmetry • Turbostratic • Rod	4.2–6.4	505–830	0.55–1.25	• First 2D MCN • Tunable textural properties • Highest adsorption capacity • Bifunctional basic and acidic sites • Controlled rod shape • CO_2 adsorption capacity
MCN-2	SBA-16	• Carbon tetrachloride • Ethylenediamine	4–4.15	3D cage	0.8	3.45	0.81	First 3D MCN
MCN-3	IBN-4	• Carbon tetrachloride • Ethylenediamine	2.3	• *p6mm* symmetry • Rod-like	3.8	645	0.67	• Nano-sized MCN • Transesterification
MCN-4	SBA-15	Amino guanidine	0.56–0.64	• 2D hexagonal • *p6mm* symmetry	3.1–5.8	152–321	0.30–0.66	Friedel–Crafts acylation of benzene
MCN-5 MCN-ATN	KIT-6	3-Amino-1,2,4-triazine	0.92	• 3D cubic • *Ia3d* group	5.5–6.0	472–635	0.71–0.99	Highly selective sensing performance for acidic molecules
MCN-6	KIT-6	• Carbon tetrachloride • Ethylenediamine	4.3–4.7	• 3D cubic • *Ia3d* group • Irregular	3.5–5.0	558–637	0.81–0.90	• High basicity • Knoevenagel condensation reaction
MCN-7	FDU-12	• Carbon tetrachloride • Ethylenediamine	2.15–2.99	• 3D cage	3.4–8.3	632–901	0.40–1.10	Large mesopore and high surface area for CO_2 capture
UF-MCN	INC-2	• Urea • Formaldehyde	2.28–2.30	• 2D hexagonal • *P6mm* group • Graphitic • Disk shape	2.5–3.5	350–500	0.30–0.60	Metal-free oxidation of cyclic olefins with H_2O_2
Meso CN spheres	Cellular silica foams	• Carbon tetrachloride • Ethylenediamine	4.55	Spheres with hierarchical 3D mesostructures	4.0–43	~550	~0.9	CO_2 uptake
mpg-C_3N_4	SiO_2 12 nm	Cyanamide	0.71	Disordered spherical pore	12	86–439	—	Cyclotrimerisation of nitriles into triazine and cyclisation of alkynes
g-CN	Colloidal silica	Cyanamide	0.72–0.74	Highly uniform ordered pore	~260	—	—	C_3N_4 network with tri-*s*-triazine rings (C_6N_7) by trigonal N atoms
C_3N_4-G-r	SiO_2 12 nm	Guanidinium chloride	0.73	Graphitic	1.8–13.4	146–215	0.57–0.84	Friedel–Crafts acylation reaction
CN-H-SBA15	SBA-15	Hexamethylenetetramine	4.04	• 2D hexagonal • *p6mm* symmetry	3.76	788	0.68	Transesterification of β-keto esters
DUT-1	SBA-15	Hexamethylenetetramine	—	• 2D hexagonal • *p6mm* symmetry	4.8–11	971–1124	1.31–1.79	Superior dehydrogenation catalyst at 750 °C of pyrolysis temperature
2D-meso-CN	SBA-15	Cyanamide	0.88	2D hexagonal	2.78	361	0.50	H_2 adsorbent
3D-meso-CN	FDU-15			3D cubic	2.45	343	0.67	
mpg-CN	Silica	Ammonium thiocyanate	0.75	g-C_3N_4	11.9	129	0.49	Photocatalytic hydrogen evolution
ompg-CN	SBA-15				5.3	171	0.24	
mpg-C_xN_y	Triton X100	Dicyandiamide	0.69–0.89	Graphite-like packing	3.1–3.4	16–116	0.05–0.28	First report on mpg-C_xN_y by a soft-template
	P123		0.82–2.06		3.8–4.3	10–299	0.03–0.13	
CNBF	$BmimBF_4$	Dicyandiamide	0.65	Sponge-like mesopore	>9.5	444	0.32	Metal-free catalysts for cyclohexane oxidation
g-C_3N_4	P123	Melamine	0.69	Worm-like pore	11.0	27–90	—	Photocatalytic H_2 evolution
CN-T	Triton X100	• Melamine • Glutaraldehyde	—	Graphite-like structure	3.8 40	172–221	0.02–0.21	Lipase immobilization support

In 2005, Vinu *et al.* firstly reported the preparation of hexagonally-ordered MCN materials (MCN-1) through a polymerization between ethylenediamine (EDA) and carbon tetrachloride (CTC) using SBA-15 as hard template (Scheme 1-3).[80] XRD measurements showed that MCN-1 has the

2D hexagonal structure same as SBA-15, and nitrogen adsorption measurements showed that MCN-1 has uniform mesopores. The results of CHN analysis, XPS measurement, and energy-filtering transmission electron microscopy (EF-TEM) observation showed that MCN-1 was mainly composed of carbon and nitrogen. XPS measurements showed that no Si atoms were detected in MCN-1 after template removal, but CHN analysis showed the presence of 12.1 wt% of other elements.

Scheme 1-3 Preparation of MCN-1.[74]

Vinu also reported controlling the pore size and the nitrogen content of MCN-1.[75] As the pore diameter of SBA-15, the template, increased, the pore diameter of MCN-1 also increased. The relationship between the weight ratio of EDA and CTC and the C/N ratio of MCN-1 is shown in Figure 1-16. The nitrogen content of MCN-1 significantly increased when the EDA to CTC weight ratio was increased. Therefore, it can be concluded that the pore size and nitrogen content of MCN-1 can be easily controlled.

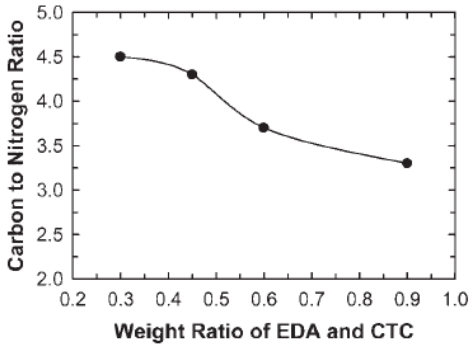

Figure 1-16 Effect of EDA and CTC weight ratio on the nitrogen content of MCN-1.[75]

Zhang *et al.* reported the effect of carbonization temperature on the composition and textual properties of MCN-1.[81] Figure 1-17 shows XRD patterns of MCN-1 with different carbonization temperatures. Since a diffraction peak was observed at 1.10–1.20° for all MCN-1 samples, the structure of samples was considered to be a replication of the template SBA-15. The peak intensity increased with increasing carbonization temperature, which is considered to increase the structural order. In the high-angle region (Figure 1-17B), a broad diffraction peak was observed around 25.3°,

which corresponds to the interplanar stacking peaks of aromatic systems in graphitic materials.[75, 82] The N_2 adsorption isotherms of all MCN-1 samples were type IV, suggesting the presence of mesopores. Textural properties measured by N_2 adsorption and chemical compositions measured by CHN elemental analysis are summarized in Table 1-10. The nitrogen content of carbonized products decreased with increasing nitridation temperature. This could be explained by the low thermodynamic stability of nitrogen species in the carbon materials.[83] As a result of investigating the nitrogen species by XPS measurement, it was found that the percentage of pyridine nitrogen decreased and the percentage of tricoordinated nitrogen and/or amino groups increased with carbonization temperature.

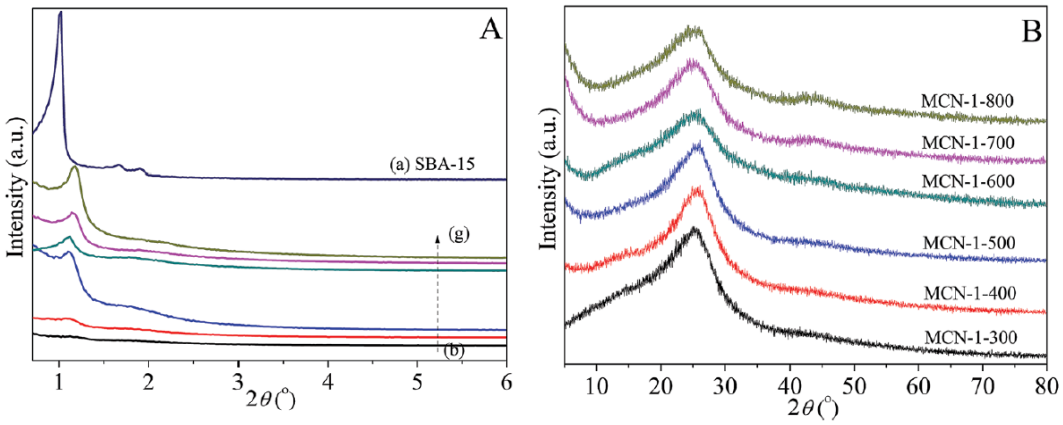

Figure 1-17 XRD patterns of (a) template SBA-15 and MCN-1-T samples (T : carbonization temperature / °C, T = (b) 300, (c) 400, (d) 500, (e) 600, (f) 700, and (g) 800).[81]

Table 1-10 Textural properties and chemical compositions of MCN-1-T and SBA-15 samples.[81]

			Pore diameter[c] (nm)		Composition (wt%)			
Sample	S_{BET}[a] ($m^2\ g^{-1}$)	V_{pore}[b] ($cm^3\ g^{-1}$)	Primary mesopore diameter	Large mesopore diameter	C	N	H	Other possible elements (Si, O, Cl and Na)
MCN-1-300	19.4	0.016	—	—	56.91	24.15	3.80	15.14
MCN-1-400	306.4	0.22	—	6.27	57.29	23.52	3.25	15.94
MCN-1-500	491.4	0.42	3.36	7.30	61.83	21.69	2.94	13.54
MCN-1-600	618.4	0.67	3.56	8.08	65.76	15.75	2.55	15.94
MCN-1-700	790.3	0.95	3.71	9.27	68.54	12.97	2.22	16.27
MCN-1-800	711.4	0.93	3.92	9.41	75.67	8.69	1.45	14.19
SBA-15	1015.5	1.07	8.06	—	—	—	—	—

[a] BET surface area. [b] Total pore volume obtained at $P/P_0 = 0.99$. [c] Most probable pore size.

1.3.2 Characterization of carbon nitride

XRD measurements have been widely used to investigate the periodic structure of porous carbon nitride. Figure 1-18 shows XRD spectra of mesoporous carbon nitride MCN-1 and template SBA-15.[80] The pattern of MCN-1 was similar to the pattern of template SBA-15, suggesting the existence of a hexagonal arrangement of cylindrical pores.

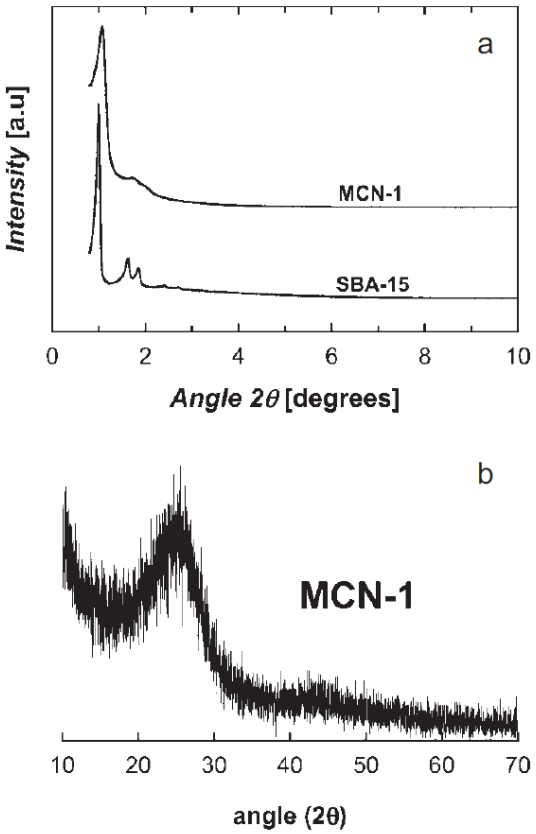

Figure 1-18 (a) XRD patterns of MCN-1and SBA-15. (b) XRD pattern of XRD at high angle range.[80]

N_2 adsorption is used to confirm the presence of mesopores and to investigate the pore size distribution. The order of carbon nitride can be studied from the intensity ratio of the D (disordered) band to the G (graphitic) band in the Raman spectrum.[84]

Combustion method and XPS measurement were often used for investigation on nitrogen content of nitrided materials. In general, porous carbon nitrides contain not only carbon and nitrogen, but also hydrogen and oxygen due to moisture or ethanol adsorbed on the surface, or amine group on porous carbon nitride. EF-TEM is also used to investigate the distribution of elements.[80, 85]

XPS measurements can be used to investigate the state of carbon and nitrogen atoms as well as the composition of porous carbon nitride. Figure 1-19 shows XPS spectra of DUCN-1, one of mesoporous carbon nitrides. The peak observed at 284.7 and 288.2 eV in C1s XPS spectrum (Figure 1-19(a)), which are attributed to graphitic carbon and sp^2-bonded carbon (N-C=N) in the nitrogen-containing aromatic rings, respectively.[86] In general, the latter carbon species is the major one in porous carbon nitride. The N 1 s spectrum can be deconvolved into four signals centered at 398.7, 399.7, 401.1, and 404.6 eV, which correspond to the sp^2-bonded N involved in the triazine

rings (C-N=C)[87], the tertiary nitrogen bonded to three carbon atoms (N-$(C)_3$)[88], the primary or secondary amine groups (-NH_2 or -NH-)[89], and the to the quaternary nitrogen species and/or charging effect (N^+– $(C)_4$)[90], respectively.

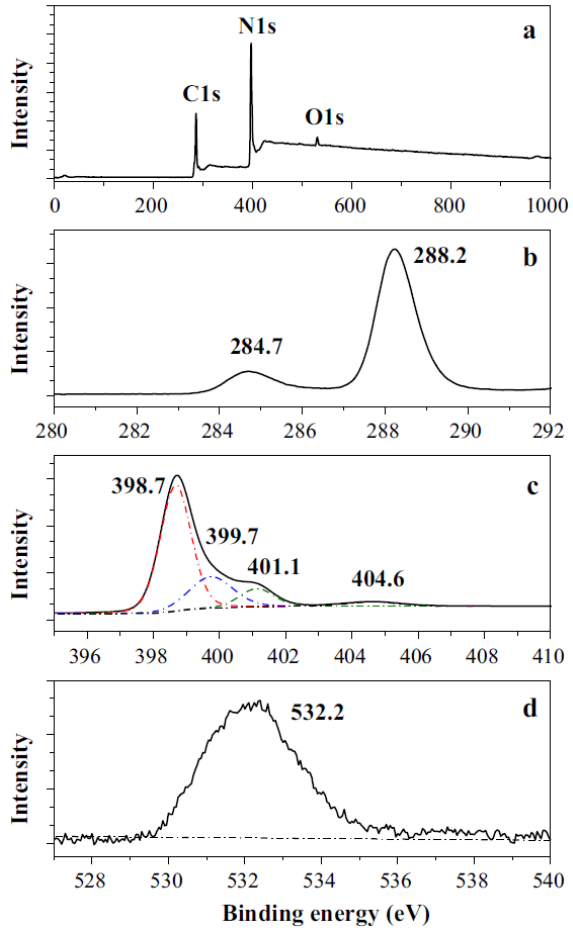

Figure 1-19 XPS spectra of DUCN-1 : (a) survey, (b) C1s, (c) N1s, and (d) O1s spectra.[85]

1.3.3 Application of carbon nitride

Porous carbon nitrides are expected to be used in various fields such as catalysis, energy storage, sensing, and adsorption due to their large surface area, semiconductivity, basicity, intercalating and adsorption properties, and excellent physicochemical properties.

Zhang *et al.* reported the effect of the carbonization temperature on the catalytic activity of MCN-1.[81] MCN-1 with different nitrogen content were prepared by controlling the carbonization temperature. Comparing the composition and conversion of each catalyst, a correlation was found between the amount of tricoordinated nitrogen and/or amino groups rather than the total nitrogen content (Figure 1-20). Therefore, it is revealed that the catalytic activity of MCN-1 is determined by the surface nitrogen species. The catalytic stability of MCN-1 was also investigated. In the case of

MCN-1 carbonized at 400°C, the conversion kept higher than 90% within five repeated runs of Knoevenagel condensation between benzaldehyde and malononitrile. Therefore, MCN-1 materials are considered to be reusable catalysts.

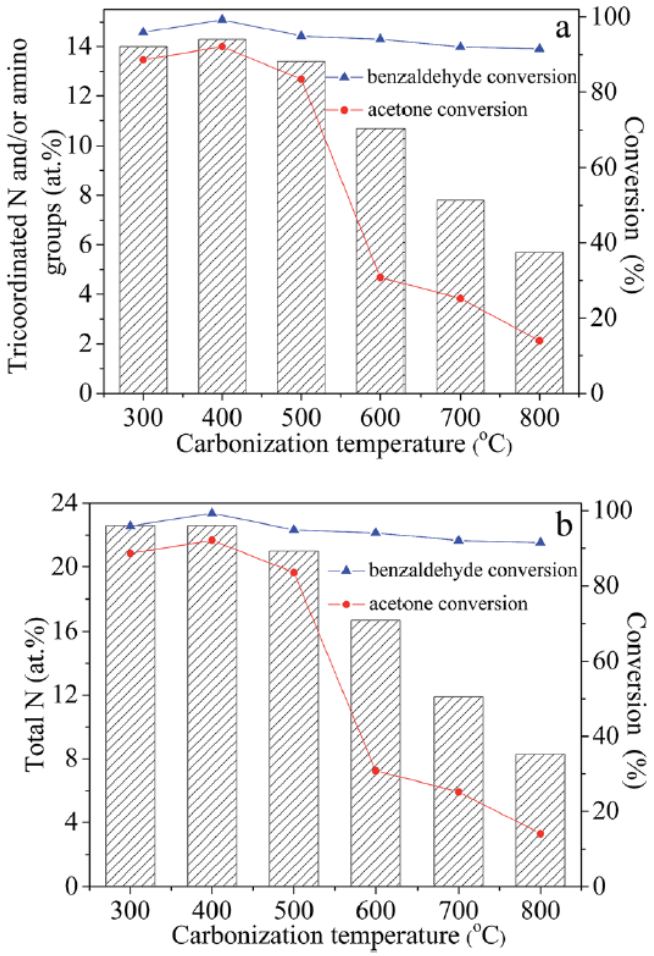

Figure 1-20 Plots for the benzaldehyde and acetone conversions obtained in the Knoevenagel condensations of benzaldehyde or acetone and malononitrile against (a) the surface concentrations of tricoordinated nitrogen and/or amino groups and (b) total nitrogen species.[81]

Similar studies have been conducted on graphitic carbon nitride, DUCN.[85] The order of catalytic activities of nitrogen species in DUCN for the Knoevenagel condensation was $-NH_2$ > -NH- > $N(-C)_3$ > C=N-C. DUCN was stable and reusable in the reaction.

1.4 Amine functionalized silica

By immobilizing amine groups on the surface of the silica material, it can be used as a solid base. A various types of amine groups have been reported to be tethered on silica surfaces (Figure 1-21).[2] The material is denoted as amine functionalized silica, amino functionalized silica, amine grafted silica, amine modified silica, and so on.

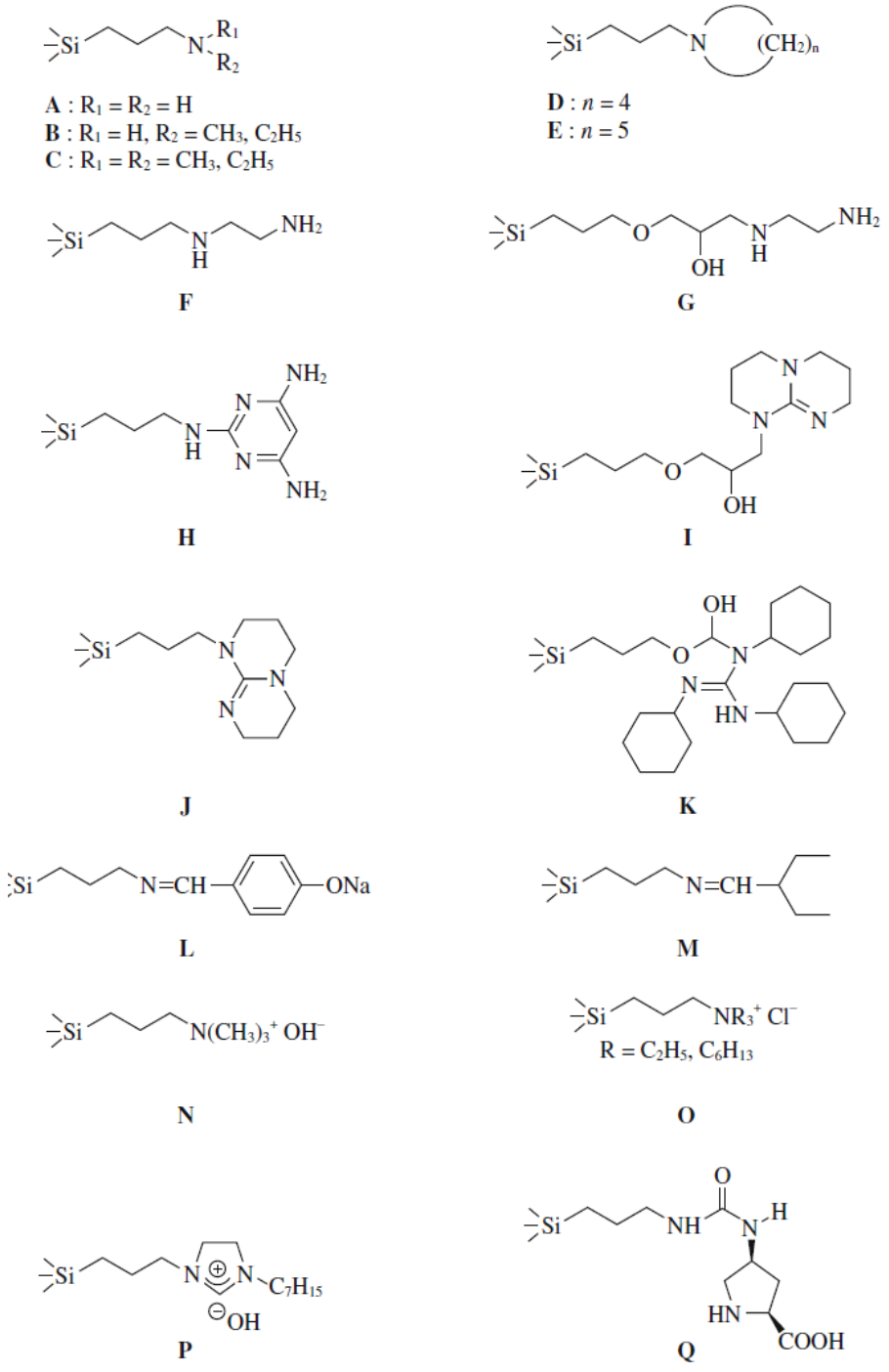

Figure 1-21 Amine groups tethered to silica materials.[2]

1.4.1 Preparation of amine functionalized silica

There are two known methods for the preparation of amine functionalized silica: post-synthesis grafting method and direct co-condensation method (Figure 1-22).[91] The post-synthesis method is the most common method of amine functionalized silica synthesis and is carried out by the reaction of silanol groups on the silica surface with silane coupling agents. A variety of amine groups have been modified on the surface of various silica materials (such as MCM-41[92-96], SBA-15[85, 97-99], FAU[100], FAU/EMT[101]) by post-synthetic methods. In the direct co-condensation method, trialkoxysilanes with amine groups are used as one of the raw materials to synthesize silica materials. Introduction of carious amine groups to mesoporous silica (MCM-41[94, 102-105], SBA-15[106-110]) by direct co-condensation method has been reported.

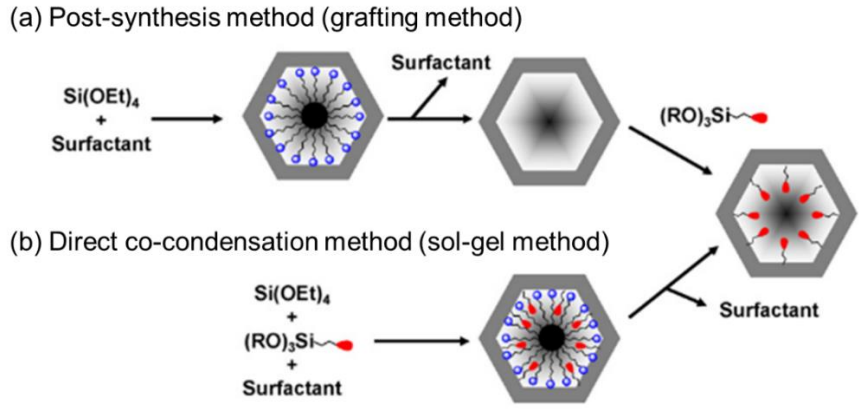

Figure 1-22 Preparation of amine functionalized silica.[91]

Macquarrie *et al.* compared the post-synthesis method with the direct co-condensation method.[96] Amine functionalized MCM-41 and Kieselgel 60 were prepared by post-synthesis method using 3-aminopropyltriethoxysilane. Hexagonal mesoporous silica and amorphous silica with aminopropyl groups were prepared from tetraethoxysilane and 3-aminopropyltrimethoxysilane by direct co-condensation method. Amine-functionalized silica prepared by direct co-condensation method are less active than those obtained by grafting method for nitroaldol reaction and Michael addition. This is probably because some of the amines are incorporated within the siliceous framework, reducing the number of active sites that the reactants can access.

Pineda *et al.* carried out the post-synthesis of amine functionalized mesoporous silica (HMS and SBA-15) by varying the amount of silane coupling agent.[97] The textural properties of functionalized SBA-15 are summarized in Table 1-11. As the amount of silane coupling agent used in the synthesis increases, the amount of amine to be modified also increases, but about 10 wt% is the maximum value.

Table 1-11 Textural properties of SBA-15 functionalized with various amount of aminopropyl groups. The content of aminopropyl groups was measured by TG.[97]

Sample	Mean pore size (nm)	Pore volume ($mL\ g^{-1}$)	S_{BET} ($m^2\ g^{-1}$)	Aminopropyl loading (wt.%)
SBA-15	5.4	0.54	706	–
SBA-15-5%APTES	2.4	0.21	221	5.4
SBA-15-10%APTES	<2.0	0.35	256	7.0
SBA-15-20%APTES	<2.0	0.32	226	9.0
SBA-15-30%APTES	<2.0	0.21	239	8.6

1.4.2 Characterization of amine functionalized silica

In this section, the characterization method of the amine functionalized silica obtained by the post-synthesis method is described.

XRD measurements are widely used to investigate the structural changes before and after grafting. Figure 1-23 shows XRD patterns of APTES-functionalized mesoporous silica before and after grafting.[98] The peak position hardly changes after grafting process, suggesting that mesoporous structure is preserved.

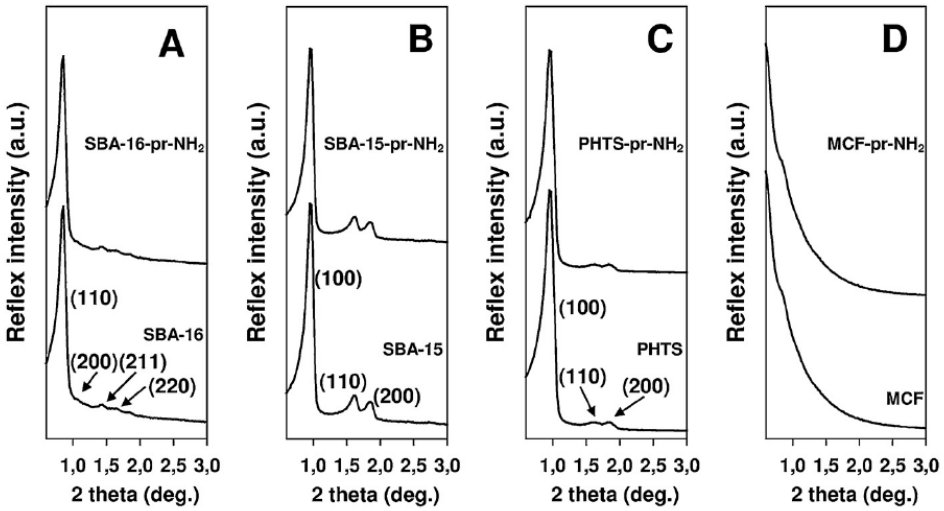

Figure 1-23 XRD patterns of mother and APTES-functionalized mesoporous silicas: (A) SBA-16, (B) SBA-15, (C) PHTS, and (D) MCF.[98]

Many researchers used N_2 adsorption measurement in order to investigate textual properties of amine functionalized silica materials. In general, the type of adsorption isotherm does not change before and after grafting process. In addition, after grafting process, the surface area and pore volume decrease due to the presence of organic functions inside the mesopores.[98]

The amount of functionalized amine groups is measured by thermogravimetric analysis, CHN analysis, and the argentometric titration using $AgNO_3$. The content of all amine groups in the bulk is measured by CHN analysis. On the other hand, the content of amine groups only on the surface is measured by titration.[94, 111]

The functionalized amine group is confirmed by FT-IR spectroscopy[97, 112, 113], XPS measurement[108, 113-116], and ^{13}C NMR.[97, 113] Figure 1-24 shows FT-IR spectra of silica and amine-functionalized silica.[112] The peak at 3400-3200 cm^{-1} is different depending on the amine series.

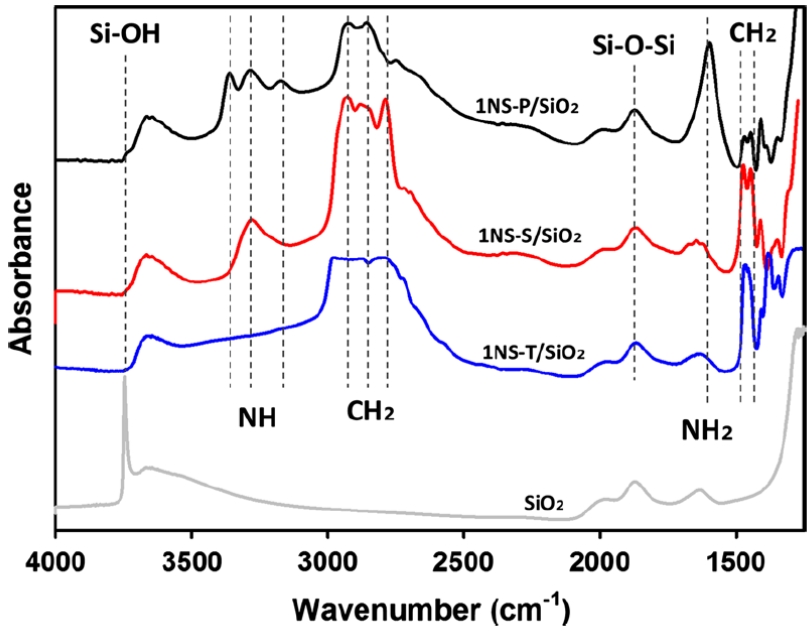

Figure 1-24 FT-IR spectra of silica and amine-functionalized silica. 1NS-P/SiO_2, 1NS-S/SiO_2, and 1NS-T/SiO_2 means (3-aminopropyl)trimethoxysilane, [3-(methylamino)propyl]trimetoxysilane, and [3-(diethylamino)propyl]trimethoxysilane functionalized silica, respectively.[112]

1.4.3 Application of amine functionalized silica

Amine functionalized mesoporous silica has attracted much attention as a solid base catalyst. It catalyzes epoxidation and C-C bond formation reactions, such as Knoevenagel condensation, aldol condensation reaction, Michael addition reaction, Claisen-Schmidt reaction, and nitroaldol reaction.[117-120]

Zhang *et al.* reported the effect of the functionalized group on the catalytic activity of amine functionalized silica.[85] (3-aminopropyl)trimethoxysilane, bis(trimethoxysilylpropyl)amine, and 2-(2-pyridylethyl)trimethoxysilane were grafted onto the surface of SBA-15. Their nitrogen content and surface area were not significantly different. The catalytic activities of amine functionalized

SBA-15 materials were investigated by Knoevenagel condensation. The order of catalytic activities of nitrogen species in amine functionalized silica was -NH_2 > -NH- > C=N-C (Table 1-12).

Table 1-12 Catalytic results of amine functionalized SBA-15 materials for different Knoevenagel condensation reactions.[85]

Entry	Catalyst	*X* (%)[a]	*S* (%)[b]	Entry	Catalyst	*X* (%)[a]	*S* (%)[b]
I. Benzaldehyde + malononitrile				*III. Benzaldehyde + ethyl cyanoacetate*			
1	None	9.8	89.5	11	None	5.8	0
2	SBA-15	16.2	93.6	12	SBA-15	7.0	0
3	NH_2-SBA-15	100	98.7	13	NH_2-SBA-15	100	97.9
4	NH-SBA-15	100	98.1	14	NH-SBA-15	100	97.2
5	N-SBA-15	100	96.5	15	N-SBA-15	32.6	94.0
II. Acetone + malononitrile				*IV. Acetone + ethyl cyanoacetate*			
6	None	0.17	92.6	16	None	0	–
7	SBA-15	0.30	96.6	17	SBA-15	0	–
8	NH_2-SBA-15	100	98.1	18	NH_2-SBA-15	81.9	97.7
9	NH-SBA-15	100	97.8	19	NH-SBA-15	18.1	96.9
10	N-SBA-15	39.9	95.4	20	N-SBA-15	0	–

[a] *X*: the conversion of benzaldehyde or acetone.
[b] *S*: the selectivity to benzylidene malononitrile (I), isopropylidenemalononitrile (II), ethyl α-cyanocinnamate (III), or ethyl 2-cyano-3-methylcrotonate (IV). Reactions conditions: 40 °C, 1 mmol benzaldehyde or acetone, 3 mmol malononitrile or ethyl cyanoacetate, 20 mg catalyst, 2 h for reactions (I) and (II), and 6 h for reactions (III) and (IV).

The catalytic stability of aminopropyl modified MCM-41 was reported.[115] The conversion kept 95% within three repeated runs of Knoevenagel condensation between benzaldehyde and diethyl malonate. Therefore, amine functionalized silica is considered to be a reusable catalyst.

Amine functionalized mesoporous silica is also expected to be used as an adsorbent for toxic heavy metal ions (e.g., Hg^{2+}, Cu^{2+}, Zn^{2+}, Cr^{3+}, and Ni^{2+}) and CO_2. From the perspective of CCUS (carbon capture, utilization and storge), it has been especially studied as a CO_2 adsorbent.[91, 121, 122] Amine functionalized silica showed higher thermal stability than amine sorbents.[123]

Hiyoshi *et al.* reported the adsorption characteristics of CO_2 on amine functionalized SBA-15.[114] 3-aminopropyltriethoxysilane (APS), *N*-(2-aminoethyl)-3-aminopropyltrimethoxysilane (AEAPS) and (3-trimethoxysilylpropyl)diethylenetriamine (TA) were used as grafting agents. Figure 1-25(a) shows relationship between amine content and CO_2 adsorption capacity. The CO_2 adsorption capacity increased with increasing amine content, but the relationship was not linear. Focusing on amine efficiency (η = adsorbed CO_2 (mmol/g) / nitrogen content (mmol/g)), a correlation was observed between surface amine density and amine efficiency (Figure 1-25 (b)). This is thought to be because the pair amine sites are more likely to form than isolated amine sites due to the increase in surface amine density, and the pair amine sites adsorb CO_2 by generating carbamates (Figure 1-26).

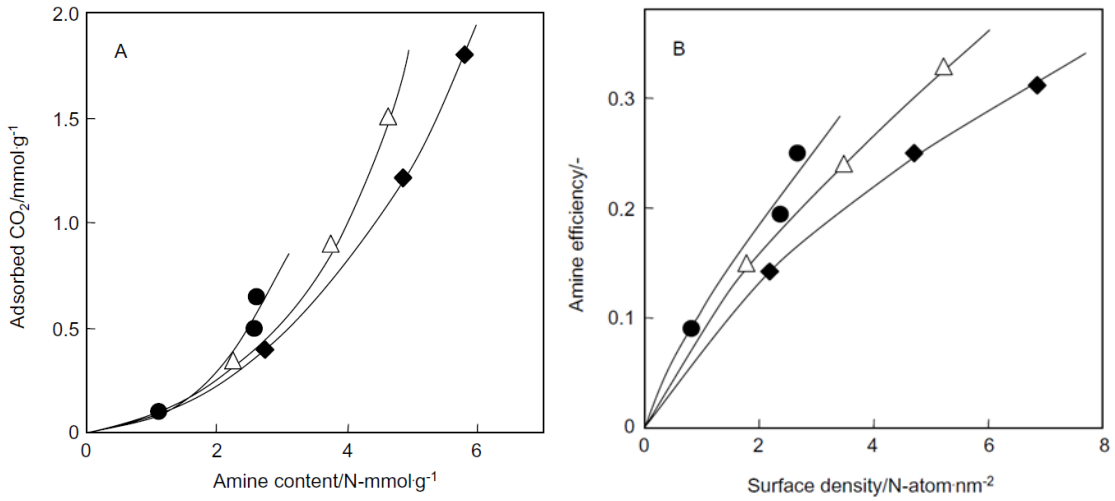

Figure 1-25 Relationship between (a) amine content and CO_2 adsorption capacity and (b) that between surface density of amine and amine efficiency. ●:APS-, △:AEAPS-, and ◆: TA-functionalized SBA-15. The adsorption was conducted at 333 K with 15 kPa CO_2 and 12 kPa H_2O with N_2 balance.[114]

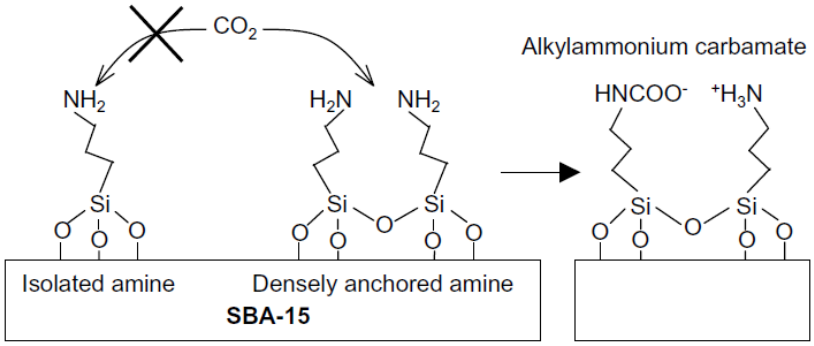

Figure 1-26 Adsorption of CO_2 on amine functionalized SBA-15.[114]

The effect of amine species on CO_2 adsorption was also investigated by Hiyoshi *et al.*[114] 3-aminopropyltriethoxysilane (APS, primary amine), *N*-methylaminopropyltrimethoxysilane (MAPS, secondary amine), and (*N,N*-dimethyl-3-aminopropyl)trimethoxysilane (DMAPS, tertiary amine) reacted with SBA-15. The amine efficiency of APS-SBA-15, MAPS-SBA-15, and DMAPS-SBA-15 was 0.25, 0.13, and 0.03, respectively. The amine efficiency is considered to be more strongly influenced by steric hindrance caused by the bulky groups attached to the nitrogen atom than the type of amine.

1.5 Objectives of this thesis

As mentioned in the previous chapter 1.1, base catalyzed reactions are used in a variety of fields such as fine chemicals, drugs, and cosmetics industries. Since solid base catalysts have many advantages over liquid base catalysts, there is a need to develop novel solid base catalysts.

I focused on the following five properties of solid base catalysts: **activities, durabilities, selectivities, accessibilities and safeties of the synthesis method**. Nitrogen-containing porous catalysts were selected as the target solid base catalysts. These catalysts are known to exhibit higher selectivities compared to alkali metal oxides.[41] In addition, the porosity increases the surface area, resulting in higher accessibility.

As mentioned above, various nitrogen sites have been reported to work as base sites. The nitrogen sites in the nitrogen-containing porous solid base catalysts are summarized in Table 1-13. In this dissertation, by comparing the properties of various nitrogen sites, effects of nitrogen sites on base catalytic properties were investigated. Based on the results, design guidelines for new solid base catalysts were developed.

Table 1-13 Nitrogen sites in the nitrogen-containing porous solid base catalysts.

Catalyst	Nitrogen site
Nitrided silica	Si-NH_2
	Si-NH-Si
	N-$(Si)_3$
Carbon nitride	Graphitic N
	Pyridinic N
	Pyrrolic N
	C-NH_2
	C-NH-C
	N-$(C)_3$
Amine-functionalized silica	C-NH_2
	C-NH-C
	N-$(C)_3$

1.6 Outline of this thesis

The framework of this dissertation is shown in Figure 1-27.

In Chapter 1, general research backgrounds and research objective of this dissertation are described. In particular, solid base catalysts which nitrogen species are the active sites were summarized.

In Chapter 2, nitrogen sites in nitrided silica were studied. By comparing the catalytic properties of nitrided zeolite and nitrided delaminated zeolite, the effect of the type and location of nitrogen sites on the catalytic properties was discussed.

In Chapter 3, nitrogen sites of nitrided silica were compared with those of carbon nitride. The effect of the functional groups attached to the nitrogen sites on the catalytic properties was investigated.

In Chapter 4, nitrogen sites of nitrided silica were compared with those of amine-functionalized silica. A variety of nitrogen sites were modified on the silica surface by a grafting method, and the properties of each nitrogen site were investigated by comparing them.

In Chapter 5, the basicity of nitrogen-containing catalysts was evaluated by CO_2 adsorption.

Finally, general conclusions and future perspectives are described in Chapter 6.

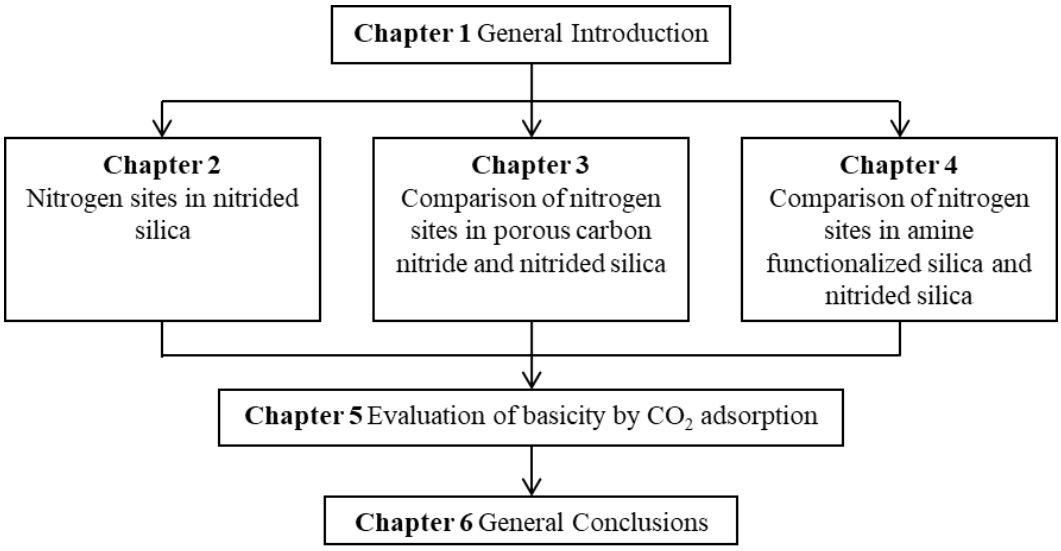

Figure 1-27 Framework of this dissertation.

References

[1] H. Hattori, Solid base catalysts: fundamentals and their applications in organic reactions, Applied Catalysis a-General, 504 (2015) 103-109.

[2] Y. Ono, H. Hattori, Solid Base Catalysis, Springer Berlin Heidelberg, 2012.

[3] S. Coluccia, A. Barton, A.J. Tench, REACTIVITY OF LOW-COORDINATION SITES ON THE SURFACE OF MAGNESIUM-OXIDE, Journal of the Chemical Society-Faraday Transactions I, 77 (1981) 2203-2207.

[4] K. Akutu, H. Kabashima, T. Seki, H. Hattori, Nitroaldol reaction over solid base catalysts, Applied Catalysis a-General, 247 (2003) 65-74.

[5] H. Kabashima, T. Katou, H. Hattori, Conjugate addition of methanol to 3-buten-2-one over solid base catalysts, Applied Catalysis a-General, 214 (2001) 121-124.

[6] 小野 嘉夫, 八嶋 建明, ゼオライトの科学と工学, 講談社, 2000..

[7] T. Yashima, K. Sato, N. Hara, T. Hayasaka, ALKYLATION ON SYNTHETIC ZEOLITES .3. ALKYLATION OF TOLUENE WITH METHANOL AND FORMALDEHYDE ON ALKALI CATION EXCHANGED ZEOLITES, Journal of Catalysis, 26 (1972) 303-&.

[8] K. Hatada, Y. Ono, SYNTHETIC ZEOLITES AS CATALYSTS FOR RING CONVERSION OF GAMMA-BUTYROLACTONE INTO 1-SUBSTITUTED 2-PYRROLIDINONES, Bulletin of the Chemical Society of Japan, 50 (1977) 2517-2521.

[9] J. Sjoberg, R. Pompe, NITRIDATION OF AMORPHOUS SILICA WITH AMMONIA, Journal of the American Ceramic Society, 75 (1992) 2189-2193.

[10] G.T. Kerr, G.F. Shipman, REACTION OF HYDROGEN ZEOLITE Y WITH AMMONIA AT ELEVATED TEMPERATURES, Journal of Physical Chemistry, 72 (1968) 3071-3072.

[11] S. Ernst, M. Hartmann, S. Sauerbeck, T. Bongers, A novel family of solid basic catalysts obtained by nitridation of crystalline microporous aluminosilicates and aluminophosphates, Applied Catalysis a-General, 200 (2000) 117-123.

[12] F. Dogan, K.D. Hammond, G.A. Tompsett, H. Huo, W.C. Conner, S.M. Auerbach, C.P. Grey, Searching for Microporous, Strongly Basic Catalysts: Experimental and Calculated ^{29}Si NMR Spectra of Heavily Nitrogen-Doped Y Zeolites, Journal of the American Chemical Society, 131 (2009) 11062-11079.

[13] V. Agarwal, G.W. Huber, W.C. Conner, Jr., S.M. Auerbach, DFT study of nitrided zeolites: Mechanism of nitrogen substitution in HY and silicalite, Journal of Catalysis, 269 (2010) 53-63.

[14] D. Verboekend, T.C. Keller, S. Mitchell, J. Perez-Ramirez, Hierarchical FAU- and LTA-Type Zeolites by Post-Synthetic Design: A New Generation of Highly Efficient Base Catalysts, Advanced Functional Materials, 23 (2013) 1923-1934.

[15] C.M. Zhang, Z. Xu, K. Wan, Q. Liu, Synthesis, characterization and catalytic properties of nitrogen-incorporated ZSM-5 molecular sieves with bimodal pores, Applied Catalysis a-General, 258 (2004) 55-61.

[16] X.X. Guan, N. Li, G.J. Wu, F.X. Zhang, J.X. Chen, N.J. Guan, Nitridation of HZSM-5 and its application in ethylation of ethylbenzene with ethanol to para-diethylbenzene, Chinese Journal of Catalysis, 26 (2005) 634-636.
[17] X.X. Guan, N. Li, G.J. Wu, J.X. Chen, F.X. Zhang, N.J. Guan, Para-selectivity of modified HZSM-5 zeolites by nitridation for ethylation of ethylbenzene with ethanol, Journal of Molecular Catalysis a-Chemical, 248 (2006) 220-225.
[18] G.J. Wu, X. Wang, Y.L. Yang, L.D. Li, G.C. Wang, N.J. Guan, Confirmation of NH species in the framework of nitrogen-incorporated ZSM-5 zeolite by experimental and theoretical studies, Microporous and Mesoporous Materials, 127 (2010) 25-31.
[19] J.H. Lyu, H.L. Hu, J.Y. Rui, Q.F. Zhang, J. Cen, W.W. Han, Q.T. Wang, X.K. Chen, Z.Y. Pan, X.N. Li, Nitridation: A simple way to improve the catalytic performance of hierarchical porous ZSM-5 in benzene alkylation with methanol, Chinese Chemical Letters, 28 (2017) 482-486.
[20] Z.-X. Zhang, B. Hu, Y. Li, K. Li, Q. Lu, Selective preparation of 1-hydroxy-3,6-dioxabicyclo 3.2.1 octan-2-one by fast pyrolysis of cellulose catalyzed with metal-loaded nitrided HZSM-5, Bioresource technology, 309 (2020) 123370-123370.
[21] H.K. Min, S.H. Cha, S.B. Hong, Nitrided ITQ-2 as an efficient Knoevenagel condensation catalyst, Chemical Communications, 49 (2013) 1115-1117.
[22] K. Narasimharao, M. Hartmann, H.H. Thiel, S. Ernst, Novel solid basic catalysts by nitridation of zeolite beta at low temperature, Microporous and Mesoporous Materials, 90 (2006) 377-383.
[23] K.D. Hammond, F. Dogan, G.A. Tompsett, V. Agarwal, W.C. Conner, C.P. Grey, S.M. Auerbach, Spectroscopic Signatures of Nitrogen-Substituted Zeolites, Journal of the American Chemical Society, 130 (2008) 14912-14913.
[24] J. Perez-Ramirez, C.H. Christensen, K. Egeblad, J.C. Groen, Hierarchical zeolites: enhanced utilisation of microporous crystals in catalysis by advances in materials design, Chemical Society Reviews, 37 (2008) 2530-2542.
[25] A. Kawano, T. Moteki, M. Ogura, Effect of delamination on active base site formation over nitrided MWW-type zeolite for Knoevenagel condensation, Microporous and Mesoporous Materials, 299 (2020).
[26] M.J. Climent, A. Corma, V. Fornes, A. Frau, R. GuilLopez, S. Iborra, J. Primo, Aluminophosphates oxynitrides as base catalysts: Nature of the base sites and their catalytic implications, Journal of Catalysis, 163 (1996) 392-398.
[27] J.M. Xiong, Y.J. Ding, H.J. Zhu, L. Yan, X.M. Liu, L.W. Lin, Nitrogen-incorporated SAPO-11 molecular sieve: Synthesis, characterization, and properties, Journal of Physical Chemistry B, 107 (2003) 1366-1369.
[28] X.X. Guan, F.X. Zhang, G.J. Wu, N.J. Guan, Synthesis and characterization of a basic molecular sieve: Nitrogen-incorporated SAPO-34, Materials Letters, 60 (2006) 3141-3144.
[29] T. Asefa, M. Kruk, N. Coombs, H. Grondey, M.J. MacLachlan, M. Jaroniec, G.A. Ozin, Novel route

to periodic mesoporous aminosilicas, PMAs: Ammonolysis of periodic mesoporous organosilicas, Journal of the American Chemical Society, 125 (2003) 11662-11673.

[30] U. Patil, A. Fihri, A.H. Emwas, V. Polshettiwar, Silicon oxynitrides of KCC-1, SBA-15 and MCM-41 for CO_2 capture with excellent stability and regenerability, Chemical Science, 3 (2012) 2224-2229.

[31] G.J. Wu, S.L. Jiang, L.D. Li, F.X. Zhang, Y.L. Yang, N.J. Guan, M. Mihaylov, H. Knozinger, Physico-chemical characterization of nitrided mesoporous silicon MCM-41, Microporous and Mesoporous Materials, 135 (2010) 2-8.

[32] F. Hayashi, K. Ishizu, M. Iwamoto, Fast and Almost Complete Nitridation of Mesoporous Silica MCM-41 with Ammonia in a Plug-Flow Reactor, Journal of the American Ceramic Society, 93 (2010) 104-110.

[33] F. Hayashi, K. Ishizu, M. Iwamoto, Effect of Pore Structure on the Nitridation of Mesoporous Silica with Ammonia, European Journal of Inorganic Chemistry, (2010) 2235-2243.

[34] Y.D. Xia, R. Mokaya, Highly ordered mesoporous silicon oxynitride materials as base catalysts, Angewandte Chemie-International Edition, 42 (2003) 2639-2644.

[35] Y.D. Xia, R. Mokaya, Mesoporous MCM-48 aluminosilica oxynitrides: Synthesis and characterization of bifunctional solid acid-base materials, Journal of Physical Chemistry C, 112 (2008) 1455-1462.

[36] B. Singh, K.R. Mote, C.S. Gopinath, P.K. Madhu, V. Polshettiwar, SBA-15-Oxynitrides as a Solid-Base Catalyst: Effect of Nitridation Temperature on Catalytic Activity, Angewandte Chemie-International Edition, 54 (2015) 5985-5989.

[37] N. Chino, T. Okubo, Nitridation mechanism of mesoporous silica: SBA-15, Microporous and Mesoporous Materials, 87 (2005) 15-22.

[38] K. Wan, Q. Liu, C.M. Zhang, J.C. Wang, The basicity and catalytic activity of ordered mesoporous silicon nitride oxide, Bulletin of the Chemical Society of Japan, 77 (2004) 1409-1414.

[39] A. Bendjeriou-Sedjerari, J.D.A. Pelletier, E. Abou-Hamad, L. Emsley, J.M. Basset, A well-defined mesoporous amine silica surface via a selective treatment of SBA-15 with ammonia, Chemical Communications, 48 (2012) 3067-3069.

[40] J.C. Wang, Q. Liu, Structural change and characterization in nitrogen-incorporated SBA15 oxynitride mesoporous materials via different thermal history, Microporous and Mesoporous Materials, 83 (2005) 225-232.

[41] T. Hasegawa, C.K. Krishnan, M. Ogura, Promising catalytic performance and shape-selectivity of nitrogen-doped siliceous MFI zeolite for base-catalyzed reactions, Microporous and Mesoporous Materials, 132 (2010) 290-295.

[42] T. Moteki, Y. Koga, M. Ogura, Primary, secondary, and tertiary silanamine sites formed on nitrided SBA-15 for base catalytic C-C bond formation reactions, Journal of Catalysis, 378 (2019) 131-139.

[43] Y. Inaki, Y. Kajita, H. Yoshida, K. Ito, T. Hattori, New basic mesoporous silica catalyst obtained by

ammonia grafting, Chemical Communications, (2001) 2358-2359.
[44] J. El Haskouri, S. Cabrera, F. Sapina, J. Latorre, C. Guillem, A. Beltran-Porter, D. Beltran-Porter, M.D. Marcos, P. Amoros, Ordered mesoporous silicon oxynitrides, Advanced Materials, 13 (2001) 192-195.
[45] M. Bouhrara, C. Ranga, A. Fihri, R.R. Shaikh, P. Sarawade, A.H. Emwas, M.N. Hedhili, V. Polshettiwar, Nitridated Fibrous Silica (KCC-1) as a Sustainable Solid Base Nanocatalyst, Acs Sustainable Chemistry & Engineering, 1 (2013) 1192-1199.
[46] A.S.L. Thankamony, C. Lion, F. Pourpoint, B. Singh, A.J.P. Linde, D. Carnevale, G. Bodenhausen, H. Vezin, O. Lafon, V. Polshettiwar, Insights into the Catalytic Activity of Nitridated Fibrous Silica (KCC-1) Nanocatalysts from ^{15}N and ^{29}Si NMR Spectroscopy Enhanced by Dynamic Nuclear Polarization, Angewandte Chemie-International Edition, 54 (2015) 2190-2193.
[47] M. Srasra, S. Delsarte, E.M. Gaigneaux, Effects of the Nitridation of Y and USY Zeolites on their Catalytic Activity for the Base Catalyzed Knoevenagel Condensation, Topics in Catalysis, 52 (2009) 1541-1548.
[48] M. Srasra, S. Delsarte, E.M. Gaigneaux, Nitrided Zeolites: A Spectroscopic Approach for the Identification and Quantification of Incorporated Nitrogen Species, Journal of Physical Chemistry C, 114 (2010) 4527-4535.
[49] K.D. Hammond, M. Gharibeh, G.A. Tompsett, F. Dogan, A.V. Brown, C.P. Grey, S.M. Auerbach, W.C. Conner, Optimizing the Synthesis of Nitrogen-Substituted Zeolites, Chemistry of Materials, 22 (2010) 130-142.
[50] L.Y. Zhang, L. Xu, J.J. Sun, J.G. Jiang, Y.M. Liu, H.H. Wu, P. Wu, Enhancement of Alkene Epoxidation Activity of Titanosilicates by Gas-Phase Ammonia Modification, Chinese Journal of Chemistry, 30 (2012) 2205-2211.
[51] Y.F. Zhao, Y. Qi, Y.X. Wei, Y.Y. Zhang, S.G. Zhang, Y. Yang, Z.M. Liu, Incorporation of Ag nanostructures into channels of nitrided mesoporous silica, Microporous and Mesoporous Materials, 111 (2008) 300-306.
[52] J.L. Bischoff, F. Lutz, D. Bolmont, L. Kubler, USE OF MULTILAYER TECHNIQUES FOR XPS IDENTIFICATION OF VARIOUS NITROGEN ENVIRONMENTS IN THE SI/NH_3 SYSTEM, Surface Science, 251 (1991) 170-174.
[53] P.S. Wang, S.G. Malghan, S.M. Hsu, T.N. Wittberg, X-RAY-INDUCED AES STUDY OF THE EFFECT OF CHEMICALLY BOUND HYDROGEN ON THE OXIDATION-KINETICS OF AN SI3N4 POWDER, Surface and Interface Analysis, 21 (1994) 155-159.
[54] R. Franke, C. Girgenrath, S. Kohn, M. Jansen, An X-ray photoelectron spectroscopic study of novel SiON glasses, Fresenius Journal of Analytical Chemistry, 361 (1998) 587-590.
[55] T.N. Taylor, D.P. Butt, C.G. Pantano, Auger parameter determination of bonding states on thinly oxidized silicon nitride, Surface and Interface Analysis, 26 (1998) 134-143.

[56] R.K. Brow, C.G. Pantano, THERMOCHEMICAL NITRIDATION OF MICROPOROUS SILICA FILMS IN AMMONIA, Journal of the American Ceramic Society, 70 (1987) 9-14.

[57] H.N. Liu, D.C. Bertolet, J.W. Rogers, THE SURFACE-CHEMISTRY OF ALUMINUM NITRIDE MOCVD ON ALUMINA USING TRIMETHYLALUMINUM AND AMMONIA AS PRECURSORS, Surface Science, 320 (1994) 145-160.

[58] P.S. Wang, S.G. Malghan, S.M. Hsu, T.N. Wittberg, THE OXIDATION OF AN ALUMINUM NITRIDE POWDER STUDIED BY BREMSSTRAHLUNG-EXCITED ANGER ELECTRON-SPECTROSCOPY AND X-RAY PHOTOELECTRON-SPECTROSCOPY, Journal of Materials Research, 10 (1995) 302-305.

[59] H. Liu, D.C. Bertolet, J.W. Rogers, REACTIONS OF TRIMETHYLALUMINUM AND AMMONIA ON ALUMINA AT 600 K - SURFACE CHEMICAL ASPECTS OF ALN THIN-FILM GROWTH, Surface Science, 340 (1995) 88-100.

[60] M. Wolff, J.W. Schultze, H.H. Strehblow, LOW-ENERGY IMPLANTATION AND SPUTTERING OF TIO2 BY NITROGEN AND ARGON AND THE ELECTROCHEMICAL REOXIDATION, Surface and Interface Analysis, 17 (1991) 726-736.

[61] B. Siemensmeyer, K. Bade, J.W. Schultze, XPS AND ELECTROCHEMICAL STUDIES OF THIN TIN LAYERS, Berichte Der Bunsen-Gesellschaft-Physical Chemistry Chemical Physics, 95 (1991) 1461-1469.

[62] I. Milosev, H.H. Strehblow, B. Navinsek, M. Metikoshukovic, ELECTROCHEMICAL AND THERMAL-OXIDATION OF TIN COATINGS STUDIED BY XPS, Surface and Interface Analysis, 23 (1995) 529-539.

[63] N.C. Saha, H.G. Tompkins, TITANIUM NITRIDE OXIDATION CHEMISTRY - AN X-RAY PHOTOELECTRON-SPECTROSCOPY STUDY, Journal of Applied Physics, 72 (1992) 3072-3079.

[64] F. Márquez, R. Guil-López, V. Fornés, A. Corma, First evidences on the stability of nitride species in ALPON catalysts, in: Catalysis Communications, 2000, pp. 21-24.

[65] N. Fripiat, M.A. Centeno, P. Grange, Identification and stability of the nitrogenous species in zirconium phosphate oxynitride catalysts, Chemistry of Materials, 11 (1999) 1434-1445.

[66] J.J. Benitez, A. Diaz, Y. Laurent, P. Grange, J.A. Odriozola, Diffuse reflectance infrared (DRIFTS) and mass spectrometry study of thermal stability of aluminophosphate oxynitrides (AlPON), Zeitschrift Fur Physikalische Chemie-International Journal of Research in Physical Chemistry & Chemical Physics, 202 (1997) 21-29.

[67] M.J. Remy, D. Stanica, G. Poncelet, E.J.P. Feijen, P.J. Grobet, J.A. Martens, P.A. Jacobs, Dealuminated H-Y zeolites: Relation between physicochemical properties and catalytic activity in heptane and decane isomerization, Journal of Physical Chemistry, 100 (1996) 12440-12447.

[68] R.B. Borade, A. Adnot, S. Kaliaguine, ACID SITES IN DEHYDROXYLATED Y ZEOLITES - AN X-RAY PHOTOELECTRON AND INFRARED SPECTROSCOPIC STUDY USING PYRIDINE AS A

PROBE MOLECULE, Journal of the Chemical Society-Faraday Transactions, 86 (1990) 3949-3956.
[69] Y.D. Xia, R. Mokaya, Ordered mesoporous MCM-41 silicon oxynitride solid base materials with high nitrogen content: synthesis, characterisation and catalytic evaluation, Journal of Materials Chemistry, 14 (2004) 2507-2515.
[70] M. Ogura, S. Fukuzawa, S. Fukunaga, H. Yamazaki, J.N. Kondo, M. Morimoto, R. Guillet-Nicolas, M. Thommes, Identification of the Basic Sites on Nitrogen-Substituted Microporous and Mesoporous Silicate Frameworks Using CO_2 as a Probe Molecule, Langmuir, 34 (2018) 1376-1385.
[71] K. Sugino, N. Oya, N. Yoshie, M. Ogura, A Simple Modification Creates a Great Difference: New Solid-Base Catalyst Using Methylated N-Substituted SBA-15, Journal of the American Chemical Society, 133 (2011) 20030-20032.
[72] K. Yamazaki, T. Moteki, M. Ogura, Carbonate synthesis from carbon dioxide and cyclic ethers over methylated nitrogen-substituted mesoporous silica, Molecular Catalysis, 454 (2018) 38-43.
[73] K. Yamazaki, T. Moteki, M. Ogura, Reaction Pathways in the Chemical Transformation of CO_2 with beta,gamma-Unsaturated Alcohols into Cyclic Carbonates Catalyzed by Methylated Nitrogen-substituted SBA-15, Journal of the Japan Petroleum Institute, 63 (2020) 149-157.
[74] K.S. Lakhi, D.H. Park, K. Al-Bahily, W. Cha, B. Viswanathan, J.H. Choy, A. Vinu, Mesoporous carbon nitrides: synthesis, functionalization, and applications, Chemical Society Reviews, 46 (2017) 72-101.
[75] A. Vinu, Two-dimensional hexagonally-ordered mesoporous carbon nitrides with tunable pore diameter, surface area and nitrogen content, Advanced Functional Materials, 18 (2008) 816-827.
[76] Y. Wang, Q. Jiang, J.K. Shang, J. Xu, Y.X. Li, Advances in the Synthesis of Mesoporous Carbon Nitride Materials, Acta Physico-Chimica Sinica, 32 (2016) 1913-1928.
[77] G.P. Mane, D.S. Dhawale, C. Anand, K. Ariga, Q. Ji, M.A. Wahab, T. Mori, A. Vinu, Selective sensing performance of mesoporous carbon nitride with a highly ordered porous structure prepared from 3-amino-1,2,4-triazine, Journal of Materials Chemistry A, 1 (2013) 2913-2920.
[78] Y. Wang, X.C. Wang, M. Antonietti, Y.J. Zhang, Facile One-Pot Synthesis of Nanoporous Carbon Nitride Solids by Using Soft Templates, ChemSusChem, 3 (2010) 435-439.
[79] Y. Wang, J.S. Zhang, X.C. Wang, M. Antonietti, H.R. Li, Boron- and Fluorine-Containing Mesoporous Carbon Nitride Polymers: Metal-Free Catalysts for Cyclohexane Oxidation, Angewandte Chemie-International Edition, 49 (2010) 3356-3359.
[80] A. Vinu, K. Ariga, T. Mori, T. Nakanishi, S. Hishita, D. Golberg, Y. Bando, Preparation and characterization of well-ordered hexagonal mesoporous carbon nitride, Advanced Materials, 17 (2005) 1648-1652.
[81] L. Zhang, H. Wang, Z. Qin, J. Wang, W. Fan, Synthesis of two-dimensional mesoporous carbon nitride under different carbonization temperatures and investigation of its catalytic properties in Knoevenagel condensations, Rsc Advances, 5 (2015) 22838-22846.

[82] Y. Qiu, L. Gao, Chemical synthesis of turbostratic carbon nitride, containing C-N crystallites, at atmospheric pressure, Chemical Communications, (2003) 2378-2379.
[83] S.N. Talapaneni, S. Anandan, G.P. Mane, C. Anand, D.S. Dhawale, S. Varghese, A. Mano, T. Mori, A. Vinu, Facile synthesis and basic catalytic application of 3D mesoporous carbon nitride with a controllable bimodal distribution, Journal of Materials Chemistry, 22 (2012) 9831-9840.
[84] M.S. Dresselhaus, F. Villalpando-Paez, G.G. Samsonidze, S.G. Chou, G. Dresselhaus, J. Jiang, R. Saito, A.G. Souza, A. Jorio, M. Endo, Y.A. Kim, Raman scattering from one-dimensional carbon systems, Physica E-Low-Dimensional Systems & Nanostructures, 37 (2007) 81-87.
[85] L.N. Zhang, H. Wang, W.Z. Shen, Z.F. Qin, J.G. Wang, W.B. Fan, Controlled synthesis of graphitic carbon nitride and its catalytic properties in Knoevenagel condensations, Journal of Catalysis, 344 (2016) 293-302.
[86] Y.W. Zhang, J.H. Liu, G. Wu, W. Chen, Porous graphitic carbon nitride synthesized via direct polymerization of urea for efficient sunlight-driven photocatalytic hydrogen production, Nanoscale, 4 (2012) 5300-5303.
[87] G.G. Zhang, J.S. Zhang, M.W. Zhang, X.C. Wang, Polycondensation of thiourea into carbon nitride semiconductors as visible light photocatalysts, Journal of Materials Chemistry, 22 (2012) 8083-8091.
[88] J.H. Yang, X.T. Wu, X.F. Li, Y. Liu, M. Gao, X.Y. Liu, L.N. Kong, S.Y. Yang, Synthesis and characterization of nitrogen-rich carbon nitride nanobelts by pyrolysis of melamine, Applied Physics a-Materials Science & Processing, 105 (2011) 161-166.
[89] Q.X. Guo, Y. Xie, X.J. Wang, S.C. Lv, T. Hou, X.M. Liu, Characterization of well-crystallized graphitic carbon nitride nanocrystallites via a benzene-thermal route at low temperatures, Chemical Physics Letters, 380 (2003) 84-87.
[90] N.D. Shcherban, P. Maki-Arvela, A. Aho, S.A. Sergiienko, P.S. Yaremov, K. Eranen, D.Y. Murzin, Melamine-derived graphitic carbon nitride as a new effective metal-free catalyst for Knoevenagel condensation of benzaldehyde with ethylcyanoacetate, Catalysis Science & Technology, 8 (2018) 2928-2937.
[91] T. Yokoi, Y. Kubota, T. Tatsumi, Amino-functionalized mesoporous silica as base catalyst and adsorbent, Applied Catalysis a-General, 421 (2012) 14-37.
[92] E. Angeletti, C. Canepa, G. Martinetti, P. Venturello, SILICA-GEL FUNCTIONALIZED WITH AMINO-GROUPS AS A NEW CATALYST FOR KNOEVENAGEL CONDENSATION UNDER HETEROGENEOUS CATALYSIS CONDITIONS, Tetrahedron Letters, 29 (1988) 2261-2264.
[93] E. Angeletti, C. Canepa, G. Martinetti, P. Venturello, AMINO-GROUPS IMMOBILIZED ON SILICA-GEL - AN EFFICIENT AND REUSABLE HETEROGENEOUS CATALYST FOR THE KNOEVENAGEL CONDENSATION, Journal of the Chemical Society-Perkin Transactions 1, (1989) 105-107.
[94] T. Yokoi, H. Yoshitake, T. Tatsumi, Synthesis of amino-functionalized MCM-41 via direct

co-condensation and post-synthesis grafting methods using mono-, di- and tri-amino-organoalkoxysilanes, Journal of Materials Chemistry, 14 (2004) 951-957.

[95] Y.W. Xie, K.K. Sharma, A. Anan, G. Wang, A.V. Biradar, T. Asefa, Efficient solid-base catalysts for aldol reaction by optimizing the density and type of organoamine groups on nanoporous silica, Journal of Catalysis, 265 (2009) 131-140.

[96] D.J. Macquarrie, R. Maggi, A. Mazzacani, G. Sartori, R. Sartorio, Understanding the influence of the immobilization procedure on the catalytic activity of aminopropylsilicas in C-C forming reactions, Applied Catalysis a-General, 246 (2003) 183-188.

[97] A. Pineda, A.M. Balu, J.M. Campelo, A.A. Romero, R. Luque, Activity of amino-functionalised mesoporous solid bases in microwave-assisted condensation reactions, Catalysis Communications, 33 (2013) 1-6.

[98] M. Geszke-Moritz, M. Moritz, APTES-modified mesoporous silicas as the carriers for poorly water-soluble drug. Modeling of diflunisal adsorption and release, Applied Surface Science, 368 (2016) 348-359.

[99] D. Majda, B.D. Napruszewska, M. Zimowska, W. Makowski, Porosity of SBA-15 after functionalization of the surface with aminosilanes, Microporous and Mesoporous Materials, 234 (2016) 98-106.

[100] E. Perozo-Rondon, R.A. Martin-Aranda, B. Casal, C.J. Duran-Valle, W.N. Lau, X.F. Zhang, K.L. Yeung, Sonocatalysis in solvent free conditions: An efficient eco-friendly methodology to prepare chalcones using a new type of amino grafted zeolites, Catalysis Today, 114 (2006) 183-187.

[101] O.G. Nik, B. Nohair, S. Kaliaguine, Aminosilanes grafting on FAU/EMT zeolite: Effect on CO_2 adsorptive properties, Microporous and Mesoporous Materials, 143 (2011) 221-229.

[102] C.E. Fowler, S.L. Burkett, S. Mann, Synthesis and characterization of ordered organo-silica-surfactant mesophases with functionalized MCM-41-type architecture, Chemical Communications, (1997) 1769-1770.

[103] C. Venkatesan, A.P. Singh, Selective mono-methylation of phenylacetonitrile to 2-phenyl propionitrile over 3-aminopropylsilyl functionalized MCM-41, Catalysis Letters, 80 (2002) 7-10.

[104] S. Huh, J.W. Wiench, J.C. Yoo, M. Pruski, V.S.Y. Lin, Organic functionalization and morphology control of mesoporous silicas via a co-condensation synthesis method, Chemistry of Materials, 15 (2003) 4247-4256.

[105] T. Yokoi, H. Yoshitake, T. Yamada, Y. Kubota, T. Tatsumi, Amino-functionalized mesoporous silica synthesized by an anionic surfactant templating route, Journal of Materials Chemistry, 16 (2006) 1125-1135.

[106] X.G. Wang, K.S.K. Lin, J.C.C. Chan, S.F. Cheng, Direct synthesis and catalytic applications of ordered large pore aminopropyl-functionalized SBA-15 mesoporous materials, Journal of Physical Chemistry B, 109 (2005) 1763-1769.

[107] X.G. Wang, Y.H. Tseng, J.C.C. Chan, S.F. Cheng, Direct synthesis of highly ordered large-pore functionalized inesoporous SBA-15 silica with methylaminopropyl groups and its catalytic reactivity in flavanone synthesis, Microporous and Mesoporous Materials, 85 (2005) 241-251.

[108] X.G. Wang, J.C.C. Chan, Y.H. Tseng, S.F. Cheng, Synthesis, characterization and catalytic activity of ordered SBA-15 materials containing high loading of diamine functional groups, Microporous and Mesoporous Materials, 95 (2006) 57-65.

[109] Sujandi, E.A. Prasetyanto, S.E. Park, Synthesis of short-channeled amino-functionalized SBA-15 and its beneficial applications in base-catalyzed reactions, Applied Catalysis a-General, 350 (2008) 244-251.

[110] S.L. Hruby, B.H. Shanks, Acid-base cooperativity in condensation reactions with functionalized mesoporous silica catalysts, Journal of Catalysis, 263 (2009) 181-188.

[111] A.B. Bourlinos, T. Karakostas, D. Petridis, "Side chain" modification of MCM-41 silica through the exchange of the surfactant template with charged functionalized organosiloxanes: An efficient route to valuable reconstructed MCM-41 derivatives, Journal of Physical Chemistry B, 107 (2003) 920-925.

[112] J.M. Celedonio, J.H. Park, Y.S. Ko, FT-IR study on CO_2 adsorbed species of CO_2 sorbents, Research on Chemical Intermediates, 42 (2016) 141-154.

[113] A.S.M. Chong, X.S. Zhao, Functionalization of SBA-15 with APTES and characterization of functionalized materials, Journal of Physical Chemistry B, 107 (2003) 12650-12657.

[114] N. Hiyoshi, K. Yogo, T. Yashima, Adsorption characteristics of carbon dioxide on organically functionalized SBA-15, Microporous and Mesoporous Materials, 84 (2005) 357-365.

[115] K.M. Parida, D. Rath, Amine functionalized MCM-41: An active and reusable catalyst for Knoevenagel condensation reaction, Journal of Molecular Catalysis a-Chemical, 310 (2009) 93-100.

[116] V. Zelenak, D. Halamova, L. Gaberova, E. Bloch, P. Llewellyn, Amine-modified SBA-12 mesoporous silica for carbon dioxide capture: Effect of amine basicity on sorption properties, Microporous and Mesoporous Materials, 116 (2008) 358-364.

[117] J.Y. Ying, C.P. Mehnert, M.S. Wong, Synthesis and applications of supramolecular-templated mesoporous materials, Angewandte Chemie-International Edition, 38 (1999) 56-77.

[118] M.E. Davis, Ordered porous materials for emerging applications, Nature, 417 (2002) 813-821.

[119] D.T. On, D. Desplantier-Giscard, C. Danumah, S. Kaliaguine, Perspectives in catalytic applications of mesostructured materials, Applied Catalysis a-General, 253 (2003) 545-602.

[120] A.P. Wight, M.E. Davis, Design and preparation of organic-inorganic hybrid catalysts, Chemical Reviews, 102 (2002) 3589-3613.

[121] A. Cherevotan, J. Raj, S.C. Peter, An overview of porous silica immobilized amines for direct air CO_2 capture, Journal of Materials Chemistry A, 9 (2021) 27271-27303.

[122] S. Choi, J.H. Drese, C.W. Jones, Adsorbent Materials for Carbon Dioxide Capture from Large Anthropogenic Point Sources, ChemSusChem, 2 (2009) 796-854.

[123] N. Hiyoshi, K. Yogo, T. Yashima, Adsorption of carbon dioxide on amine modified SBA-15 in the presence of water vapor, Chemistry Letters, 33 (2004) 510-511.

Chapter 2. Nitrogen sites in nitrided silica

2.1 Introduction

Zeolites are microporous crystalline materials that have been widely used in industries such as sorbents and acid catalysts.[1] Recently, a nitrided zeolite has been reported as a novel base catalyst.[2-5] This material is synthesized by reacting with ammonia to substitute the framework oxygen by nitrogen under high temperature condition, forming primary (Si–OH + NH_3 → Si–NH_2 + H_2O) and/or secondary (Si–O–Si + NH_3 → Si–NH–Si + H_2O) amine species.[2] The basicity of this material arises from the presence of a lone pair on the framework nitrogen atom, and it is potentially affected by the type of mother framework structure and crystallographic nitrogen site (N-site) location.[2] Although the number of N-site on a nitrided zeolite is generally smaller than that on a nitrided mesoporous silica,[6, 7] N-sites on zeolite showed higher base-catalytic activity per active site than those on mesoporous silica maybe because of their crystallinity.[8] When the nitridation temperature is in a proper range, the substitution proceeds without collapsing the original porous structure of zeolite.[2, 4, 9] Therefore, the molecular sieve effect would remain on the material even after the nitridation. This feature would, however, prevent its application from base catalysis to form large products via a C–C bond formation reaction. If a larger molecule compared to the micropore window is involved in the reaction as a reactant or a product, the size constraints on accessibility or diffusibility would restrict the reaction.

Increasing the external surface area of zeolites would be an approach to overcome the drawback, which allows catalytic sites to be exposed on the surface and relatively increases the number of accessible sites.[10] Delamination of lamellar zeolite precursors with maintaining the structure of mother layers has been known as an effective approach.[11] For example, delaminated MCM-22(P), called ITQ-2, was successfully synthesized via swelling the layers by template intercalation and dispersing them by ultrasonic treatment.[12] ITQ-2 is made of a MCM-22(P) sheet of 2.5 nm in thickness, which possesses open 12-membered ring hemicavities on the external surface.[12] Min et al. carried out the successful nitridation of ITQ-2 with maintaining the original crystalline structure.[13] They also revealed that, when it was used in the reaction involving bulky molecules, the high accessibility of surface active sites improved both the base catalytic property and the catalyst life compared to the nitrided MCM-22 zeolite.[13] The report clearly shows an effectiveness of the combination of base catalysis for large molecule and high accessibility of high surface area zeolite.

In this chapter, I further investigated the effect of delamination on the catalytic behavior. It was proposed that the key of delamination is not to increase the external surface area but to increase a unique catalytic site on the surface. Nitrided MCM-22(P)-derived materials were synthesized with different degrees of delamination treatment (denoted as NMCM-22-Del) by controlling the treatment

temperature and time. The chemical and the textural properties of delaminated products before and after nitridation were characterized by various techniques (XRD, nitrogen adsorption, elemental analysis, TEM, and FT-IR). The base catalytic property of the prepared products was evaluated by a typical base-catalyzed reaction of Knoevenagel condensation between benzaldehyde and ethyl cyanoacetate. A critical parameter affecting the catalytic property would be investigated by comparing the initial product formation rates and the textural properties of the catalysts.

2.2 Experimental

2.2.1 Synthesis of catalysts

MCM-22(P) product was prepared by hydrothermal synthesis.[14] Typically, sodium aluminate (0.536 g, Al/NaOH = 0.80, Wako) and sodium hydroxide (0.375g, 97.0%, Kanto Chemical) were dissolved in distilled water (62.88 g), and then hexamethyleneimine (4.056 g, 98%, Aldrich) and fumed silica (4.92 g, Aldrich) were added consecutively. The chemical composition of the final mixture was 2.6 Na_2O : Al_2O_3 : 30 SiO_2: 15 SDA : 1367 H_2O. The mixture was stirred vigorously for 2 h at room temperature. The crystallization of MCM-22(P) was performed at 423 K for 7 days under autogenous pressure under dynamic condition tumbled at 60 rpm using a 23 mL PTFE-lined stainless-steel autoclave (Parr, model #4649). The obtained product was filtered, washed with distilled water, and dried at 373 K for 24 h in an oven.

Delaminated products (MCM-22-Del) were prepared by swelling and dispersing the lamellar precursor MCM-22(P).[12] Practically, the dried MCM-22(P) (0.54 g) was dispersed in distilled water (9.62 g), and then hexadecyltrimethylammonium bromide (3.05 g, 99%, Wako) and an aqueous solution of tetrapropylammonium hydroxide (3.3 g, 40 wt%, TCI) were added. The resultant mixture was heated at different temperature from 313 to 373 K (i.e., 40 to 100 °C) and vigorously stirred for 16 or 46 h to facilitate the swelling of the precursor by intercalation of the large cation (hexadecyltrimethylammonium cation). The suspension was sonicated in an ultrasound bath (40 kHz) for 1 h to disperse the individual layers. Then, the pH was adjusted to 2.0 by adding 2 M HCl solution dropwisely to flocculate the delaminated products, which was recovered by centrifugation (6000 rpm, 15 min) and washed with distilled water. The obtained products were calcined for 12 h at 813 K in air. As a control product, a 3D microporous MCM-22 zeolite was obtained by calcination of the dried MCM-22(P) products in air for 12 h at 813 K.[14]

Nitrogen-substituted catalysts were prepared by nitridation of the products. All the products were placed in a quartz tube and heated at 973 K for 7 or 10 h with the ramping rate of 5 $K \cdot min^{-1}$ under ammonia gas flow of 0.5 $L \cdot min^{-1}$ (99.999%, TAIYO NIPPON SANSO). Products were cooled down to room temperature under nitrogen atmosphere.

Nitrided SBA-15 (NSBA-15) was prepared for comparison.

SBA-15 was prepared by hydrothermal treatment.[15] Typically, triblock copolymer poly(ethylene glycol)-block-poly(propylene glycol)-block-poly(ethylene glycol), Pluronic P-123 (4.0 g, PEG 30 wt%, average M_n of 5800, Aldrich), was dissolved in 2 M aqueous hydrochloric acid solution (118.6 g, for Volumetric Analysis, FUJIFILM Wako Pure Chemical) and distilled water (29.2 g) under stirring at 313 K for 3 h. TEOS (8.6 g, 95.0%, FUJIFILM Wako Pure Chemical) was then dripped to the solution, and hydrolyzed at 313 K for 24 h under stirring. The chemical composition of the final mixture was SiO_2 : 0.017 P123 : 6HCl : 190 H_2O. The resultant solution was placed in an electric oven for hydrothermal treatment at 373 K for 24 h. The obtained sample was filtered and washed with distilled water. The sample was calcined at 823 K for 6 h to remove the template surfactants.

Nitrogen-substituted catalysts were prepared by nitridation of the products. 0.1 g of SBA-15 was placed in a quartz tube and heated at 973–1173 K for 2 or 10 h with the ramping rate of 5.0 $K \cdot min^{-1}$ under ammonia gas flow of 1.0 $L \cdot min^{-1}$ (99.999%, TAIYO NIPPON SANSO). Products were cooled down to room temperature under nitrogen atmosphere.

2.2.2 Product characterization

Powder XRD patterns of the products were collected by a RINT2100 diffractometer (Rigaku) using Cu Kα radiation (λ = 0.1541 nm). The data were recorded in the 2θ range of 2–40° with an angular step size of 0.02°. Nitrogen sorption measurement was conducted by a Quadrasorb evo (Quantachrome) at 77 K to determine total surface area, micropore volume, micropore surface area, and external surface area of the products. Prior to the measurement, the products were degassed in vacuum at 575 K for 3 h. The total surface area was calculated by the BET isothermal equation. The micropore volume, the micropore surface area, and the external surface area were evaluated by the *t*-plot method. The quantitative analysis of nitrogen content was carried out by a vario MICRO cube elemental analyzer (Elementer). The FT-IR spectra of the products were collected by a 4100 FT-IR spectrometer (JASCO). The measurements were carried out with a self-supporting product wafer put in an *in-situ* quartz cell. The product was pretreated at 673 K in vacuum for 1 h, and the spectra were recorded at room temperature under vacuum condition with a resolution of 4.0 cm^{-1}. Transmission electron microscopy measurement was performed to obtain bright field STEM images using a JEM-ARM200F (JEOL, 200 kV).

2.2.3 Catalytic test

Knoevenagel condensation was performed as a model base-catalyzed reaction. A mixture of benzaldehyde (10 mmol, 98.0%, Wako), ethyl cyanoacetate (10 mmol, 98%, Wako), and toluene as a solvent (40 mL, 99.5%, Wako) were introduced into the round-bottom flask. The flask was heated in a thermostatic oil bath and the mixture was stirred by a magnetic stirrer. After the temperature was reached to 353 K, catalyst (50 mg) was added into the mixture. Small portion of liquid products

(about 0.1 mL) were collected as needed from the reaction mixture with a syringe. The obtained products were analyzed with a gas chromatograph GC-14B (Shimadzu) equipped with an FID detector and a ZB-1 capillary column.

For the NSBA-15 catalyst, the experiment was conducted with a different procedure. A mixture of benzaldehyde (1 mmol, 98.0%, FUJIFILM Wako Pure Chemical), malononitrile (1 mmol, 98%, FUJIFILM Wako Pure Chemical) or ethyl cyanoacetate (1 mmol, 98%, FUJIFILM Wako Pure Chemical), and toluene as a solvent (10 mmol, 99.5%, FUJIFILM Wako Pure Chemical) were introduced into the test tube. The tube was heated in a thermostatic oil bath and the mixture was stirred by a magnetic stirrer. After the temperature was reached to 333 K, catalyst (10 mg) was added into the mixture. The mixture was heated for 3 h. The obtained products were analyzed with a gas chromatograph GC-14B (Shimadzu) equipped with an FID detector and a ZB-1 capillary column.

2.3 Results and discussion

2.3.1 Catalyst preparation

The powder XRD patterns of the nitrided and its original products are shown in Figure 2-1. The XRD patterns of as-made MCM-22(P) and calcined MCM-22 products (Figure 2-1(a)) were identical to those shown in the previous report,[14] so that successful synthesis of zeolitic layered precursor was achieved. In the previous report,[12] ITQ-2 did not show the diffraction at 7.2° due to the lack of the long-range order of layer stacking, whereas the diffraction peaks originated from the crystalline layer remain in the higher angle region.[12] On the other hand, in our delaminated products, the small peak at 7.2° was observed besides the higher angle region peaks (Figure 2-1(a)). Although the complete reproduction of ITQ-2 was not achieved, the smaller peak of post-treated product compared to the original MCM-22 suggests the partial delamination. The intensity of the peak at 7.2° decreased with an increase of post treatment temperature (Figure 2-1(a)), indicating the gradual disorder of long-range layer stacking structure. In other words, delamination of the layer may proceed in a small portion along with the increase of the temperature. The XRD pattern of each product was not changed before and after nitridation (Figure 2-1(b)), which indicates that the crystalline framework structure of the product was preserved even after the high-temperature nitridation treatment at 973 K.

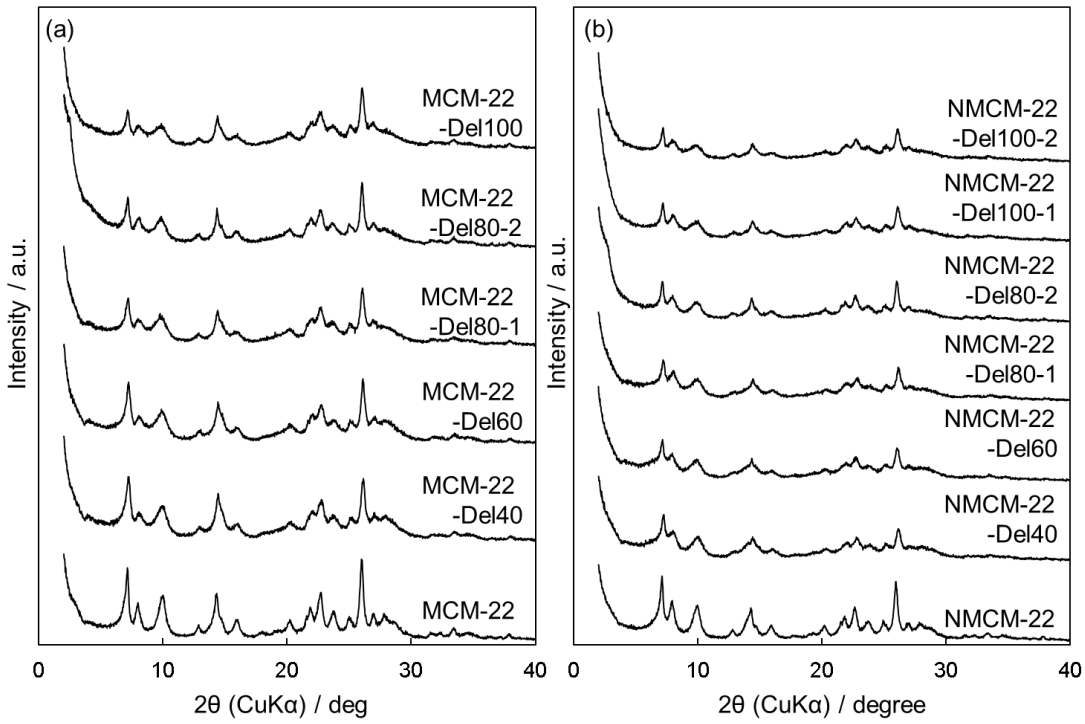

Figure 2-1. X-ray diffraction patterns of (a) MCM-22 and delaminated products before delamination and (b) NMCM-22 and NMCM-22-Del products.

To further confirm the partial delamination, TEM measurement was performed. TEM images of a representative delaminated product (NMCM-22-Del80-2) are shown in Figure 2-2. The morphology of the crystals was a plate-like shape in size of 0.3 μm (Figure 2-2 (a)), which is typical for MCM-22(P)-derived materials.[14] Although a single layer of MCM-22(P) (i.e., ITQ-2) was not observed,[12] the cross-section image clearly showed that layers were cleaved from the edge of the crystal to the planar direction (Figure 2-2 (b)). The high-resolution image showed that each crystal is build-up by stacking of thin layers with the thickness of 2.5 nm (Figure 2-2 (c)), which was the thickness of a MCM-22(P) sheet. This result is consistent with the changes in the XRD patterns discussed above. Therefore, XRD and TEM measurements reveal that the products are successfully delaminated in part and the crystalline structure is maintained after nitridation procedures.

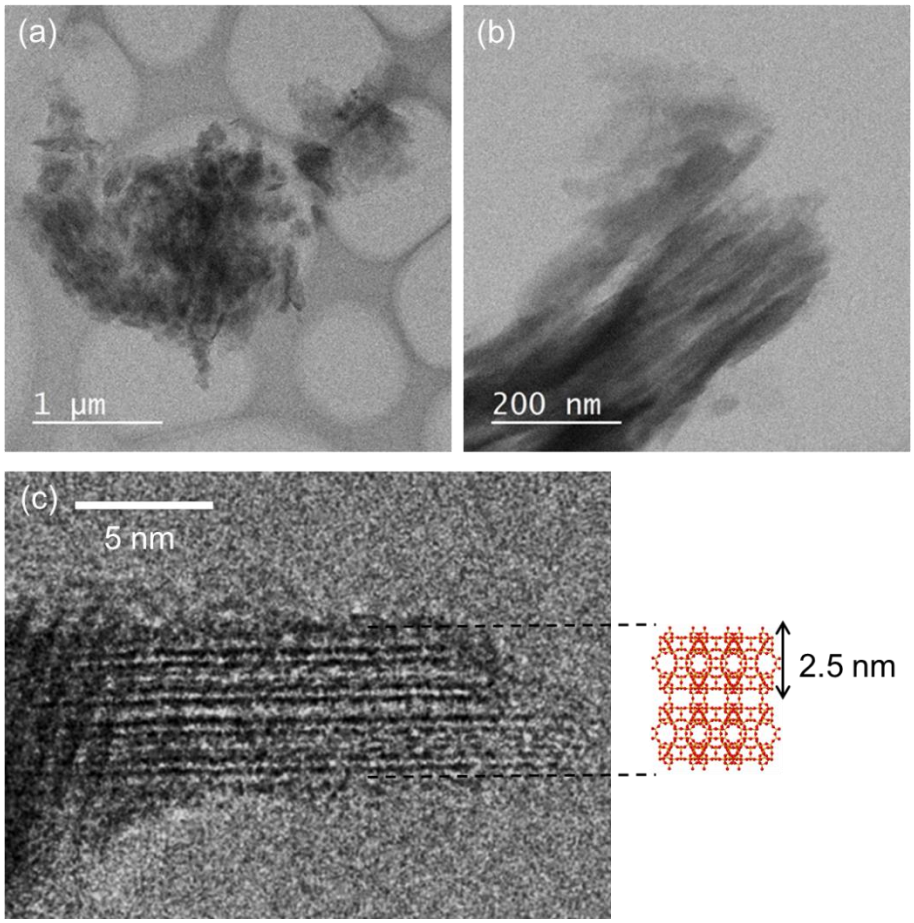

Figure 2-2. TEM images of NMCM-22-Del80-2 product, as a representative of delaminated product. (a) low magnification image, (b) cross-section image, and (c) high-resolution cross-section image.

The N_2 adsorption isotherms of the mother MCM-22 and the delaminated products are shown in Figure 2-3. Hysteresis due to slit mesopores was observed in the relative pressure range of 0.8–1.0 in all the delaminated products. The textural properties of delaminated products based on N_2 sorption measurement are summarized in Table 2-1. The product before nitridation possessed micropore volume larger than 0.15 $cc \cdot g^{-1}$, suggesting that the zeolitic porous framework structure is maintained during the delamination process. Decrease in the micropore surface area was observed with increase of delamination temperature. This could be explained by the disappearance of large 1.8 × 0.7 × 0.7 nm "inside cavities" changed into the "surface cup structures" by delamination. In some products, the order of external surface area did not correlate with the order of delamination temperature (e.g., MCM-22-Del80-2 has a larger external surface area than MCM-22-Del100). This might be due to different mother MCM-22(P) synthesized in a different batch. These results show that the series of delaminated products are successfully prepared with a different external surface area.

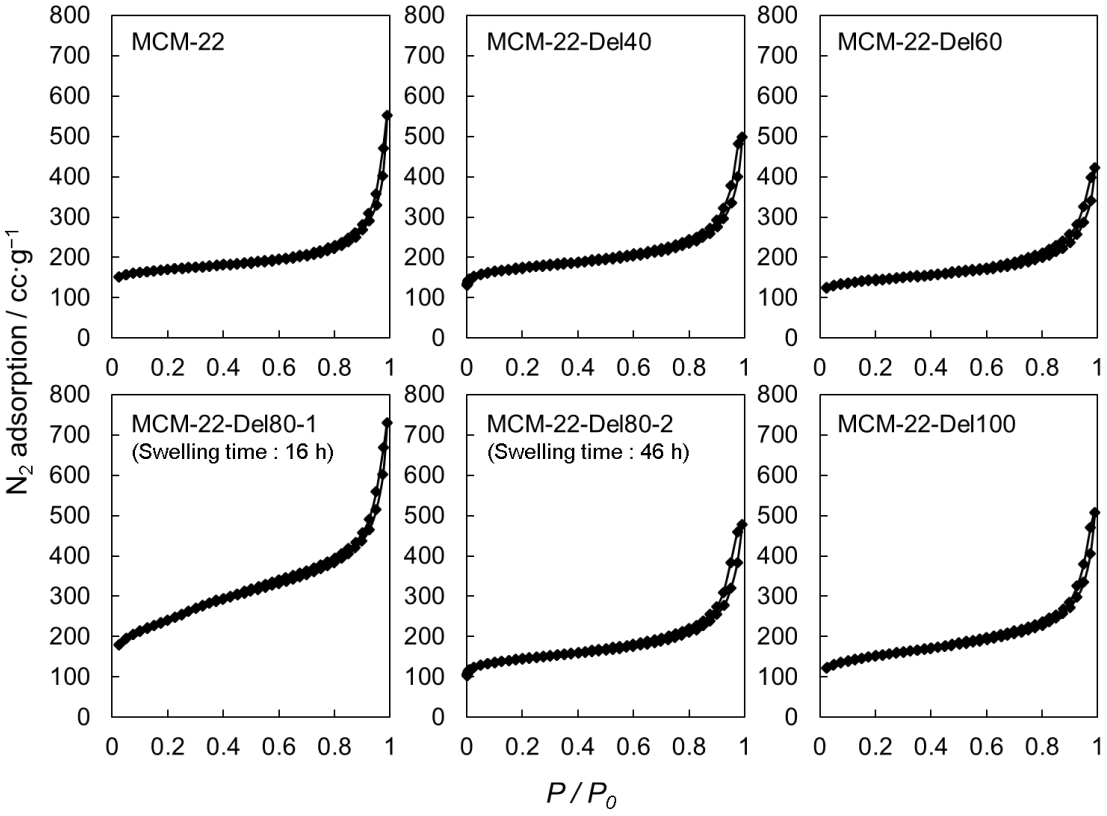

Figure 2-3. N_2 adsorption isotherms of MCM-22 and delaminated samples.

Table 2-1. Textural properties of samples before and after delamination at different conditions.

Product	Delamination temperature / °C	Delamination time / h	S_{ext} / $m^2 \cdot g^{-1}$	S_{micro} / $m^2 \cdot g^{-1}$	V_{micro} / $cc \cdot g^{-1}$
MCM-22	–	–	118	531	0.216
MCM-22-Del40	40	16	147	500	0.206
MCM-22-Del60	60	16	131	402	0.166
MCM-22-Del80-1	80	46	151	384	0.160
MCM-22-Del100	100	16	197	358	0.152
MCM-22-2	–	–	146	547	0.227
MCM-22-Del80-2	80	16	368	481	0.244

The N_2 adsorption isotherms of the nitrided products are shown in Figure 2-4. In all the nitrided samples, hysteresis was observed in the relative pressure range of 0.8–1.0. Therefore, it is considered that the slit mesopores are still present after nitridation. The textural properties of delaminated products based on N_2 sorption measurement are summarized in

Table 2-2. After nidation, a decrease in the surface area of micropores was observed in all products. It suggests that a partial collapse of the micropore structure occurred.

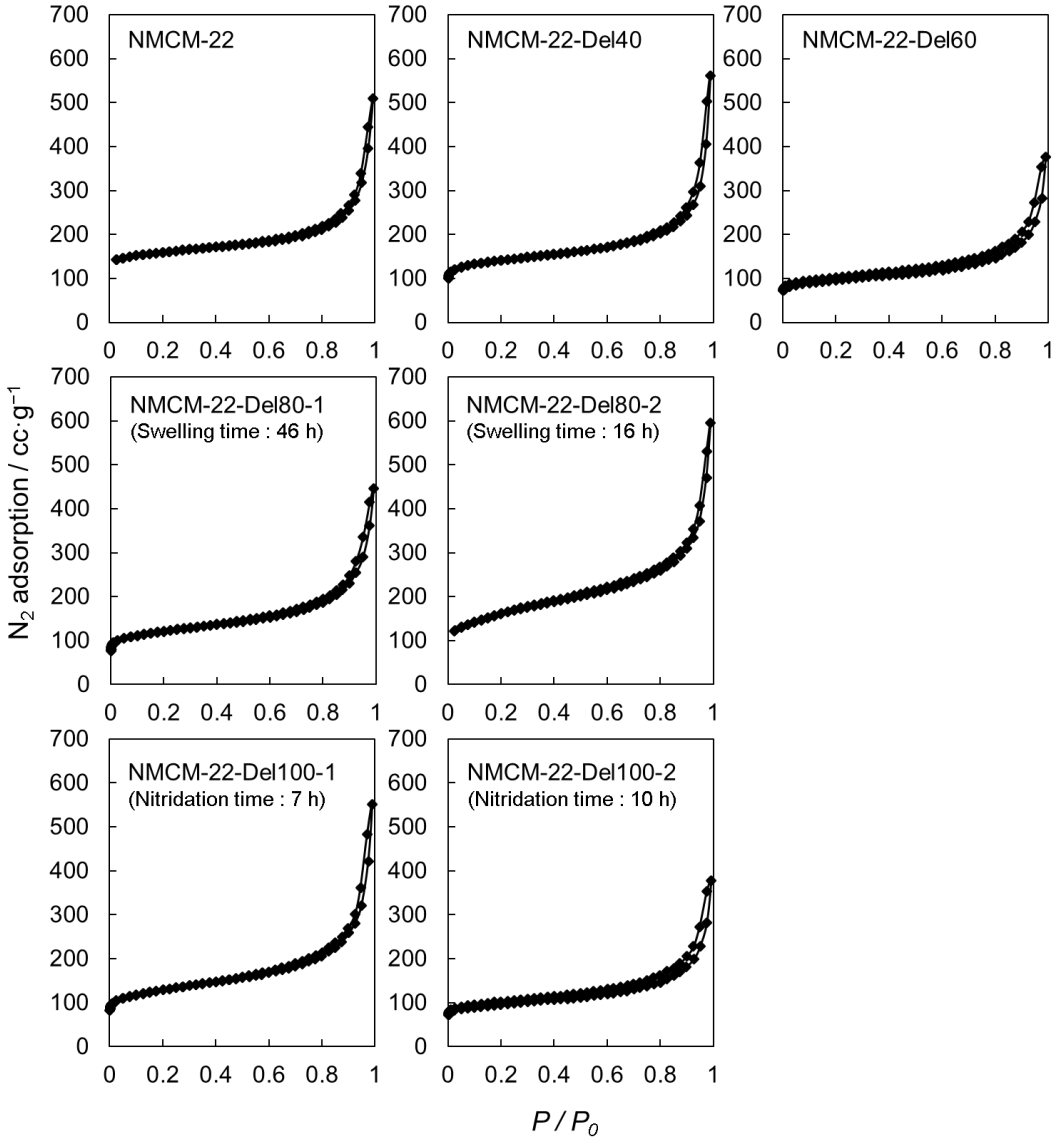

Figure 2-4. N_2 adsorption isotherms of NMCM-22 and nitridated delaminated products.

Table 2-2. Textural properties and nitrogen contents of nitrided products.

Product	Nitridation time / h	S_{ext} / $m^2 \cdot g^{-1}$	S_{micro} / $m^2 \cdot g^{-1}$	V_{micro} / $cc \cdot g^{-1}$	N content[a] / wt%	N_{ext} content[b] / wt%
NMCM-22	10	151	433	0.180	4.90	1.27
NMCM-22-Del40	10	146	377	0.157	5.21	1.45
NMCM-22-Del60	10	113	240	0.101	4.88	1.56
NMCM-22-Del80-1	10	154	282	0.122	6.53	2.30
NMCM-22-Del80-2	10	255	311	0.146	7.17	3.23
NMCM-22-Del100-1	10	187	278	0.122	5.64	2.27
NMCM-22-Del100-2	7	183	244	0.107	4.00	1.72

[a] calculated from elemental analysis. [b] N_{ext} content = N content × S_{ext} / (S_{ext} + S_{micro})

The nitrogen contents of nitrided products measured by elemental analysis are also listed in Table 2-2. The contents were similar to the values reported in the nitrided zeolites in the previous studies (e.g., zeolite Y, ZSM-5, MCM-22, and ITQ-2).[4, 5, 13] There was no clear correlation between the amount of nitrogen and the nitridation conditions (e.g., temperature or time), maybe due to the difference of mother MCM-22(P) materials synthesized in different batches. Compared to the well-studied nitrided mesoporous silica materials,[6-8, 16] the nitrogen contents of N-zeolite used in this study and previous zeolitic nitrided material were relatively small. Because zeolites possess more stable crystalline framework and much less silanol groups on the pore wall, the amount of nitrogen substituted in the zeolite framework is much less than that in mesoporous framework treated under the same nitridation condition. For example, nitrogen content reached up to 36.3 wt% on MCM-41 material by nitridation (600 $mL \cdot min^{-1}$, 1273 K, 10 h),[7] whereas only reached to 15.6 wt% on ZSM-5 zeolite obtained under similar nitridation condition (500 $mL \cdot min^{-1}$, 1373 K, 10 h).[5] The nitridation of pure silica material proceeds mainly in two-stage reactions at different temperatures.[17] At a lower temperature, Si–NH_2 groups are formed from silanol groups (Si–OH + NH_3 → Si–NH_2 + H_2O). On the other hand, siloxane bond starts to react at a higher temperature (Si–O–Si + NH_3 → Si–NH–Si + H_2O, and/or → Si–NH_2 + HO–Si). In this point of view, the delamination treatment increases the accessible silanol groups by exposing the interlayer surfaces. Even though the amount of surface silanol group is not so many (e.g., 4 oxygen atoms form silanol groups out of 144 oxygen atoms per unit cell in MWW-type framework), delaminated zeolites should have more chance to form Si–NH_2 groups compared to the conventional 3D crystalline zeolites, and they would show different catalytic features.

Assuming that the diffusion of ammonia molecule into the micropore is fast enough and the nitridation of the external and internal surfaces proceeds at the same rate,[4] the nitrogen content of

external surface (N_{ext} content) could be calculated from the ratio of the external surface area to the total surface area. The estimated amount of N_{ext} content is listed in Table 2-2. It is clear that about 30–45% of nitrogen atoms are exposed to the external space on the NMCM-22-Del, whereas about 25% of nitrogen atoms are exposed on NMCM-22 (Table 2-2). The presence of different amine species on the nitrided products are confirmed by FT-IR spectroscopy. Figure 2-5 shows FT-IR spectra of the nitrided products in the range from 3000 to 3600 cm^{-1}. The bands at 3415, 3367, and 3258 cm^{-1} could be assigned to Si–NH_2, Si–NH–Si(Al), and Si–NH_2···Al groups, respectively.[17] On a proton-form aluminosilicate zeolite, the previous report proposed the formation of isolated and bridged primary amines (i.e., Si–NH_2 and Si–NH_2···Al, respectively) at a lower temperature through the amination of surface silanol and Brønsted acid site (i.e., Si–OH and Si–OH···Al), respectively.[18] It should be noted that, our products made with sodium cation were also changed into proton-form because of the acidic treatment to flocculate the dispersed products (see Experimental Section). The result indicates that all these types of N-atom were formed on all nitrided products, and the proposed surface N-sites are illustrated in Figure 2-6. Different from conventional 3-D zeolites, a layered zeolite formed from 2-D zeolitic precursor possesses structurally prescribed surface silanol groups (e.g., MWW-type zeolite as shown in Figure 2-6). Therefore, primary amine generally formed on a silanol site is unique and number-limited on the surface. Furthermore, the number of silanol site would have a linear correlation with the surface area. On the other hand, secondary amine could be formed as far as nitridation proceeds. I estimate that, in this sense, degree of delamination can be directly connected to the surface area and eventually to the number of surface silanol sites, which would be equal to the number of primary amine species formed by nitridation.

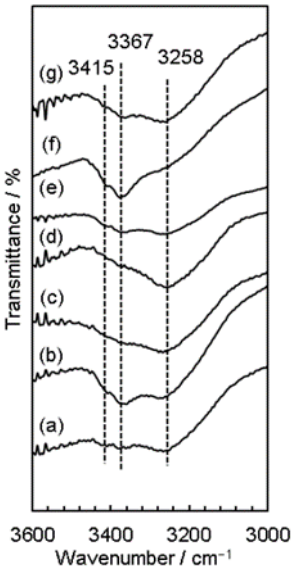

Figure 2-5. FT-IR spectra of nitrided products in the range from 3000 to 3600 cm^{-1}. (a) NMCM-22, (b) NMCM-22-Del40, (c) NMCM-22-Del60, (d) NMCM-22-Del80-1, (e) NMCM-22-Del80-2, (f) NMCM-22-Del100-1, and (g) NMCM-22-Del100-2 products.

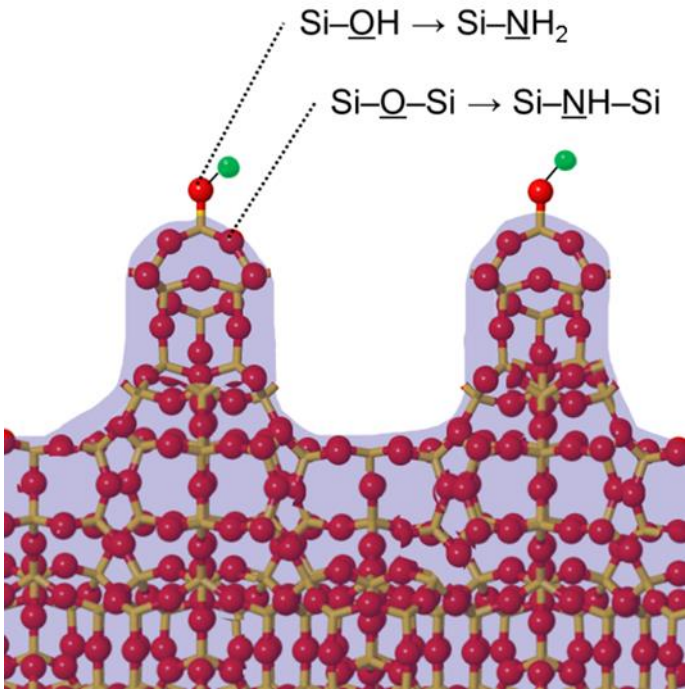

Figure 2-6. Schematic illustration of external surface structure of MWW-type zeolite. Oxygen, silicon, and hydrogen atoms are depicted in red, yellow, and green, respectively. The blue and white area are internal and external area, respectively.

The powder XRD pattern of mother SBA-15 is shown in Figure 2-7. Three peaks were observed at 0.95, 1.59, and 1.82°. The peaks assigned to*100*, *110*, and *200* diffractions of 2D-hexagonal structure. The lattice spacing of *001* plane (d_{100}) was 9.3 nm and the lattice parameter (a_0) was 10.7 nm. In previous reports, the lattice parameter of SBA-15 is 10.22–10.67 nm.[19-22] Therefore, the mother sample was conventional SBA-15.

The powder XRD patterns of NSBA-15 products are also shown in Figure 2-7. Three peaks assigned to *100*, *110*, and *200* diffractions of 2D-hexagonal structure were observed in all products, indicating the preservation of periodic structure after high temperature treatment. The three peaks shifted to a higher angle with increasing nitridation temperature. It suggests that the high temperature treatment caused the shrinkage of the periodic structure.[7, 20, 22-24] Figure 2-8(a) shows the nitrogen adsorption-desorption isotherm of the series of NSBA-15 products. The typical type-IV isotherms were observed in all products, indicating the presence of mesopores. Figure 2-8(b) shows the BJH adsorption pore size distribution of the series of NSBA-15. Table 2-3 summarizes the textural properties of NSBA-15 products based on XRD measurement and nitrogen sorption measurement. a_0 is the average lattice parameter calculated based on d_{100} values. The BET surface area and the micropore volume decreased with the increase of nitridation temperature. Moreover, the mean pore diameter and the wall thickness decreased with increasing nitridation temperature. It suggests that the shrinkage of the structure occurred. This result is consistent with the changes in the previous report.[7, 20, 22-24] The shrinkage was caused by condensation of silanamine groups (Si–NH_2 + Si–NH_2 → Si–NH–Si + NH_3, Si–NH–Si + Si–NH_2 → N–$(Si)_3$ + NH_3) in higher temperature nitridation process.[20, 24, 25]

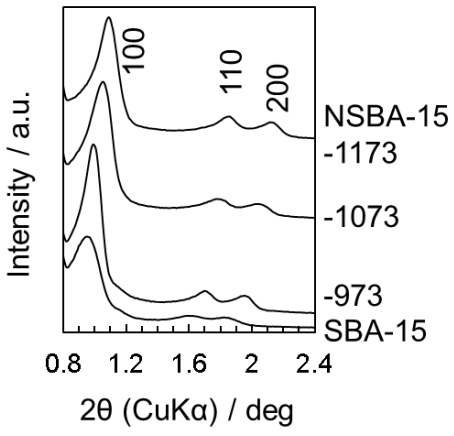

Figure 2-7. XRD patterns of mother SBA-15 and series of nitrided samples (NSBA-15) prepared at different temperature from 973 to 1173 K (ammonia flow rate of 1.0 L min^{-1} for 10 h).

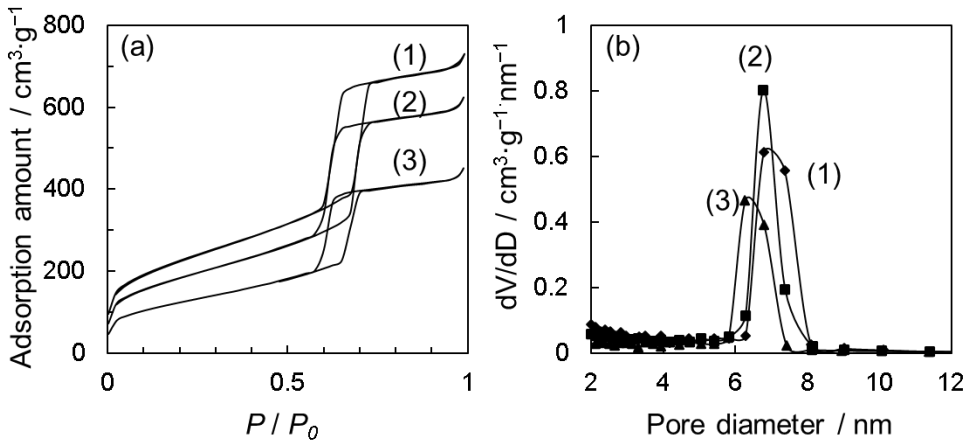

Figure 2-8. (a) N_2 adsorption isotherms and (b) BJH adsorption pore size distribution of (1) NSBA-15-973, (2) NSBA-15-1073, and (3) NSBA-15-1173.

Table 2-3. Structural properties of mother SBA-15 and nitrided SBA-15 (NSBA-15) prepared at different temperature (973–1173 K).

Product	Nitridation temperature / K	Nitridation time / h	d_{100} / nm	a_0 / nm	BET surface area / $m^2 \cdot g^{-1}$ [a]	Total pore volume / $cm^3 \cdot g^{-1}$ [a]	Mean pore diameter / nm [b]	Wall thickness / mm [c]
SBA-15	–	–	9.3	10.7	806	0.89	8.1	2.6
NSBA-15-973	973	10	8.9	10.3	790	1.05	7.1	3.2
NSBA-15-973-2	973	2	–	–	660	0.95	7.4	–
NSBA-15-1073	1073	10	8.4	9.7	640	0.92	6.8	2.9
NSBA-15-1173	1173	10	8.1	9.4	424	0.68	6.6	2.8

[a] Measured by nitrogen sorption measurements.

[b] Calculated by BJH method with adsorption isotherm.

[c] Calculated as a difference of lattice parameter and pore diameter.

The nitrogen contents of nitrided products were measured by elemental analysis. The nitrogen contents of NSBA-15-973, NSBA-15-973-2, NSBA-15-1073, and NSBA-15-1173 were 7.86 wt% (5.61 $mmol \cdot g^{-1}$), 2.90 wt% (2.07 $mmol \cdot g^{-1}$) 13.1 wt% (9.36 $mmol \cdot g^{-1}$), and 18.2 wt% (13.0 $mmol \cdot g^{-1}$), respectively. The nitrogen contents increased with increasing nitridation temperature and time. The nitrogen content of obtained NSBA-15 in this study was comparable to the previous reports applying similar nitridation condition.[20, 26, 27] The maximum amount of oxygen atoms

existing on the pore surface of mother SBA-15 is calculated to be 12.6 mmol·g^{-1}.[26] Therefore, as the nitridation processes from the pore surface, all of the oxygen atoms on the pore surface would be replaced with nitrogen atoms in NSBA-15-1173 case.

In order to identify nitrogen species, XPS measurement was performed. Figure 2-9 shows the XPS spectra of N1s levels for NSBA-15 samples. The peak was observed at around 398 eV and shifted to lower binding energy with increasing nitridation temperature. This would be attributed to the condensation of silanamine and the formation of secondary and tertiary silanamine species.[17, 28] The XPS spectra was deconvoluted to three peaks as blue lines shown in Figure 2. The peak at 399.8 eV is attributed to the primary silanamine (Si-$\underline{N}H_2$). The peak at 398.0 eV is attributed to the secondary silanamine (Si-$\underline{N}$H-Si). The peak at 397.3 eV is attributed to the tertiary silanamine ($\underline{N}$-(Si)$_3$).[4, 17, 20, 27-30] The nitrogen and silanamine contents of nitrided SBA-15 calculated by XPS are listed in Table 2-4. The content of tertiary silanamine species increased with increasing nitridation temperature. In nitridation process, primary silanamine species were formed first (Si–OH + NH_3 → Si–NH_2 + H_2O) at lower temperature around 773 K.[31] At higher temperature, secondary/tertiary silananime species were subsequently formed (Si–O–Si + NH_3 → Si–NH–Si + H_2O, Si–NH–Si + Si–NH_2 → N–(Si)$_3$ + NH_3).[6]

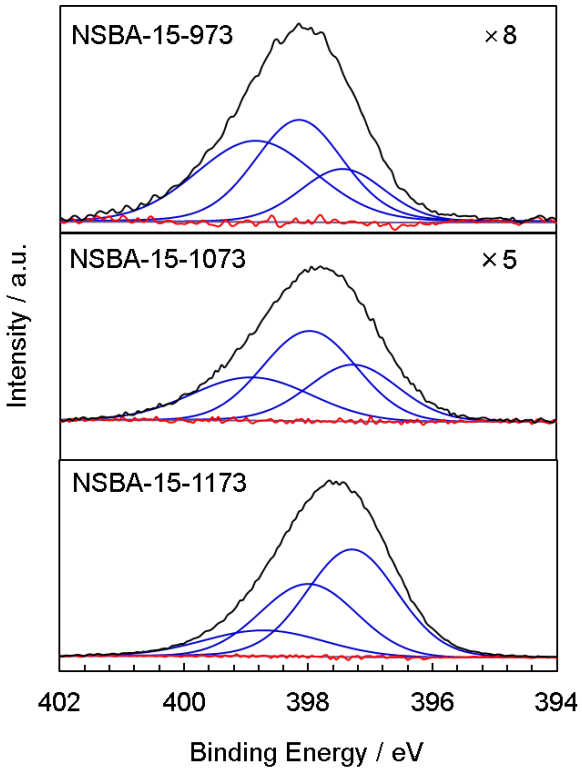

Figure 2-9. XPS spectra of N 1s levels for series of nitrided samples (NSBA-15) prepared at different temperature from 973 to 1173 K (ammonia flow rate of 1.0 L min^{-}1 for 10 h). Black curves

and blue curves are measured data and fitting curves, respectively. The deconvoluted peaks are assigned to primary, secondary, and tertiary silanamine with the binding energy of 398.7, 398.0, and 397.3 eV, respectively. Red curves show difference between measured data and sum of fitting curves.

Table 2-4. Nitrogen and silanamine contents of nitrided SBA-15 (NSBA-15) prepared at different temperature (973–1173 K) measured by CHN elemental analysis and XPS. The values from CHN analysis are the average of 3 measurements.

	CHN	XPS					
Product	N content / wt%	N content / atomic%	Si content / atomic%	O content / atomic%	Silanamine content / wt%*1 (molar percentage / %)		
					$Si\text{-}NH_2$	Si-NH-Si	$N\text{-}(Si)_3$
NSBA-15-973	7.86	5.85	30.6	63.6	3.22 (41.0)	3.15 (40.1)	1.49 (18.9)
NSBA-15-973-2*2	2.90	–	–	–	1.19 (41.0)	1.16 (40.1)	0.55 (18.9)
NSBA-15-1073	13.1	12.3	28.8	58.8	3.56 (27.2)	5.82 (44.4)	3.72 (28.4)
NSBA-15-1173	18.2	26.1	34.2	39.6	2.77 (15.2)	6.24 (34.3)	12.7 (50.5)

*1 Silanamine content = N content (measured by CHN) × silanamine percentage

*2 Calculated assuming equal percentage of silanamine in NSBA-15-973 and NSBA-15-973-2

2.3.2 Catalytic reactions

Knoevenagel condensation of benzaldehyde with ethyl cyanoacetate was performed as a model base-catalyzed reaction. Figure 2-10 shows the changes of product yields along with the reaction time catalyzed by the series of nitrided products as listed in Table 2-2. The yield increased monotonously with increasing reaction time over all the catalysts. At every data point, the selectivity towards the desired product, ethyl α-cyanocinnamate, was over 99%. The initial rates are summarized in Table 2-5, which were calculated from the slope of initial 1 hour based on the linear approximation. The rates were, however, neither proportional to the delamination temperature nor identical to each other, and it was unclear what was the major factor that contributes to the formation rate. Because the size of ethyl α-cyanocinnamate (0.57 nm) is larger than the size of 10-membered ring window open in MCM-22 crystal (0.40 × 0.55 nm), N-sites on the internal pore surface would not be catalytic active sites. Thus, it is simply estimated that the catalyst possessing larger external

nitrogen content shows higher formation rate per gram of catalyst. To identify the major parameter that affects the product formation rate, the relationship between the formation rates and the textual properties was examined.

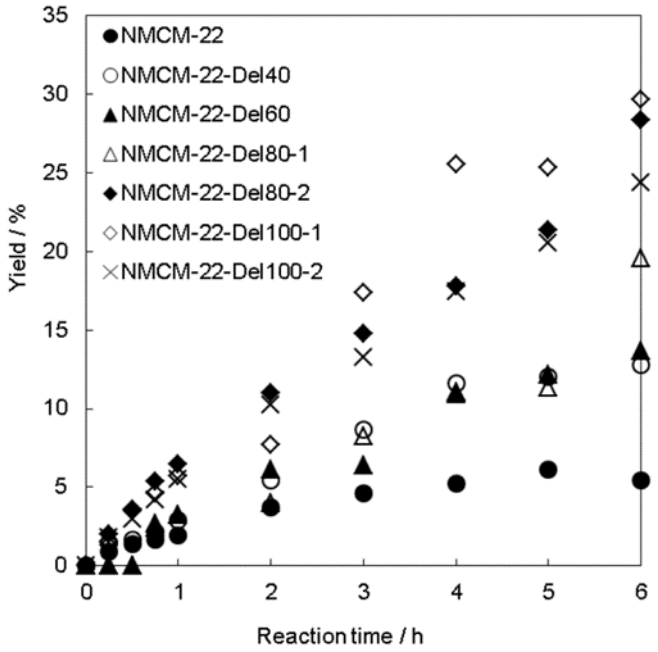

Figure 2-10. Changes in the product yield of Knoevenagel condensation reaction as a function of reaction time over NMCM-22 and NMCM-22-Del catalysts (10 mmol benzaldehyde, 10 mmol ethyl cyanoacetate, 40 mL toluene, 50 mg catalyst, 353K).

Table 2-5. Initial formation rate of the Knoevenagel condensation reaction between benzaldehyde and ethyl cyanoacetate on NMCM-22 and NMCM-22-Del catalysts.

Product	Initial formation rate[a] / $mmol_{product} \cdot h^{-1} \cdot g_{catalyst}^{-1}$
NMCM-22-Del40	0.29
NMCM-22-Del60	0.26
NMCM-22-Del80-1	0.24
NMCM-22-Del80-2	0.27
NMCM-22-Del100-1	0.54
NMCM-22-Del100-2	0.60

[a] calculated by a linear approximation in the initial one hour established in Figure 2-10.

The initial rates (Table 2-5) were plotted as a function of micropore surface area (Figure 2-11(a)), total nitrogen content (Figure 2-11(b)), external surface area (Figure 2-11(c)), and external nitrogen content (Figure 2-11(d)). Clear correlation was not observed with micropore surface area (Figure

2-11(a)) nor with total nitrogen content (Figure 2-11(b)). This clearly indicates that; 1) active sites, where both reactants and the product can access, were not uniformly distributed on the internal and external surfaces, and 2) not all the nitrogen is the active site. As discussed above, this would be explained by the structural size constraints between the framework window and the products/reactants.

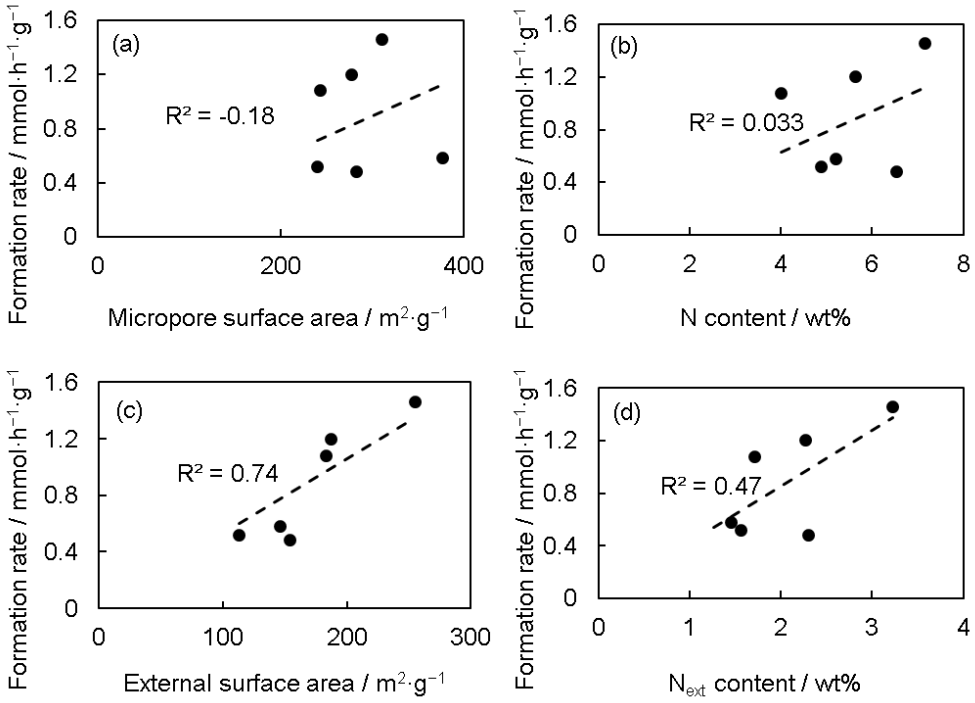

Figure 2-11. Correlation of initial formation rate in Knoevenagel condensation with (a) micropore surface area, (b) nitrogen content, (c) external surface area, and (d) external nitrogen content over NMCM-22-Del catalysts. The dashed lines joining the points are approximation curves. R^2 represented the coefficient of determination calculated by Microsoft Excel.

A proportional relationship between the initial product formation rate and the external surface area was observed with the coefficient of determination (R^2) of 0.74 (Figure 2-11(c)). This suggested that the reaction mainly proceeds on the external surface. It was, however, incomprehensive that the nitrogen content on the external surface showed less liner correlation with the formation rate (R^2 of 0.47 in Figure 2-11(d)). If all the N-sites on the external surface were active sites, the correlation value should be expected to be similar in the both the external surface area and the number of external N-site. Thus, based on these experimental facts, the major active site is assumed to be a number-limited (i.e., structurally unique) nitrogen on the external surface. In the previous study on the nitrided mesoporous silica, Si–$\underline{N}H_2$ group has been reported to be more active than Si–$\underline{N}$H–Si group for Knoevenagel condensation.[32] As shown in Figure 2-6 and described above, silanol

group that sits on the external surface reacts to form Si–NH_2 group at a lower temperature than siloxane group. Even though the primary amine group would also be formed from the reaction via siloxane cleavage (Si–O–Si + NH_3 → Si–NH_2 + HO–Si), this pair site might be subsequently dehydrated to form secondary amine (Si–NH_2 + HO–Si → Si–NH–Si + H_2O).[3] The Si–NH_2 formed from surface silanol is, however, unique because it never turns into Si–NH–Si due to the lack of neighboring silanol groups (Figure 2-6). A bridged primary amine (Si–NH_2···Al) is expected to be less active because the lone pair of nitrogen is interacting with the neighboring aluminum atom. When MCM-22(P) was completely delaminated to form dispersed monolayers, the theoretical maximum of nitrogen content of Si–NH_2 formed from surface silanol groups is about 1.5 wt%. Because the nitrogen contents of all products in this study exceeded this value (Table 2-2), it is straightforward to imagine all the silanol groups are turned into Si–NH_2 at the nitridation temperature of 973 K, and further nitridation on the siloxane bond results to form Si–NH_2, Si–NH–Si, and Si–NH_2···Al groups. This would explain why the external surface area showed higher linear correlation with the initial product formation rate (Figure 2-11(c)) rather than the N_{ext} content (Figure 2-11(d)). Although further detailed analysis is ongoing to determine the shape and to count the number of active sites, here, it can be concluded that Si–NH_2 is the most plausible active site on the NMCM-22 catalyst, which is mainly formed by the nitridation of the surface silanol group.

Figure 2-12 shows the relationship between the yields and the nitrogen content of the catalysts. At every data point, the selectivity towards the desired product, benzalmalononitrile or ethyl α-cyanocinnamate, was over 99%. Therefore, NSBA-15 showed good selectivity for Knoevenagel condensation. The contribution of each amine species in the reaction between benzaldehyde with ethyl cyanoacetate was calculated by the least-squares method according to previous report,[20] and it was 96.3% for primary amines, −7.11% for secondary amines, and 10.8% for tertiary amines. There was a rough correlation between the amount of primary silanamine and the catalytic activity like previous report.[20]

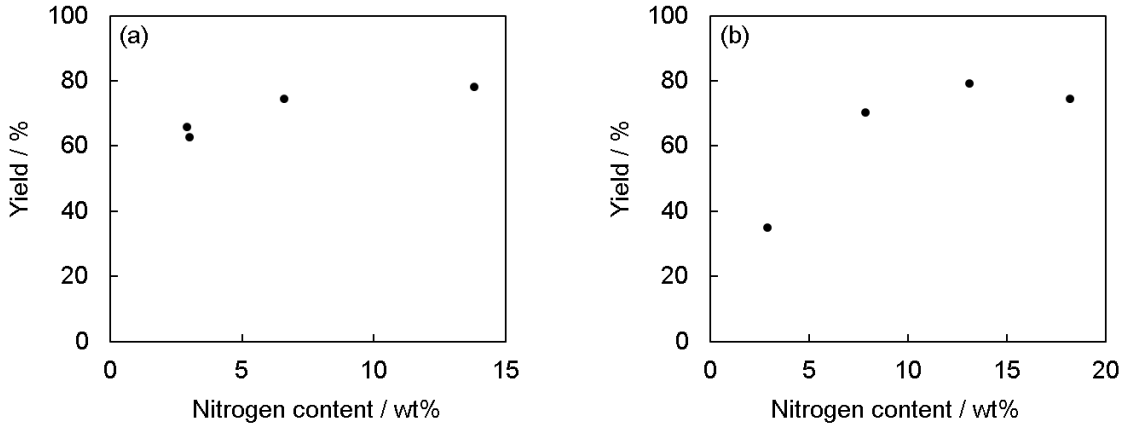

Figure 2-12. The relationship between the yields at three hours after the start of the reaction and the nitrogen content of the catalysts in Knoevenagel condensation between benzaldehyde and (a) malononitrile (pK_a : 11.1) or (b) ethyl cyanoacetate (pK_a : 13.1).

Figure 2-13 shows the changes of product yields along with the reaction time catalyzed by NSBA-15-973-2. At every data point, the selectivity towards the desired product, ethyl α-cyanocinnamate, was over 99%. The initial rate is 1.63 $mmol_{product} \cdot h^{-1} \cdot g_{catalyst}^{-1}$, which was calculated from the slope of initial 1 hour based on the linear approximation.

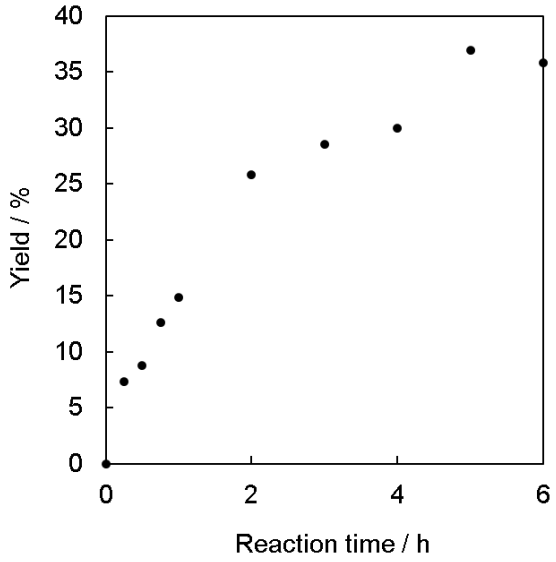

Figure 2-13. Changes in the product yield of Knoevenagel condensation reaction as a function of reaction time over NSBA-15-973-2 catalyst (10 mmol benzaldehyde, 10 mmol ethyl cyanoacetate, 40 mL toluene, 50 mg catalyst, 353K).

2.3.3 Comparison between nitrided zeolite and nitrided mesoporous silica

In both NMCM-22-Del and NSBA-15 catalysts, the amount of primary amines on the accessible micropore external surface was key factor for catalytic activity. The amount of primary amines was listed in Table 2-6. Figure 2-14 shows schematic illustration of MWW-type zeolite unit cell viewed from the c-axis direction. Two oxygen atoms of the silanol group are present on the unit cell surface (1.79×10^{-18} m^2). Assuming that all the external surfaces of MCM-22-Del were layer surfaces, the amount of primary amines was estimated from the external surface area (Table 2-6). The primary amine content of NSBA-15-973-2 was calculated based on the XPS measurement results of NSBA-15-973 (Table 2-4). The initial rates were plotted as a function of the amount of primary amine (Figure 2-15). A proportional relationship between the initial product formation rate and the amount of primary amine was observed. The result of NMCM-22-Del was below the dashed line connecting the zero point and the result of NSBA-15-973-2. This is probably because the actual external surfaces of NMCM-22-Del are not only the layer surfaces, so the amount of primary amines shown in Table 2-6 was higher than actual. Considering the above, the activities of primary amines in NMCM-22-Del and NSBA-15 are considered to be almost similar. Therefore, the catalytic activity of primary amines in nitrided silica was independent of the mother silica materials.

Table 2-6. Amount of primary amine nitrogen and initial formation rate of the Knoevenagel condensation reaction between benzaldehyde and ethyl cyanoacetate on NMCM-22-Del and NSBA-15 catalysts.

Product	Amount of primary amine nitrogen / wt%	Initial formation rate / $mmol_{product} \cdot h^{-1} \cdot g_{catalyst}^{-1}$
NMCM-22-Del40	0.379	0.29
NMCM-22-Del60	0.293	0.26
NMCM-22-Del80-1	0.399	0.24
NMCM-22-Del80-2	0.661	0.27
NMCM-22-Del100-1	0.475	0.54
NMCM-22-Del100-2	0.485	0.60
NSBA-15-973-2	1.18	1.63

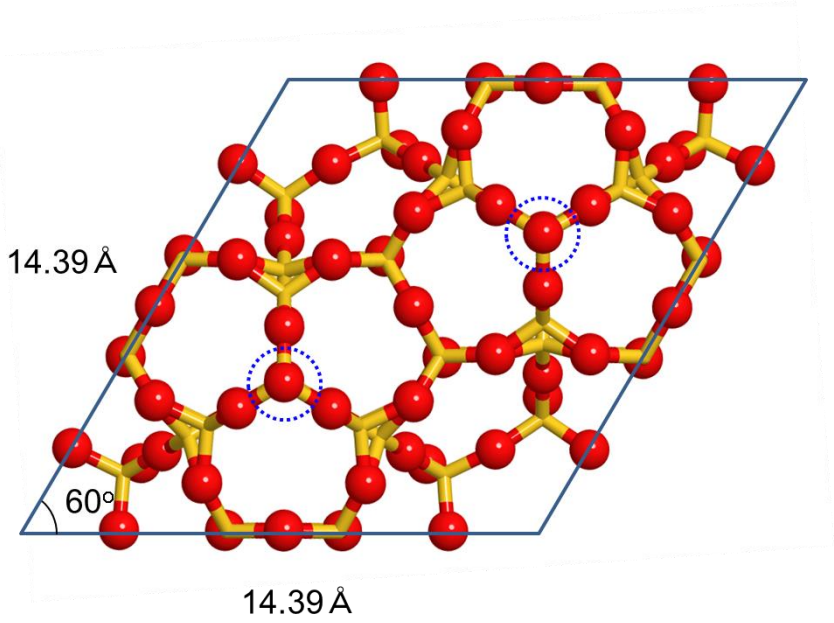

Figure 2-14. Schematic illustration of MWW-type zeolite unit cell viewed from the c-axis direction. Oxygen and silicon atoms are depicted in red and yellow, respectively. The oxygen atoms surrounded by the blue dashed lines represent the oxygen of the surface silanol groups.

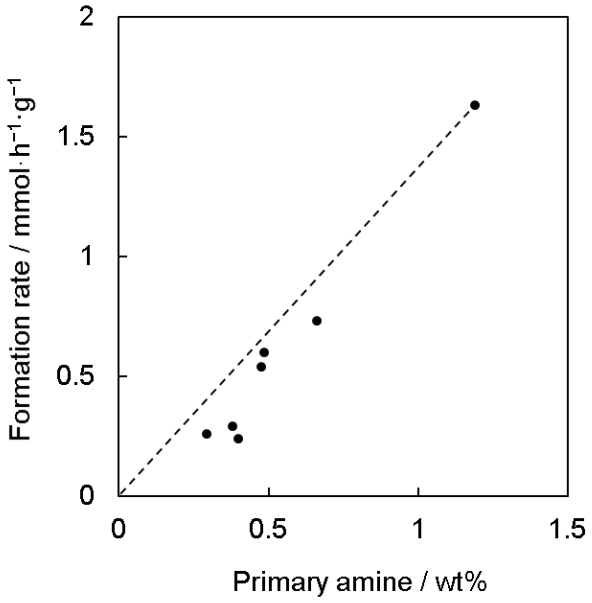

Figure 2-15. Correlation of initial formation rate in Knoevenagel condensation with primary amine content over NMCM-22-Del and NSBA-15 catalysts. The dashed line connects the zero point and the result of NSBA-15-973-2.

2.4 Conclusions

A variety of delamination of MWW zeolites was achieved by controlling the temperature or the time of the swelling step. The microstructure was preserved even after a high-temperature nitridation treatment. Elemental analysis suggests the successful substitution of nitrogen atom into the zeolite framework and Si–NH_2, Si–NH–Si, and Si–NH_2···Al groups were formed on all nitrided products. All nitrided products catalyzed Knoevenagel condensation of benzaldehyde with ethyl cyanoacetate. A proportional relationship between the initial rate and the external surface area was observed and the nitrogen content on the external surface showed less linear correlation with the formation rate. It is because the increase of the external surface area brings the increase of structurally unique Si–OH and eventually Si–NH_2, which is more active than Si–NH–Si or Si–NH_2···Al on the same surface. Therefore, delamination of lamellar zeolite precursor is an effective approach to increase the base catalytic activity of nitrided zeolites for a reaction involving larger molecules.

NSBA-15 was prepared by reacting with ammonia gas. The 2D hexagonal structure was preserved even after a high-temperature nitridation treatment. Elemental analysis and XPS measurement suggest the successful substitution of nitrogen atom into the silica framework and primary silanamine species (Si-$\underline{N}H_2$), secondary silamanime species (Si-$\underline{N}$H-Si), and tertiary silanamine species ($\underline{N}$-$(Si)_3$) were formed on all nitrided products. As the nitridation temperature increased, higher amines were formed. All nitrided products catalyzed Knoevenagel condensation of benzaldehyde with malononitrile or ethyl cyanoacetate. There was a rough correlation between the amount of primary silanamine and the initial rate.

The catalytic properties of nitrided delaminated zeolite and nitrided mesoporous silica nitride were compared. A proportional relationship between the initial product formation rate and the amount of primary amine was observed. Therefore, the catalytic activity of primary amines in nitrided silica was independent of the mother silica materials.

References

[1] K. Tanabe, W.F. Holderich, Industrial application of solid acid-base catalysts, Applied Catalysis a-General, 181 (1999) 399-434.

[2] S. Ernst, M. Hartmann, S. Sauerbeck, T. Bongers, A novel family of solid basic catalysts obtained by nitridation of crystalline microporous aluminosilicates and aluminophosphates, Applied Catalysis a-General, 200 (2000) 117-123.

[3] K. Narasimharao, M. Hartmann, H.H. Thiel, S. Ernst, Novel solid basic catalysts by nitridation of zeolite beta at low temperature, Microporous and Mesoporous Materials, 90 (2006) 377-383.

[4] M. Srasra, S. Delsarte, E.M. Gaigneaux, Effects of the Nitridation of Y and USY Zeolites on their Catalytic Activity for the Base Catalyzed Knoevenagel Condensation, Topics in Catalysis, 52 (2009) 1541-1548.

[5] C.M. Zhang, Z. Xu, K. Wan, Q. Liu, Synthesis, characterization and catalytic properties of nitrogen-incorporated ZSM-5 molecular sieves with bimodal pores, Applied Catalysis a-General, 258 (2004) 55-61.

[6] N. Chino, T. Okubo, Nitridation mechanism of mesoporous silica: SBA-15, Microporous and Mesoporous Materials, 87 (2005) 15-22.

[7] F. Hayashi, K. Ishizu, M. Iwamoto, Fast and Almost Complete Nitridation of Mesoporous Silica MCM-41 with Ammonia in a Plug-Flow Reactor, Journal of the American Ceramic Society, 93 (2010) 104-110.

[8] T. Hasegawa, C.K. Krishnan, M. Ogura, Promising catalytic performance and shape-selectivity of nitrogen-doped siliceous MFI zeolite for base-catalyzed reactions, Microporous and Mesoporous Materials, 132 (2010) 290-295.

[9] G.J. Wu, X. Wang, Y.L. Yang, L.D. Li, G.C. Wang, N.J. Guan, Confirmation of NH species in the framework of nitrogen-incorporated ZSM-5 zeolite by experimental and theoretical studies, Microporous and Mesoporous Materials, 127 (2010) 25-31.

[10] Y.S. Tao, H. Kanoh, L. Abrams, K. Kaneko, Mesopore-modified zeolites: Preparation, characterization, and applications, Chemical Reviews, 106 (2006) 896-910.

[11] W.J. Roth, P. Nachtigall, R.E. Morris, J. Cejka, Two-Dimensional Zeolites: Current Status and Perspectives, Chemical Reviews, 114 (2014) 4807-4837.

[12] A. Corma, V. Fornes, S.B. Pergher, T.L.M. Maesen, J.G. Buglass, Delaminated zeolite precursors as selective acidic catalysts, Nature, 396 (1998) 353-356.

[13] H.K. Min, S.H. Cha, S.B. Hong, Nitrided ITQ-2 as an efficient Knoevenagel condensation catalyst, Chemical Communications, 49 (2013) 1115-1117.

[14] A. Corma, C. Corell, J. Perezpariente, SYNTHESIS AND CHARACTERIZATION OF THE MCM-22 ZEOLITE, Zeolites, 15 (1995) 2-8.

[15] D.Y. Zhao, Q.S. Huo, J.L. Feng, B.F. Chmelka, G.D. Stucky, Nonionic triblock and star diblock copolymer and oligomeric surfactant syntheses of highly ordered, hydrothermally stable, mesoporous silica structures, Journal of the American Chemical Society, 120 (1998) 6024-6036.

[16] K. Sugino, N. Oya, N. Yoshie, M. Ogura, A Simple Modification Creates a Great Difference: New Solid-Base Catalyst Using Methylated N-Substituted SBA-15, Journal of the American Chemical Society, 133 (2011) 20030-20032.

[17] M. Srasra, S. Delsarte, E.M. Gaigneaux, Nitrided Zeolites: A Spectroscopic Approach for the Identification and Quantification of Incorporated Nitrogen Species, Journal of Physical Chemistry C, 114 (2010) 4527-4535.

[18] P. Fink, J. Datka, INFRARED SPECTROSCOPIC STUDIES OF AMINATION OF ZSM-5 ZEOLITES, Journal of the Chemical Society-Faraday Transactions I, 85 (1989) 3079-3086.

[19] M. Hartmann, A. Vinu, Mechanical stability and porosity analysis of large-pore SBA-15 mesoporous

molecular sieves by mercury porosimetry and organics adsorption, Langmuir, 18 (2002) 8010-8016.
[20] T. Moteki, Y. Koga, M. Ogura, Primary, secondary, and tertiary silanamine sites formed on nitrided SBA-15 for base catalytic C-C bond formation reactions, Journal of Catalysis, 378 (2019) 131-139.
[21] A. Galarneau, N. Cambon, F. Di Renzo, R. Ryoo, M. Choi, F. Fajula, Microporosity and connections between pores in SBA-15 mesostructured silicas as a function of the temperature of synthesis, New Journal of Chemistry, 27 (2003) 73-79.
[22] J.C. Wang, Q. Liu, Structural change and characterization in nitrogen-incorporated SBA15 oxynitride mesoporous materials via different thermal history, Microporous and Mesoporous Materials, 83 (2005) 225-232.
[23] Y.D. Xia, R. Mokaya, Mesoporous MCM-48 aluminosilica oxynitrides: Synthesis and characterization of bifunctional solid acid-base materials, Journal of Physical Chemistry C, 112 (2008) 1455-1462.
[24] Y.D. Xia, R. Mokaya, Highly ordered mesoporous silicon oxynitride materials as base catalysts, Angewandte Chemie-International Edition, 42 (2003) 2639-2644.
[25] Y.D. Xia, R. Mokaya, Ordered mesoporous MCM-41 silicon oxynitride solid base materials with high nitrogen content: synthesis, characterisation and catalytic evaluation, Journal of Materials Chemistry, 14 (2004) 2507-2515.
[26] K. Yamazaki, T. Moteki, M. Ogura, Carbonate synthesis from carbon dioxide and cyclic ethers over methylated nitrogen-substituted mesoporous silica, Molecular Catalysis, 454 (2018) 38-43.
[27] F. Hayashi, K. Ishizu, M. Iwamoto, Effect of Pore Structure on the Nitridation of Mesoporous Silica with Ammonia, European Journal of Inorganic Chemistry, (2010) 2235-2243.
[28] B. Singh, K.R. Mote, C.S. Gopinath, P.K. Madhu, V. Polshettiwar, SBA-15-Oxynitrides as a Solid-Base Catalyst: Effect of Nitridation Temperature on Catalytic Activity, Angewandte Chemie-International Edition, 54 (2015) 5985-5989.
[29] J.L. Bischoff, F. Lutz, D. Bolmont, L. Kubler, USE OF MULTILAYER TECHNIQUES FOR XPS IDENTIFICATION OF VARIOUS NITROGEN ENVIRONMENTS IN THE SI/NH_3 SYSTEM, Surface Science, 251 (1991) 170-174.
[30] C.H.F. Peden, J.W. Rogers, N.D. Shinn, K.B. Kidd, K.L. Tsang, THERMALLY GROWN SI3N4 THIN-FILMS ON SI(100) - SURFACE AND INTERFACIAL COMPOSITION, Physical Review B, 47 (1993) 15622-15629.
[31] A. Bendjeriou-Sedjerari, J.D.A. Pelletier, E. Abou-Hamad, L. Emsley, J.M. Basset, A well-defined mesoporous amine silica surface via a selective treatment of SBA-15 with ammonia, Chemical Communications, 48 (2012) 3067-3069.
[32] L.N. Zhang, H. Wang, W.Z. Shen, Z.F. Qin, J.G. Wang, W.B. Fan, Controlled synthesis of graphitic carbon nitride and its catalytic properties in Knoevenagel condensations, Journal of Catalysis, 344 (2016) 293-302.

Chapter 3. Comparison of nitrogen sites in porous carbon nitride and nitrided silica

3.1. Introduction

Nitrided silica (zeolite and mesoporous silica),[1, 2] amine-functionalized silica (zeolite and mesoporous silica) and carbon nitride[3] have been reported as solid base catalysts whose nitrogen atoms work as base sites.

Nitrided mesoporous silica is synthesized by reacting mesoporous silica with ammonia under high temperature condition. Oxygen atoms in the silica framework are substituted by nitrogen atoms. The basicity of this material arises from the presence of a lone pair on the framework nitrogen atom. The nitridation temperature affects on the type of nitrogen species produced. Primary amines are formed at lower temperature (873–973 K) and secondary/tertiary amines are formed at higher temperatures (above 973 K).[4, 5] Increasing the nitridation time or increasing the ammonia flow rate, i.e., increasing the total amount of ammonia to be reacted increases the amount of substituted nitrogen.[6, 7]

The catalytic performance of nitrided mesoporous silica depends on the type and amount of nitrogen species. In aldol condensation and Knoevenagel condensation, the catalytic activity was in the order of primary > secondary ~ tertiary amine sites.[5] Moreover, methylation enhances the basicity of the nitrided mesoporous silica. Methylated nitrided mesoporous silica catalyze Knoevenagel condensation of high pK_a reactant (diethyl malonate)[8] and CO_2 addition reaction.[9, 10] Nitrided silica is a solid base catalyst that is resistant to poisoning by atmospheric carbon dioxide and does not require pretreatment, but it has the disadvantage that the Si-N bond is unstable and easily hydrolyzed.[7] Another disadvantage is that toxic ammonia gas is required for synthesis.[11]

Carbon nitride material has been also studied as a novel solid base catalyst. Compared with bulk carbon nitride material, porous carbon nitride (PCN) material shows higher mass diffusion rate and higher catalytic activity because of its large surface area and nanosized pores.[3] There are two known methods for the preparation of porous carbon nitrides: the hard template method and the soft template method.[12] In the hard template method, mesoporous silica such as SBA-15 is used as a template.[13] The raw material is introduced into the template pores and carbonized by high temperature treatment. Then, the silica template is removed using hydrofluoric acid or sodium hydroxide solution to obtain porous carbon nitride. On the other hand, the soft template method uses a liquid template such as surfactant or ionic liquid.[14, 15] Unlike the hard template method, the template can be removed only by high temperature treatment. However, since template removal and carbonization occur simultaneously, the structure is destroyed, and the specific surface area tends to become smaller.

Carbon nitride contains multiple types of nitrogen species such as pyridine nitrogen and

primary/secondary/tertiary amine.[16, 17] The relationship between nitrogen species in carbon nitride and catalytic properties has been studied. Zhang and co-workers reported that the catalytic activity of porous carbon nitride for the Knoevenagel condensation of benzaldehyde or acetone and ethyl cyanoacetate was related to their amount of primary or secondary amine species.[17]

In this chapter, the catalytic properties of nitrogen species in silica-based materials and carbon-based materials were investigated (Figure 3-1). A series of nitrided mesoporous silica SBA-15 materials (denoted as NSBA-15) at different nitridation temperature was synthesized. A series of porous carbon nitride materials (PCN) at different carbonization temperature was synthesized by the hard template method. The chemical and the textural properties of the prepared products were characterized by various techniques (XRD, nitrogen adsorption, elemental analysis, and XPS). The base catalytic property of the products was evaluated by Knoevenagel condensation between benzaldehyde and malononitrile or ethyl cyanoacetate. The effect of nitrogen species on the catalytic properties was investigated by comparing the properties of the two catalysts, NSBA-15 and PCN. NSBA-15 can catalyze a basic reaction involving a higher pK_a reactant than the one that PCN can handle.

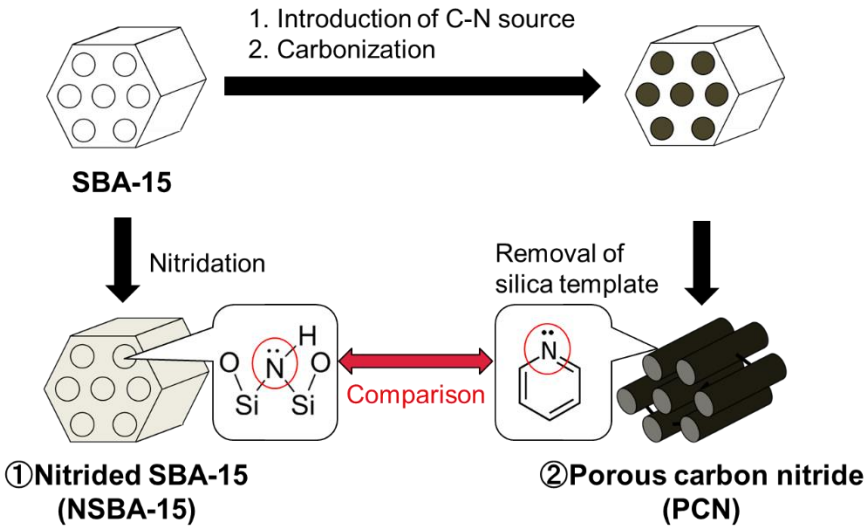

Figure 3-1. Schematic diagram of Chapter 3.

3.2. Experimental

3.2.1 Synthesis of catalyst

SBA-15 was prepared by hydrothermal treatment.[18] Typically, triblock copolymer poly(ethylene glycol)-block-poly(propylene glycol)-block-poly(ethylene glycol), Pluronic P-123 (4.0 g, PEG 30 wt.%, average M_n of 5800, Aldrich), was dissolved in 2 M aqueous hydrochloric acid solution (118.6 g, for Volumetric Analysis, FUJIFILM Wako Pure Chemical) and distilled water (29.2 g) under

stirring at 313 K for 3 h. TEOS (8.6 g, 95.0%, FUJIFILM Wako Pure Chemical) was then dripped to the solution, and hydrolyzed at 313 K for 24 h under stirring. The chemical composition of the final mixture was SiO_2 : 0.017 P123 : 6HCl : 190 H_2O. The resultant solution was placed in an electric oven for hydrothermal treatment at 373 K for 24 h. The obtained sample was filtered and washed with distilled water. The sample was calcined at 823 K for 6 h to remove the template surfactants.

Porous carbon nitride materials were prepared using mesoporous silica template (Scheme 3-1).[16] Typically, the calcined SBA-15 (0.5 g), anhydrous ethylenediamine (1.35 g, 99.0%, KANTO CHEMICAL), and carbon tetrachloride (3.0 g, 99.5%, FUJIFILM Wako Pure Chemical) were mixed in PTFE bottle. The mixture was heated at 363 K for 6 h. The obtained dark-brown-colored solid mixture was dried at 355 K for overnight. The product was placed in a quartz tube and heated at 873–1273 K for 5 h with the ramping rate of 3.0 $K \cdot min^{-1}$ under nitrogen gas flow of 2.0 $L \cdot min^{-1}$ to carbonize the polymer. The silica template was removed by hydrofluoric acid (5 wt%, MORITA CHEMICAL INDUSTRIES CO.). The obtained product was filtrated and washed in distilled water and dried at 373K.

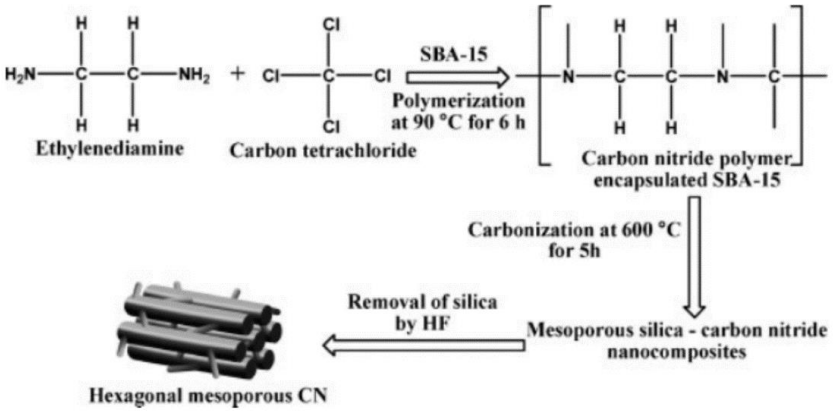

Scheme 3-1 Preparation of porous carbon nitride using SBA-15.[16]

3.2.2 Product characterization

Powder XRD patterns of the products were collected by a RINT2100 diffractometer (Rigaku) using Cu Kα radiation (λ = 0.1541 nm). The data were recorded in the 2θ range of 0.5–3.0° with an angular step size of 0.01°.

Nitrogen sorption measurement was conducted by a Quadrasorb evo (Quantachrome) at 77 K to determine total surface area, micropore volume, micropore surface area, and external surface area of the products. Prior to the measurement, the products were degassed in vacuum at 523 K for 3 h (PCN) or 573 K for 3 h (others). The total surface area was calculated by the BET isothermal equation. The pore size was obtained from the adsorption branch of the nitrogen isotherms using the Barrett-Joyner-Halenda method.

The quantitative analysis of nitrogen content was carried out by a vario MICRO cube elemental analyzer (Elementer).

X-ray photoelectron spectroscopy was conducted by a PHI Quantera SXM (ULVAC-PHI Inc.). Powder samples were hold on a sample stage with a silver paste. Prior to the measurement, the sample stage with samples was degassed in vacuum at room temperature overnight.

3.2.3 Catalytic test

Knoevenagel condensation was performed as a model base-catalyzed reaction. A mixture of benzaldehyde (1 mmol, 98.0%, FUJIFILM Wako Pure Chemical), malononitrile (1 mmol, 98%, FUJIFILM Wako Pure Chemical) or ethyl cyanoacetate (1 mmol, 98%, FUJIFILM Wako Pure Chemical), and toluene as a solvent (10 mmol, 99.5%, FUJIFILM Wako Pure Chemical) were introduced into the test tube. The tube was heated in a thermostatic oil bath and the mixture was stirred by a magnetic stirrer. After the temperature was reached to 333 K, catalyst (10 mg) was added into the mixture. The mixture was heated for 3 h. The obtained products were analyzed with a gas chromatograph GC-14B (Shimadzu) equipped with an FID detector and a ZB-1 capillary column.

In order to identify the active site, a change over time in Knoevenagel condensation was performed. A mixture of benzaldehyde (10 mmol, 98.0%, FUJIFILM Wako Pure Chemical), malononitrile (10 mmol, 98%, FUJIFILM Wako Pure Chemical), and toluene as a solvent (40 mL, 99.5%, FUJIFILM Wako Pure Chemical) were introduced into the round-bottom flask. The flask was heated in a thermostatic oil bath and the mixture was stirred by a magnetic stirrer. After the temperature was reached to 353 K, catalyst (PCN series, 10 mg) was added into the mixture. Small portion of liquid products (about 0.1 mL) were collected as needed from the reaction mixture with a syringe. The obtained products were analyzed with a gas chromatograph GC-14B equipped with an FID detector and a ZB-1 capillary column.

3.3. Results and Discussion

3.3.1 Catalyst preparation

The powder XRD patterns of PCN products are shown in Figure 3-2. The peak assigned to *100* diffractions of 2D-hexagonal structure[16] was observed only in PCN-1273, indicating the incomplete replication of SBA-15 template structure in the other samples. It was probably due to insufficient cleaning, which resulted in the presence of carbon nitride on the surface of the SBA-15 template. The carbon nitride exist on the surface was decomposed and removed during the high temperature treatment at 1273 K.

Figure 3-3 shows the powder XRD patterns of PCN products at higher angle. All products showed a single broad diffraction peak near 26°. It corresponded to non-porous carbon nitride spheres, indicating turbostratic ordering of the carbon and nitrogen atoms in the graphene layers.[19]

Therefore, the PCN products were thought to be turbostratic layers of graphene in which some of the carbon has been replaced by nitrogen.

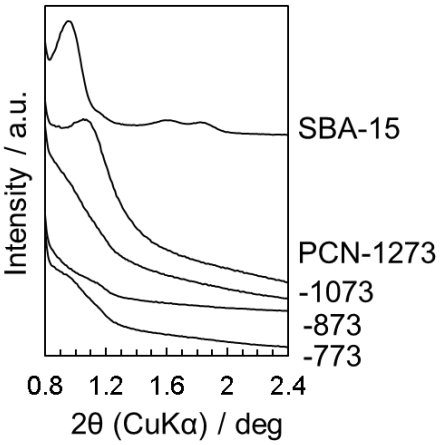

Figure 3-2. XRD patterns of mother SBA-15 and series of porous carbon nitride carbonized at different temperature (773–1273 K).

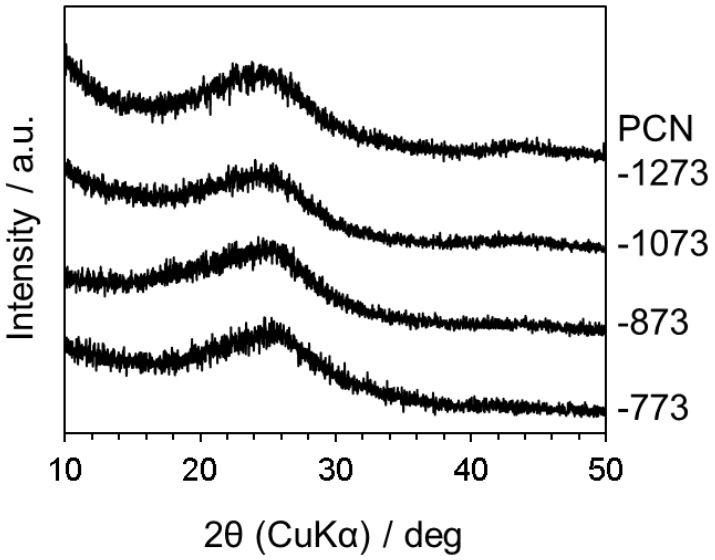

Figure 3-3. XRD patterns of series of porous carbon nitride carbonized at different temperature (773–1273 K).

Figure 3-4(a) shows the nitrogen adsorption-desorption isotherm of the series of PCN products. The typical type-IV isotherms were observed in all products, indicating the presence of mesopores. Table 3-1 summarized the textural properties of PCN products. When the carbonization temperature is less than 1073 K, the BET surface area and total pore volume increased with increasing carbonization

temperature. This result is consistent with previous reports.[17] However, PCN-1273 showed less BET surface area than PCN-1073, indicating that carbonization at higher temperature lead to structural damage.

Figure 3-4(b) shows BJH pore size distributions of the series of PCN products. PCN-773, 873, and 1073 had non-uniform pores. It suggests the incomplete replication of SBA-15 template structure. The mean pore diameter of PCN-1273 was 3.3 nm. The wall thickness of mother SBA-15 is 2.6 nm. Therefore, nitrogen adsorption-desorption measurement revealed that only PCN-1273 processed the replication structure of mother SBA-15 and other product processed the incomplete replication structure. The result was consistent with the changes in the XRD patterns discussed above.

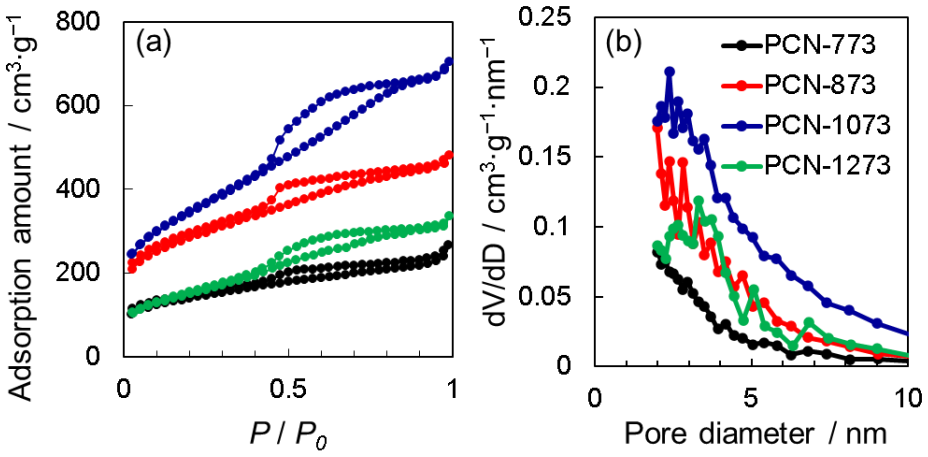

Figure 3-4. (a) N_2 adsorption isotherms and **(b)** BJH adsorption pore size distribution of PCN samples prepared at 773–1273 K.

Table 3-1. Textual properties of porous carbon nitride (PCN) carbonized at different temperature (773–1273 K) calculated from N_2 sorption measurement.

Product	BET Surface area / $m^2\ g^{-1}$	Total pore volume / $cm^3\ g^{-1}$
PCN-773	502	0.284
PCN-873	1019	0.486
PCN-1073	1214	0.855
PCN-1273	527	0.440

The nitrogen contents of nitrided products as prepared and three months after preparation measured by elemental analysis are listed in Table 3-2. The C/N ratio of products before carbonization was consistent with that of raw material (Scheme 3-1). The nitrogen content of carbonized products decreased with increasing nitridation temperature. This could be explained by the low

thermodynamic stability of nitrogen species in the carbon materials.[12, 20] Weights other than C, N, and H were thought to be mainly due to the remaining SBA-15 template.

Table 3-2. Composition of porous carbon nitride (PCN) prepared at different temperature (773–1273 K) measured by elemental analysis and XPS.

Product	CHN					XPS				
	C / wt%	N / wt%	H / wt%	Others / wt%	C/N molar ratio	C / at%	N / at%	O / at%	Si / at%	C/N molar ratio
PCN-773	56.2	31.7	2.34	9.76	2.06	69.94	24.85	4.21	1.00	2.81
PCN-873	66.4	19.7	2.11	11.8	3.92	77.82	16.42	4.87	0.88	4.74
PCN-1073	74.6	10.6	1.24	13.6	8.20	81.42	5.11	11.4	2.07	15.9
PCN-1273	81.8	6.72	0.493	11.0	14.2	89.03	7.82	2.00	1.16	11.4
Before carbonization (PCN-873)	23.3	19.3	5.60	51.8	1.40	—	—	—	—	—

To identify composition, XPS measurement was also performed. Figure 3-5 shows XPS survey spectra of carbonized products. The peaks derived from carbon, nitrogen, and oxygen atom were observed in all products. The peak at 368 eV derived from silver atom was observed in PCN-873, owing to the silver paste which was used for holding of samples. The peak at 151 eV derived from silicon atom was observed in PCN-1273, probably owing to incomplete removal of SBA-15 template. There is a correlation between the amount of Si measured by XPS and others content in the elemental analysis (Table 3-2).

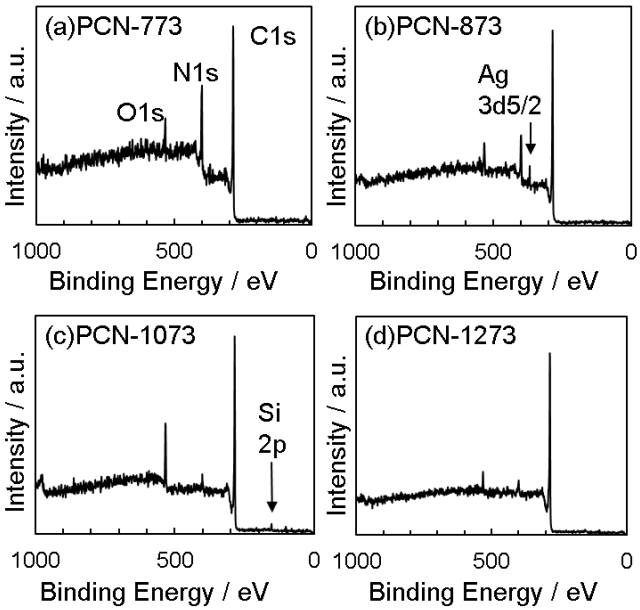

Figure 3-5. XPS survey spectra for series of porous carbon nitride (PCN) prepared at different temperature from 773 to 1273 K.

Figure 3-6 shows the XPS spectra of N1s levels for PCN samples. The XPS spectra was deconvoluted to four peaks as blue lines shown in Figure 3-6. The peak at 398.5 eV arises from the sp^2 N atoms bonded to C atoms in aromatic rings, i.e., pyridine nitrogen (C-N=C).[21, 22] The peak at 399.7 eV is attributed to tertiary nitrogen groups bonded to three carbon atoms ($N–(C)_3$). [21, 22] The peak at 400.9 eV is attributed to primary or secondary amine species ($C-NH_2$ or C-NH-C).[21, 22] The signal centered at ca. 404.4 eV is attributed to the quaternary nitrogen species and/or charging effect ($N^+–(C)_4$).[21, 22]

The content and the percentage of nitrogen species in PCN calculated from XPS spectra are listed in Table 3-3. Pyridine nitrogen content significantly decreased, and the sum of amine nitrogen contents increased with increasing carbonization temperature above 1073 K. The tendency was consistent with the previous report.[17]

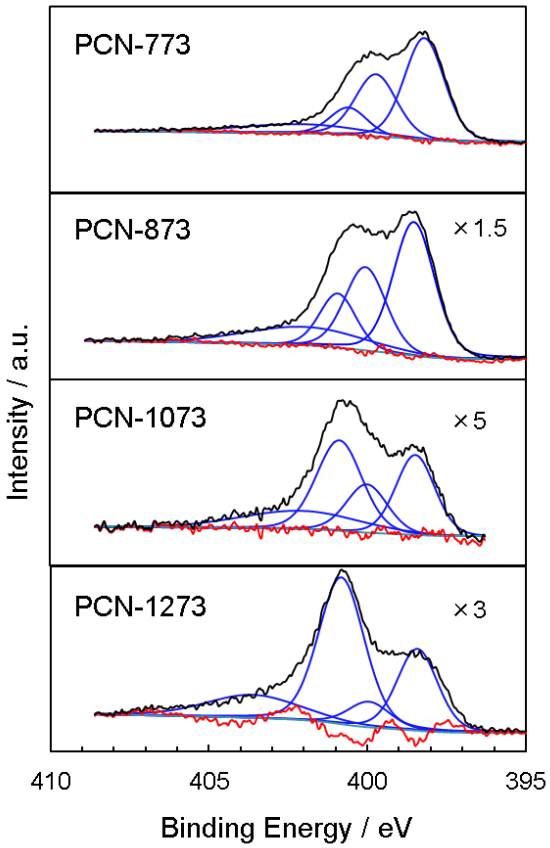

Figure 3-6. XPS spectra of N 1s levels for series of porous carbon nitride (PCN) prepared at different temperature from 773 to 1273 K. Black curves and blue curves are measured data and fitting curves, respectively. The deconvoluted peaks are assigned to pyridinic nitrogen species (C-N=C), the tertiary nitrogen bonded to three carbon atoms (N-$(C)_3$), the primary or secondary amine groups (C-NH_2 or C-NH-C), and the quaternary nitrogen species (N^+– $(C)_4$) with the binding energy of 398.5, 399.7, 400.9, and 404.4 eV, respectively. Red curves show difference between measured data and sum of fitting curves.

Table 3-3. Contents of nitrogen species in porous carbon nitride (PCN) prepared at different temperature (773–1273 K) measured by CHN and XPS.

Product	Content / wt% (molar percentage / %)			
	C=N-C	N-$(C)_3$	-NH_2 or -NH-	N-$(C)_4$
PCN-773	15.0 (47.1)	9.3 (29.4)	3.7 (11.8)	3.7 (11.7)
PCN-873	8.4 (42.5)	5.3 (26.7)	3.0 (15.1)	3.1 (15.7)
PCN-1073	2.9 (27.6)	1.9 (17.8)	3.9 (36.6)	1.9 (18.0)
PCN-1273	1.7 (25.0)	0.5 (8.0)	3.4 (50.9)	1.1 (16.1)

3.3.2 Catalytic reactions

Knoevenagel condensation of benzaldehyde with active methylene compounds was performed as a model reaction. Malononitrile (pK_a : 11.1) and ethyl cyanoacetate (pK_a : 13.1) were used as active methylene compounds. Nitrogen contents of the catalysts were measured by CHN just before the reaction was carried out.

Figure 3-7 shows the relationship between the yields and the nitrogen content of the catalysts. At every data point, the selectivity towards the desired product, benzalmalononitrile or ethyl α-cyanocinnamate, was over 99%. Therefore, PCN showed good selectivity for Knoevenagel condensation.

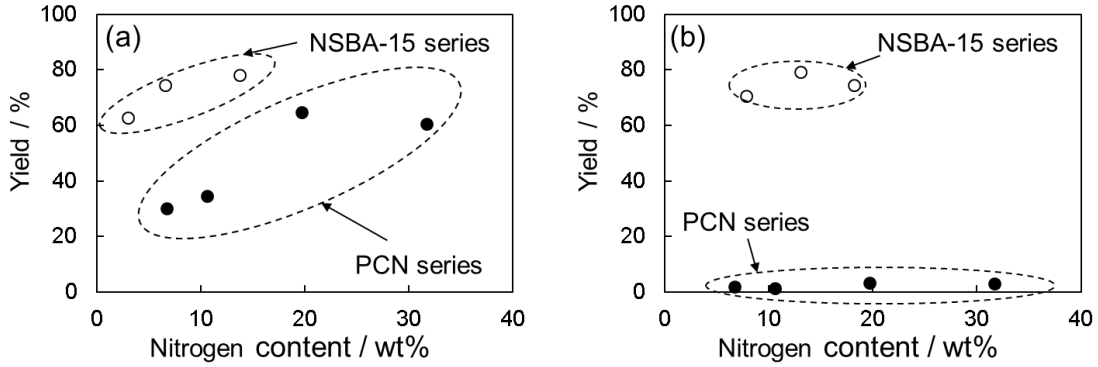

Figure 3-7. The relationship between the yields at three hours after the start of the reaction and the nitrogen content of the catalysts in Knoevenagel condensation between benzaldehyde and (a) malononitrile (pK_a : 11.1) or (b) ethyl cyanoacetate (pK_a : 13.1). The results of NSBA-15 were from Chapter 2.

A previous report revealed that the catalytic activity of porous carbon nitride depends on the content of primary or secondary amine species (C-NH_2 or C-NH-C).[17] However, there was no proposal relationship between the yield with the content of any nitrogen species. For a further investigation, the change of yield over time in Knoevenagel condensation between benzaldehyde and malononitrile was measured (Figure 3-8). Initial formation rates were calculated by a linear approximation in the initial one hour established in Figure 3-8. Although a rough correlation was found between the initial reaction rate and the nitrogen contents, the least-squares method could not identify the active species. To summarize the above results, in this study, a critical parameter affecting the catalytic property was not identified.

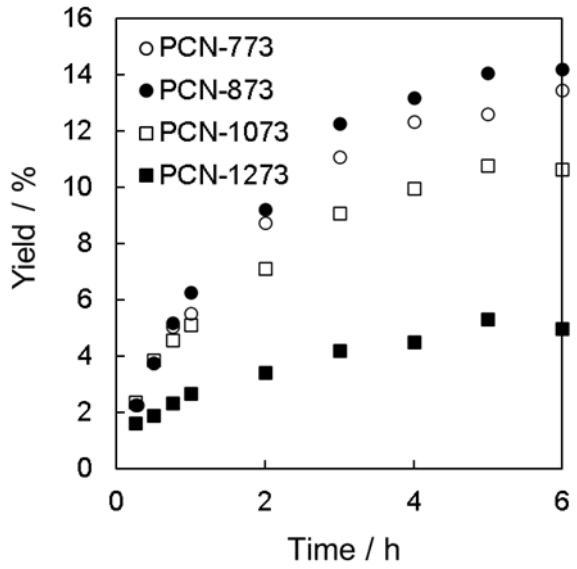

Figure 3-8. Changes in the product yield of Knoevenagel condensation reaction as a function of reaction time over PCN catalysts (10 mmol benzaldehyde, 10 mmol malononitrile, 40 mL toluene, 10 mg catalyst, 353K).

In the case of malononitrile, both NSBA-15 and PCN showed high catalytic activity (Figure 3-7(a)). On the other hand, in the case of ethyl cyanoacetate, only NSBA-15 showed high catalytic activity (Figure 3-7(b)). When diethyl malonate (pK_a : 16.4) was used as active methylene compounds, both NSBA-15 and PCN did not catalyzed the Knoevenagel condensation of benzaldehyde.[8, 23] Therefore, the limit of pK_a of active methylene compound in PCN would be lower than that in NSBA-15. That is probably because of the different of the structure of active nitrogen sites. Figure 3-9 shows the structure of active nitrogen sites in NSBA-15 and PCN. n NSBA-15, nitrogen atoms bond with silicon atoms, which is quasi-aliphatic amines (e.g., ethylamine (pK_a : 10.6)). On the other hand, nitrogen atoms in PCN are on or in aromatic rings, i.e., they are aromatic amines (e.g., pyridine (pK_a : 5.3)). Aliphatic amines generally exhibit stronger proton abstraction than aromatic ones. Therefore, NSBA-15 can catalyze a basic reaction involving a higher pKa reactant than the one that PCN can handle.

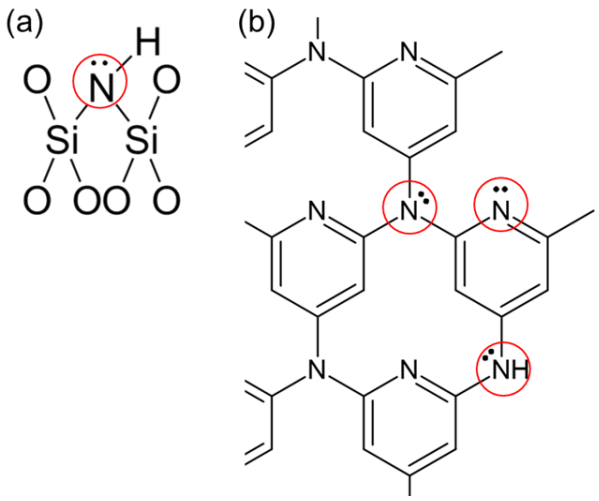

Figure 3-9. The structure of the active sites in (a) NSBA-15 and (b)PCN.

The percentage of nitrogen remaining before and after the reaction was compared. The reaction with malononitrile was conducted three months after preparation and the products were stored in air after preparation. The used catalysts were collected by filtration of reaction liquid after catalytic reaction, washed by ethanol, and dried at 373 K.

The nitrogen contents of catalysts before and after catalytic reaction are showed in Figure 3-10. In as prepared products, the nitrogen content increased with increasing nitridation temperature. The nitrogen contents decreased after three months, probably because of the decomposition of Si-N bond by water vapor in air.[7] The nitrogen contents remained after three months and PCN materials showed high stability.

Almost all nitrogen atoms remained after the reaction test in PCN, but only three-quarters nitrogen atoms remained in NSBA-15. Nitrogen atoms bond to silicon atoms in NSBA-15 and that bond to carbon atoms in PCN (Figure 3-9). Si-N bond is easily hydrolyzed. So, Si-N bond in NSBA-15 was hydrolyzed by water formed by Knoevenagel condensation. Therefore, NSBA-15 showed lower catalytic stability than PCN. The reuse tests have not been conducted yet. However, the catalytic stability of carbon nitride synthesized by the same method as the PCNs in this paper was reported.[17] The conversion kept higher than 90% within five repeated runs of Knoevenagel condensation between benzaldehyde and malononitrile. Therefore, PCN materials are considered to be reusable catalysts.

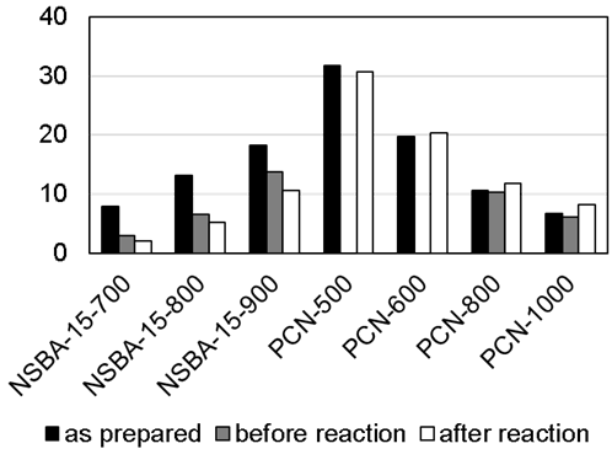

Figure 3-10. Nitrogen content of NSBA-15 and PCN as prepared, before, and after the reaction test.

3.4. Conclusions

PCN was prepared by using carbon tetrachloride and ethylenediamine as precursor and SBA-15 as template. The PCN possessed an incomplete replication of the structure of the SBA-15 template. XPS measurement suggests the presence of pyridine nitrogen species (C-N=C), primary or secondary amine species (C-NH_2 or C-NH-C), and tertiary amine species (N–$(C)_3$) on the surface of PCN.

In NSBA-15, the primary silanamine species were the most active site for Knoevenagel condensation. It was not possible to identify the most dominant nitrogen site for the reaction in PCN. NSBA-15 showed higher catalytic activity than PCN for Knoevenagel condensation between benzaldehyde and ethyl cyanoacetate probably because of their higher pK_a. PCN showed higher catalytic stability than NSBA-15 because of the lack of unstable Si-N bond. Based on the above results, a catalyst with aliphatic amines and no Si-N bond is considered to have both high activity and high stability.

References

[1] S. Ernst, M. Hartmann, S. Sauerbeck, T. Bongers, A novel family of solid basic catalysts obtained by nitridation of crystalline microporous aluminosilicates and aluminophosphates, Applied Catalysis a-General, 200 (2000) 117-123.

[2] T. Hasegawa, C.K. Krishnan, M. Ogura, Promising catalytic performance and shape-selectivity of nitrogen-doped siliceous MFI zeolite for base-catalyzed reactions, Microporous and Mesoporous Materials, 132 (2010) 290-295.

[3] X. Jin, V.V. Balasubramanian, S.T. Selvan, D.P. Sawant, M.A. Chari, G.Q. Lu, A. Vinu, Highly Ordered Mesoporous Carbon Nitride Nanoparticles with High Nitrogen Content: A Metal-Free Basic Catalyst, Angewandte Chemie-International Edition, 48 (2009) 7884-7887.

[4] N. Chino, T. Okubo, Nitridation mechanism of mesoporous silica: SBA-15, Microporous and Mesoporous Materials, 87 (2005) 15-22.
[5] T. Moteki, Y. Koga, M. Ogura, Primary, secondary, and tertiary silanamine sites formed on nitrided SBA-15 for base catalytic C-C bond formation reactions, Journal of Catalysis, 378 (2019) 131-139.
[6] F. Hayashi, K. Ishizu, M. Iwamoto, Fast and Almost Complete Nitridation of Mesoporous Silica MCM-41 with Ammonia in a Plug-Flow Reactor, Journal of the American Ceramic Society, 93 (2010) 104-110.
[7] F. Hayashi, K. Ishizu, M. Iwamoto, Effect of Pore Structure on the Nitridation of Mesoporous Silica with Ammonia, European Journal of Inorganic Chemistry, (2010) 2235-2243.
[8] K. Sugino, N. Oya, N. Yoshie, M. Ogura, A Simple Modification Creates a Great Difference: New Solid-Base Catalyst Using Methylated N-Substituted SBA-15, Journal of the American Chemical Society, 133 (2011) 20030-20032.
[9] K. Yamazaki, T. Moteki, M. Ogura, Carbonate synthesis from carbon dioxide and cyclic ethers over methylated nitrogen-substituted mesoporous silica, Molecular Catalysis, 454 (2018) 38-43.
[10] K. Yamazaki, T. Moteki, M. Ogura, Reaction Pathways in the Chemical Transformation of CO_2 with beta,gamma-Unsaturated Alcohols into Cyclic Carbonates Catalyzed by Methylated Nitrogen-substituted SBA-15, Journal of the Japan Petroleum Institute, 63 (2020) 149-157.
[11] A.J. Han, H.Y. He, J. Guo, H. Yu, Y.F. Huang, Y.C. Long, Studies on structure and acid-base properties of high silica MFI-type zeolite modified with methylamine, Microporous and Mesoporous Materials, 79 (2005) 177-184.
[12] K.S. Lakhi, D.H. Park, K. Al-Bahily, W. Cha, B. Viswanathan, J.H. Choy, A. Vinu, Mesoporous carbon nitrides: synthesis, functionalization, and applications, Chemical Society Reviews, 46 (2017) 72-101.
[13] Y. Wang, Q. Jiang, J.K. Shang, J. Xu, Y.X. Li, Advances in the Synthesis of Mesoporous Carbon Nitride Materials, Acta Physico-Chimica Sinica, 32 (2016) 1913-1928.
[14] Y. Wang, X.C. Wang, M. Antonietti, Y.J. Zhang, Facile One-Pot Synthesis of Nanoporous Carbon Nitride Solids by Using Soft Templates, ChemSusChem, 3 (2010) 435-439.
[15] Y. Wang, J.S. Zhang, X.C. Wang, M. Antonietti, H.R. Li, Boron- and Fluorine-Containing Mesoporous Carbon Nitride Polymers: Metal-Free Catalysts for Cyclohexane Oxidation, Angewandte Chemie-International Edition, 49 (2010) 3356-3359.
[16] A. Vinu, Two-dimensional hexagonally-ordered mesoporous carbon nitrides with tunable pore diameter, surface area and nitrogen content, Advanced Functional Materials, 18 (2008) 816-827.
[17] L.N. Zhang, H. Wang, Z.F. Qin, J.G. Wang, W.B. Fan, Synthesis of two-dimensional mesoporous carbon nitride under different carbonization temperatures and investigation of its catalytic properties in Knoevenagel condensations, Rsc Advances, 5 (2015) 22838-22846.
[18] D.Y. Zhao, Q.S. Huo, J.L. Feng, B.F. Chmelka, G.D. Stucky, Nonionic triblock and star diblock

copolymer and oligomeric surfactant syntheses of highly ordered, hydrothermally stable, mesoporous silica structures, Journal of the American Chemical Society, 120 (1998) 6024-6036.
[19] A. Vinu, K. Ariga, T. Mori, T. Nakanishi, S. Hishita, D. Golberg, Y. Bando, Preparation and characterization of well-ordered hexagonal mesoporous carbon nitride, Advanced Materials, 17 (2005) 1648-1652.
[20] S.N. Talapaneni, S. Anandan, G.P. Mane, C. Anand, D.S. Dhawale, S. Varghese, A. Mano, T. Mori, A. Vinu, Facile synthesis and basic catalytic application of 3D mesoporous carbon nitride with a controllable bimodal distribution, Journal of Materials Chemistry, 22 (2012) 9831-9840.
[21] N.D. Shcherban, P. Maki-Arvela, A. Aho, S.A. Sergiienko, P.S. Yaremov, K. Eranen, D.Y. Murzin, Melamine-derived graphitic carbon nitride as a new effective metal-free catalyst for Knoevenagel condensation of benzaldehyde with ethylcyanoacetate, Catalysis Science & Technology, 8 (2018) 2928-2937.
[22] L.N. Zhang, H. Wang, W.Z. Shen, Z.F. Qin, J.G. Wang, W.B. Fan, Controlled synthesis of graphitic carbon nitride and its catalytic properties in Knoevenagel condensations, Journal of Catalysis, 344 (2016) 293-302.
[23] F.Z. Su, M. Antonietti, X.C. Wang, mpg-C_3N_4 as a solid base catalyst for Knoevenagel condensations and transesterification reactions, Catalysis Science & Technology, 2 (2012) 1005-1009.

Chapter 4. Comparison of nitrogen sites in amine functionalized silica and nitrided silica

4.1 Introduction

Silane coupling agents containing amines can be used to immobilize the basic moieties to the surface of silica materials. Silica materials functionalized by amine groups are called amine-functionalized silica and have been widely studied as solid base catalysts, adsorbents, and drug carriers.[1, 2]

There are two methods to prepare amine-functionalized silica, post-synthesis grafting method and direct co-condensation method. In the grafting method, amines are functionalized by the reaction of silanol groups of silica with silane coupling agents. There have been reports of amine functionalization of silica materials such as MCM-41,[3, 4] SBA-15,[5] and X-type zeolites[6] by the grafting method. On the other hand, in the direct co-condensation method, silane coupling agent is used as one of the raw materials in the synthesis step of silica materials. For example, hexagonal mesoporous silica and amorphous silica with aminopropyl groups can be prepared from tetraethoxysilane and 3-aminopropyltrimethoxysilane.[4] Amine-functionalized silica prepared by direct co-condensation method are less active than those obtained by grafting method for nitroaldol reaction and Mihael addition.[4] This is probably because some of the amines are incorporated within the siliceous framework, reducing the number of active sites that the reactants can access.

In this chapter, in order to clarify the differences in catalytic properties of different nitrogen species, amine-functionalized SBA-15 with four different amines were prepared (Figure 4-1). The chemical and the textural properties of products were characterized by various techniques (elemental analysis, thermogravimetry, nitrogen sorption, and FT-IR). The base catalytic property of the prepared products was evaluated by a typical base-catalyzed reaction of Knoevenagel condensation and compared with those of nitrided SBA-15 (NSBA-15), porous carbon nitride (PCN), methylated nitrided SBA-15 (MeNSBA-15).

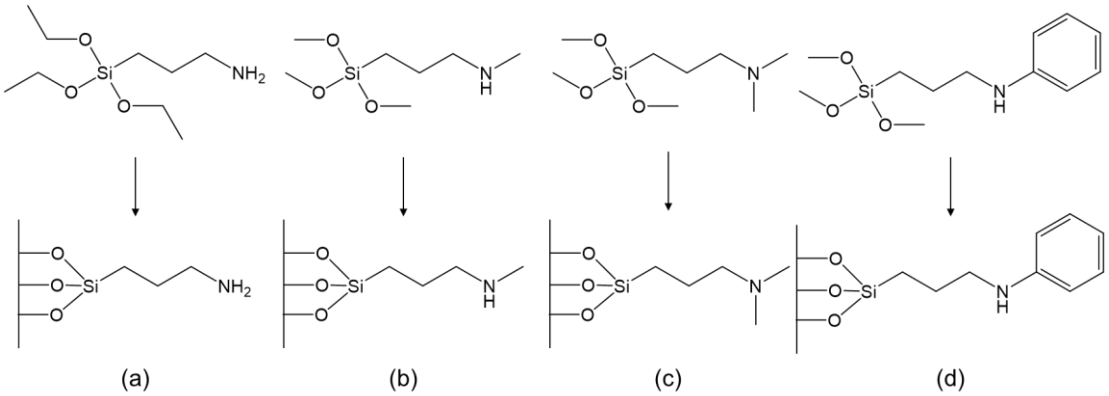

Figure 4-1 Structure of silane coupling agents (a) 3-aminopropyltriethoxysilane, (b) 3-(methylamino)propyltrimethoxysilane, (c) [3-(*N*,*N*-Dimethylamino)propyl]trimethoxysilane, and (d) trimethoxy[3-(phenylamino)propyl]silane and surface structure of amine-functionalized SBA-15.

4.2 Experimental

4.2.1 Synthesis of catalysts

SBA-15 was prepared by a hydrothermal method (Chapter 3.2.1).

SBA-15 functionalized with silane coupling agents were prepared by a grafting method.[5, 7] Obtained SBA-15 was dried at 383 K overnight for pretreatment. 0.01 mmol of silane coupling agents and 10 mL of dehydrated toluene were mixed. The silane coupling agents were 3-aminopropyltriethoxysilane (>98.0%, Tokyo Chemical Industry Co., Ltd.), 3-(methylamino)propyltrimethoxysilane (>95.0%, Tokyo Chemical Industry Co., Ltd.), [3-(*N*,*N*-Dimethylamino)propyl]trimethoxysilane (>96.0%, Tokyo Chemical Industry Co., Ltd.), and trimethoxy[3-(phenylamino)propyl]silane (>98.0%, Tokyo Chemical Industry Co., Ltd.). The dried SBA-15 was added into the mixture and refluxed at 383 K for 22 h. The mixture was filtrated and washed by 30 mL of dehydrated toluene and 30 mL of dehydrated dichloromethane. The obtained material was dried at 343 K for 2 h in vacuum. The products obtained by grafting 3-aminopropyltriethoxysilane, 3-(methylamino)propyltrimethoxysilane, [3-(*N*,*N*-Dimethylamino)propyl]trimethoxysilane, and trimethoxy[3-(phenylamino)propyl]silane on SBA-15 were denoted as AP-SBA-15 (aminopropyl-SBA-15), MAP-SBA-15 (methyl aminopropyl-SBA-15), DMAP-SBA-15 (dimethyl aminopropyl-SBA-15) and PAP-SBA-15 (phenyl aminopropyl-SBA-15), respectively.

4.2.2 Product characterization

The quantitative analysis of nitrogen content was carried out by a vario MICRO cube elemental analyzer (Elementer).

Simultaneous thermogravimetry / differential thermal analysis (TG-DTA) was conducted by

Thermo plus TG8120 (Rigaku). A sample of ca. 2 mg was heated in a flow of air (30 mL min^{-1}) at a heating rate of 10 K min^{-1} from room temperature to 873 K.

Nitrogen sorption measurement was conducted by a Quadrasorb evo (Quantachrome) at 77 K to determine total surface area, micropore volume, micropore surface area, and external surface area of the products. Prior to the measurement, the products were degassed in vacuum at 423 K for 3 h. The total surface area was calculated by the BET isothermal equation. The micropore volume, the micropore surface area, and the external surface area were evaluated by the *t*-plot method.

The FT-IR spectra of the products were collected by a 4100 FT-IR spectrometer (JASCO). 15 mg of the catalyst was pressed at 10 MPa to mold the disk and submitted to the cell for FT-IR measurement. Then, the disk was pretreated at 423 K in vacuum for 1.5 h, and the spectra were recorded at room temperature under vacuum condition with a resolution of 4.0 cm^{-1}.

4.2.3 Catalytic test

Knoevenagel condensation was performed as a model base-catalyzed reaction. A mixture of benzaldehyde (1 mmol, 98.0%, FUJIFILM Wako Pure Chemical), malononitrile (1 mmol, 98%, FUJIFILM Wako Pure Chemical) or ethyl cyanoacetate (1 mmol, 98%, FUJIFILM Wako Pure Chemical), and toluene as a solvent (10 mmol, 99.5%, FUJIFILM Wako Pure Chemical) were introduced into the test tube. The tube was heated in a thermostatic oil bath and the mixture was stirred by a magnetic stirrer. After the temperature was reached to 333 K, catalyst (10 mg) was added into the mixture. The mixture was heated for 3 h. The obtained products were analyzed with a gas chromatograph GC-14B (Shimadzu) equipped with an FID detector and a ZB-1 capillary column.

Knoevenagel condensation of benzaldehyde and diethyl malonate was also conducted. A mixture of benzaldehyde (2 mmol), diethyl malonate (2 mmol, 98%, FUJIFILM Wako Pure Chemical), and ethanol as a solvent (2.13 mL, 99.5%, FUJIFILM Wako Pure Chemical) were introduced into the flask. The flask was heated in a thermostatic oil bath and the mixture was stirred by a magnetic stirrer. After the temperature was reached to 353 K, catalyst (20 mg) was added into the mixture. The mixture was heated at 353 K for 24 h with a reflux condenser. The obtained products were analyzed with the gas chromatograph and the ZB-1 capillary column.

4.3 Results and discussion

4.3.1 Catalyst preparation

The nitrogen and carbon contents of amine-functionalized products measured by elemental analysis are listed in Table 4-1. The contents were similar to the values reported in the amine-functionalized SBA-15 in the previous study.[5] The nitrogen contents of MAP-SBA-15 and DMAP-SBA-15 were higher than that of AP-SBA-15. In previous report, that of SBA-15 functionalized with methylaminopropyl group was lower than that of SBA-15 functionalized with aminopropyl group.[8]

The difference was caused by silane coupling agents. In the previous reports, silane coupling agents with trimethoxy groups were used for grafting of aminopropyl groups and methylaminopropyl groups. However, in this study, the silane coupling agent with triethoxy groups was used for grafting of aminopropyl groups and the silane coupling agent with trimethoxy groups was used for grafting of methylaminopropyl groups. The reason why more amine groups were functionalized on MAP-SBA-15 and DMAP-SBA-15 than AP-SBA-15 would be because the trimethoxy group is more reactive than the triethoxy group. The nitrogen content of PAP-SBA-15 was lower than that of AP-SBA-15, probably due to the steric hindrance of silane coupling agents. In all products, the C/N molar ratio was higher than the C/N molar ratio of the amino group considered to be functionalized. It suggested that toluene and dichloromethane used in washing or carbon dioxide in air were adsorbed on the surface of the product.

Table 4-1 Nitrogen and carbon contents of SBA-15 and amine-functionalized SBA-15.

Product	N / wt% ($mmol \cdot g^{-1}$)	C / wt% ($mmol \cdot g^{-1}$)	C/N molar ratio	C/N molar ratio of the functionalized amino group
SBA-15	0 (0)	0.0307 (0.0256)	–	–
AP-SBA-15	1.63 (1.17)	5.52 (4.61)	3.95	3
MAP-SBA-15	1.96 (1.40)	8.05 (6.71)	4.79	4
DMAP-SBA-15	1.90 (1.36)	10.3 (8.55)	6.29	5
PAP-SBA-15	1.33 (0.947)	12.9 (10.7)	11.3	9

Figure 4-2 shows thermogravimetric analysis results for mother SBA-15 and amine-functionalized SBA-15. A weight loss and an endothermic peak below 100 °C were observed in SBA-15 (Figure 4-2 (a)). The weight loss is considered to be due to the desorption of adsorbed water. On the other hand, weight losses and exothermic peaks after 200 °C were also observed in amine-functionalized SBA-15 (Figure 4-2 (b), (c), (d) and (e)). The weight losses of amine-functionalized products were lower than that of SBA-15, suggesting that the surface of amine-functionalized products was hydrophobic. The weight loss in the second step was 5 wt% for AP-SBA-15, 9 wt% for MAP-SBA-15, 11 wt% for DMAP-SBA-15, and 10 wt% for PAP-SBA-15. Since these values are roughly consistent with the total amount of C and N measured by elemental analysis, the decrease in the second step is considered to be due to the combustion of the modified functional groups. The temperature of the second mass loss was different for each sample. The temperature of the second step was 300 °C for AP-SBA-15, 310 °C for MAP-SBA-15, 300 °C for DMAP-SBA-15, and 330 °C for PAP-SBA-15. This difference might be due to the difference in the functional groups functionalized on each sample.

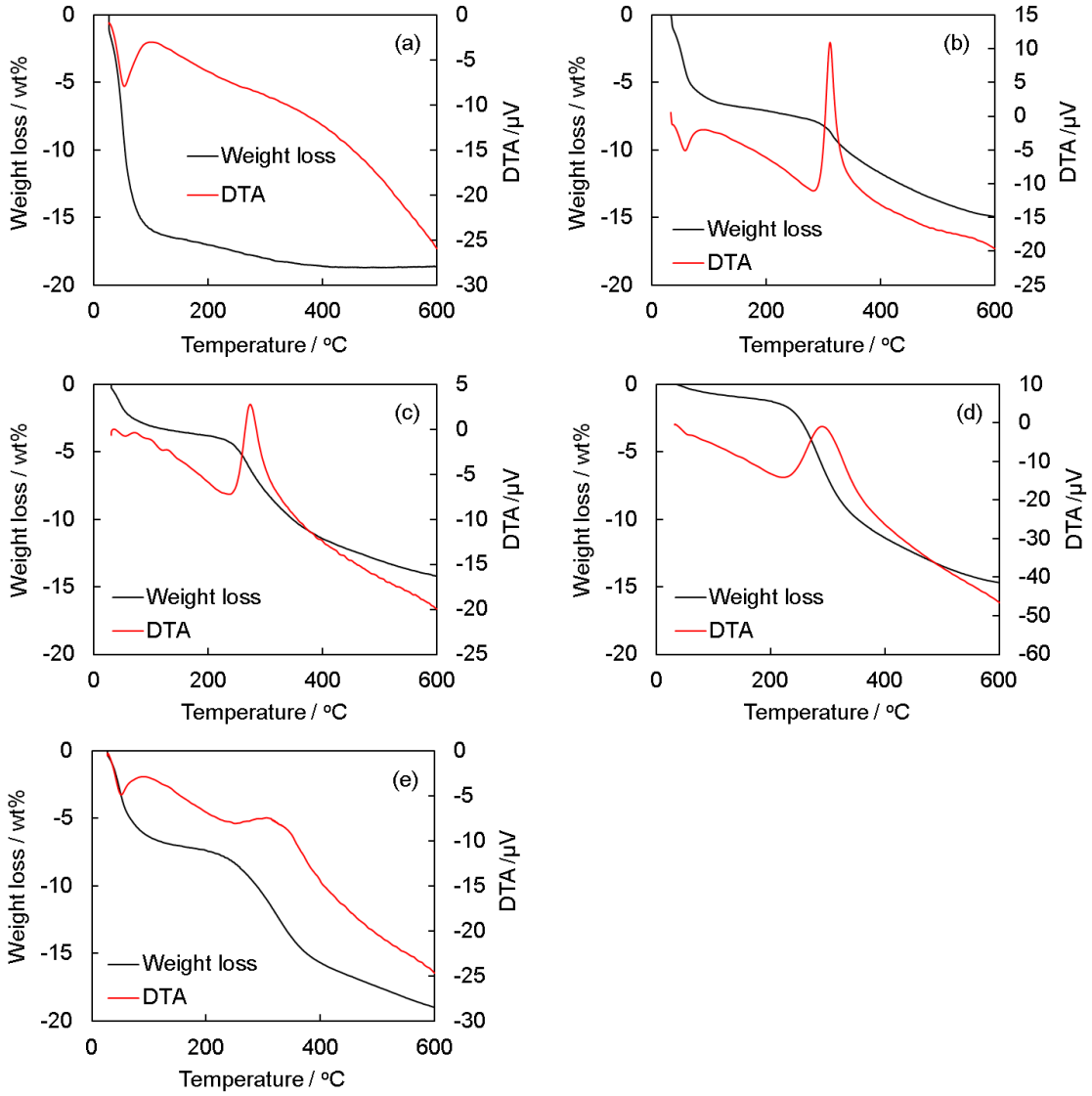

Figure 4-2 TG and DTA curves of (a) SBA-15, (b) AP-SBA-15, (c) MAP-SBA-15, (d) DMAP-SBA-15 and (e) PAP-SBA-15.

Figure 4-3 (a) shows the nitrogen adsorption-desorption isotherm of the mother SBA-15 and amine-functionalized products. The typical type-IV isotherms were observed in all products, indicating the presence of mesopores. Figure 4-3 (b) shows the BJH adsorption pore size distribution of the mother SBA-15 and amine-functionalized products. All samples possessed uniform mesopores.

Textual properties calculated by the nitrogen sorption measurement were summarized in Table 4-2. The pore diameter, the BET surface area, and micropore volume were decreased after amine functionalization. The higher the amount of amine functionalization in the sample, the more these values decreased. It suggests that the functionalized amine groups were located inside the

mesopores.[5]

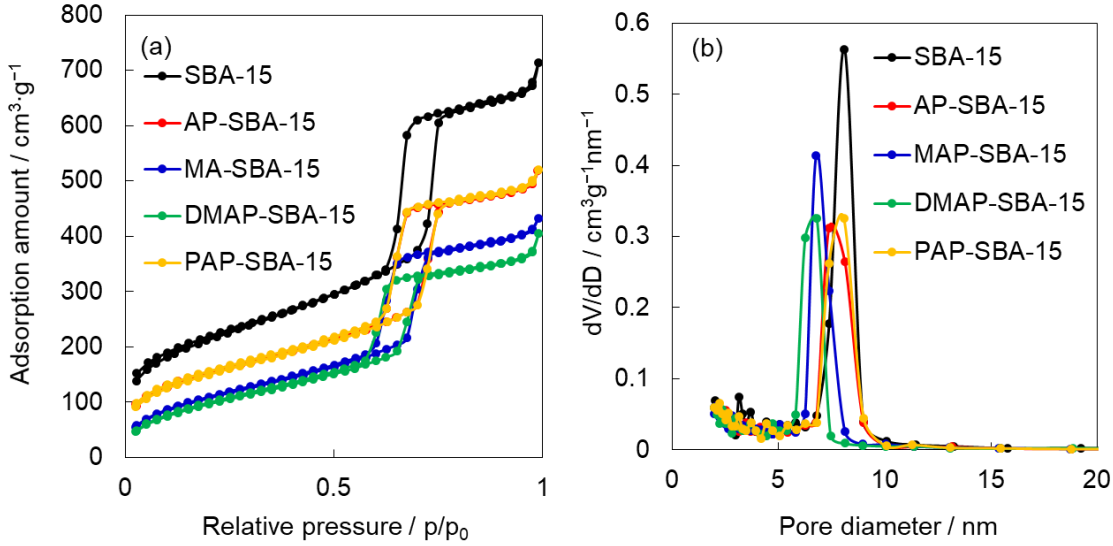

Figure 4-3 (a) N_2 adsorption isotherms and (b) BJH adsorption pore size distribution of SBA-15 and amine-functionalized SBA-15.

Table 4-2 Textual properties of mother SBA-15 and amine-functionalized products calculated from nitrogen sorption measurement.

Product	Pore diameter / nm	BET Surface area / $m^2\ g^{-1}$	Micropore volume / $cm^3\ g^{-1}$
SBA-15	8.1	783	0.10
AP-SBA-15	7.4	548	0.063
MAP-SBA-15	6.8	379	0.0
DMAP-SBA-15	6.8	339	0.0
PAP-SBA-15	8.1	531	0.053

The functional groups in the products were investigated by FT-IR spectroscopy. Figure 4-4 (a) shows FT-IR spectrum of mother SBA-15 in the range from 1300 to 4000 cm^{-1}. The band at 3740 cm^{-1} could be assigned to ν(OH) of Si-OH.[9] The broad band at 3530 cm^{-1} and the bands at 1630 cm^{-1} could be assigned to adsorbed water.[9] Figure 4-4 (b) shows FT-IR spectrum of AP-SBA-15. The bands at 3375 and 3300 cm^{-1} were observed. These bands could be assigned to ν_a(NH) and ν_s(NH) of aliphatic primary amine (C-NH_2).[10] The bands at 2935 and 2870 cm^{-1} were derived from ν_a(CH) and ν_s(CH) of methylene groups, respectively. In the low wavenumber region, bands were observed at 1630, 1600, and 1480–1415 cm^{-1}. These bands could be assigned to ν(OH) of Si-OH, ν(NH) of aliphatic primary amine, δ(CH) of methylene groups, respectively. From the above

results, the surface of AP-SBA-15 is considered to be as shown in Figure 4-1. Figure 4-4 (c) shows FT-IR spectrum of MAP-SBA-15. The FT-IR spectrum of MAP-SBA-15 is similar to that of AP-SBA-15, but there is a difference in that there is only one band around 3320 cm^{-1}. The band could be assigned to ν(NH) of aliphatic secondary amine (C-NH-C). Figure 4-4 (d) shows FT-IR spectrum of DMAP-SBA-15. The FT-IR spectrum of DMAP-SBA-15 is similar to that of AP-SBA-15, but there is a difference in that there is only one broad band around 3400 cm^{-1} assigned to adsorbed water. No peaks derived from tertiary amines were observed.[10] Figure 4-4 (e) shows FT-IR spectrum of PAP-SBA-15. The band at 3320 cm^{-1} could be assigned to ν(CH) of aromatic secondary amine. The bands at 3060 and 3020 cm^{-1} were derived from ν_a(CH) and ν_s(CH) of aromatic rings, respectively. In the low wavenumber region, strong sharp bands were observed at 1602 and 1510 cm^{-1}. These bands could be assigned to ν_a(C=C) and ν_s(C=C) of aromatic rings. Therefore, FT-IR measurements confirmed that the desired amine groups were attached on each surface of SBA-15.

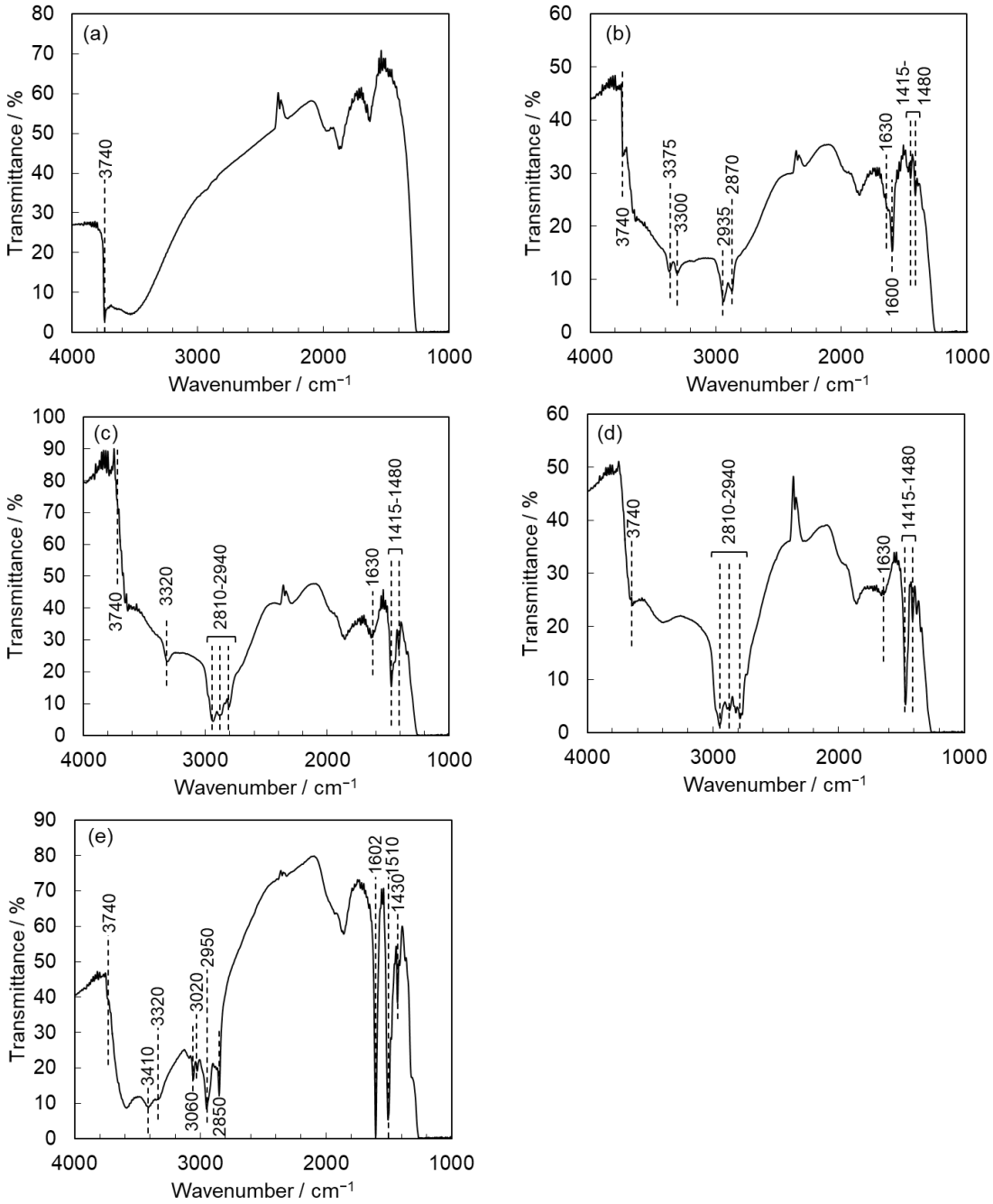

Figure 4-4 FT-IR spectra of products in the range from 1300 to 4000 cm^{-1}. (a) SBA-15, (b) AP-SBA-15, (c) MAP-SBA-15, (d) DMAP-SBA-15 and (e) PAP-SBA-15.

4.3.2 Catalytic reaction

Knoevenagel condensation of benzaldehyde with active methylene compounds was performed as a model reaction. Malononitrile (pK_a : 11.1) and ethyl cyanoacetate (pK_a : 13.1) were used as active methylene compounds.

Figure 4-5 shows the relationship between the yields and the nitrogen content of the catalysts. At every data point, the selectivity towards the desired product, benzalmalononitrile or ethyl α-cyanocinnamate, was over 99%. Therefore, amine-functionalized SBA-15 showed good selectivity for Knoevenagel condensation. In addition, no peak derived from the desorbed aminopropyl group was observed in GC, indicating that amine-functionalized SBA-15 showed good stability.

AP-SBA-15 showed high catalytic activity in the case of both malononitrile (Figure 4-5 (a)) and ethyl cyanoacetate (Figure 4-5 (b)). This trend of AP-SBA-15 was similar to that of NSBA-15. On the other hand, PAP-SBA-15 showed high catalytic activity only in the case of malononitrile. This trend of PAP-SBA-15 was similar to that of PCN. In AP-SBA-15, nitrogen atoms bond with alkyl groups and donates electrons. On the other hand, nitrogen atoms in PAP-SBA-15 bond with phenyl groups, which show electron-withdrawing properties. Therefore, AP-SBA-15 can catalyze a basic reaction involving a higher pK_a reactant than the one that PAP-SBA-15 can handle.

Comparing the catalytic activity of AP-SBA-15 with that of NSBA-15, AP-SBA-15 showed higher catalytic activity than NSBA-15 even though the nitrogen content was lower. AP-SBA-15 showed higher activity than NSBA-15 when compared by primary amine nitrogen content (Figure 4-5 (c)). The reason for the high activity of AP-SBA-15 could be the possibility that the active site of NSBA-15 is difficult to access, effect of surface silanol groups, and that AP-SBA-15 is hydrophobic. While the active sites of AP-SBA-15 are located where bulky molecules such as silane coupling agents can access, the active sites of NSBA-15 are not necessarily located only on the mesopore surface. The silanol protonates the benzaldehyde oxygen while the amine undergoes nucleophilic attack on the carbonyl carbon.[11] The hydrophobicity of catalysts provides two advantages: 1) The water produced by the condensation reaction is released rapidly. 2) Reactants (such as benzaldehyde and ethyl cyanoacetate) can easily access the catalyst surface.[12]

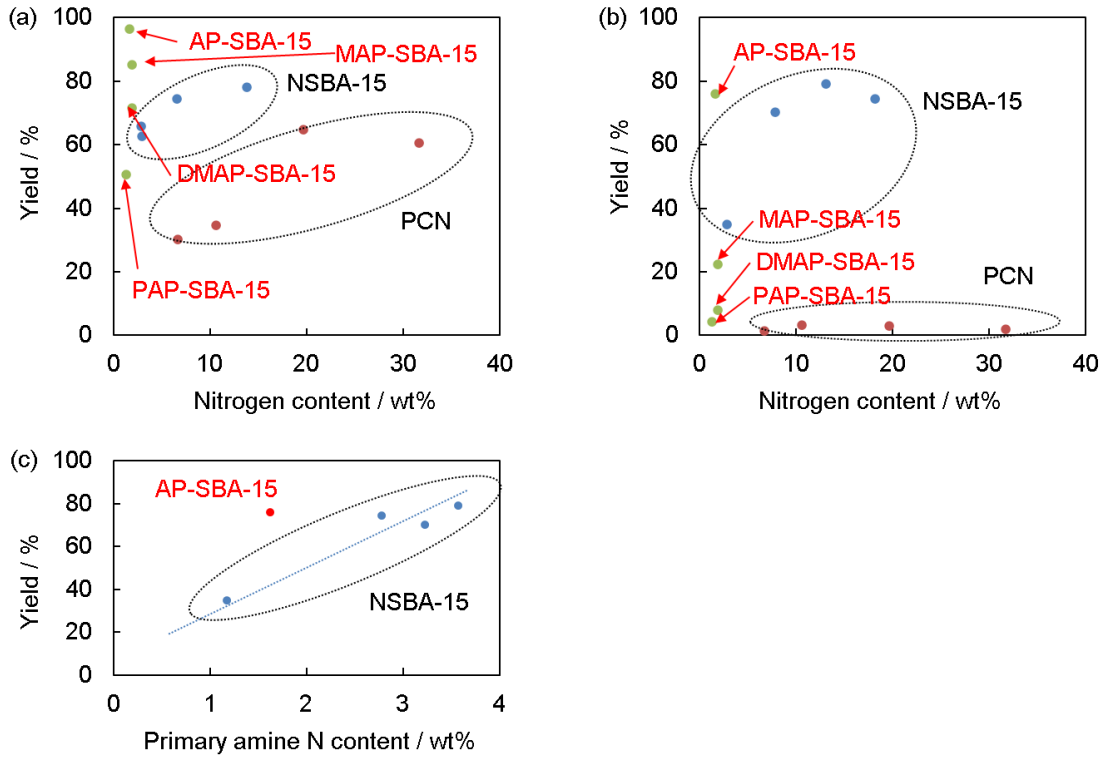

Figure 4-5 The relationship between the yields at three hours after the start of the reaction and the nitrogen content of the catalysts in Knoevenagel condensation between benzaldehyde and (a) malononitrile (pK_a : 11.1) or (b) ethyl cyanoacetate (pK_a : 13.1). (c) The relationship between the yields at three hours after the start of the reaction and the primary amine nitrogen content of the catalysts in Knoevenagel condensation between benzaldehyde and ethyl cyanoacetate. The results of NSBA-15 and PCN were from Chapter 2 and 3.

The order of catalytic activities of aliphatic amine functionalized SBA-15 catalysts for the reactions of benzaldehyde and malononitrile or ethyl cyanoacetate was AP-SBA-15 > MAP-SBA-15 > DMAP-SBA-15 (Figure 4-5). This would be explained by the difference of reaction mechanism.[13-15] Figure 4-6 shows the reaction mechanism of Knoevenagel condensation using AP-SBA-15 which was drawn based on previous reports.[14, 15] First, the primary amine group makes a nucleophilic attack on the aldehyde group of benzaldehyde. After the removal of water, a stable imine intermediate (Schiff-base) is created (step A). In step B, the Schiff-base deprotonates ethyl cyanoacetate resulting in a carbanion that initiates the carbon–carbon coupling (step C). In step D, a proton shifts from the former methylene compound to the nitrogen of primary amine group. Finally, the product is desorbed from the catalyst and the reaction is complete (step E).

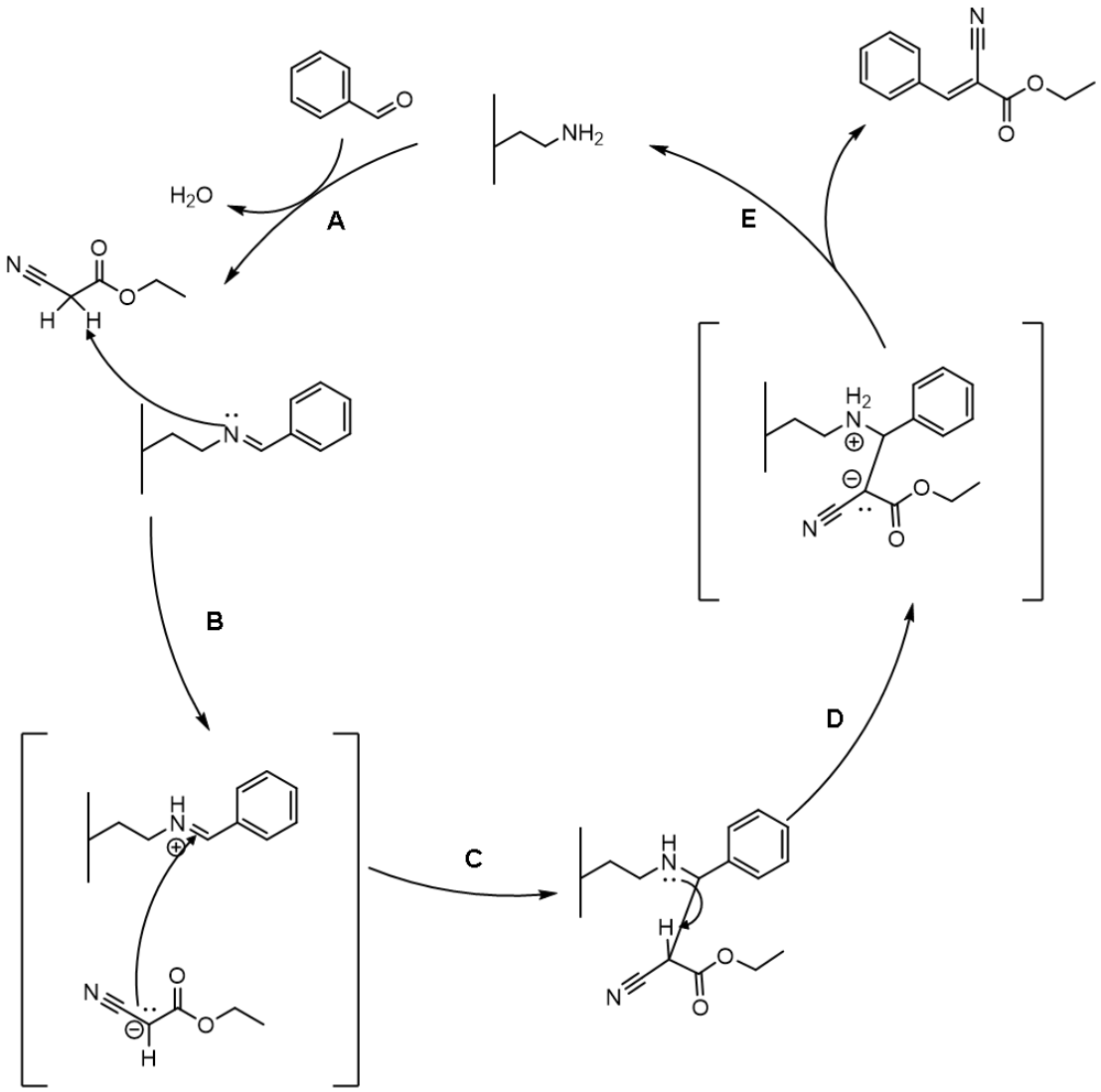

Figure 4-6 Proposed mechanism of the reaction between benzaldehyde and ethyl cyanoacetate catalyzed by AP-SBA-15 (primary amine).

On the other hand, Figure 4-7 shows the reaction mechanism of Knoevenagel condensation using MAP-SBA-15 which was drawn based on previous reports.[15, 16] First, the secondary amine group makes a double nucleophilic attack on the aldehyde group of benzaldehyde. After the removal of water, a stable intermediate is created (step A). In step B, one of the attached secondary amines deprotonates ethyl cyanoacetate. A carbanion is created in step C and then creating a stable intermediate. In step D, a proton shifts from the former methylene compound to the nitrogen of secondary amine group. Finally, the product is desorbed from the catalyst and the reaction is complete (step E). Compared to the case of AP-SBA-15 (Figure 4-6), the type of intermediates is different, and two amine groups are required for the reaction.

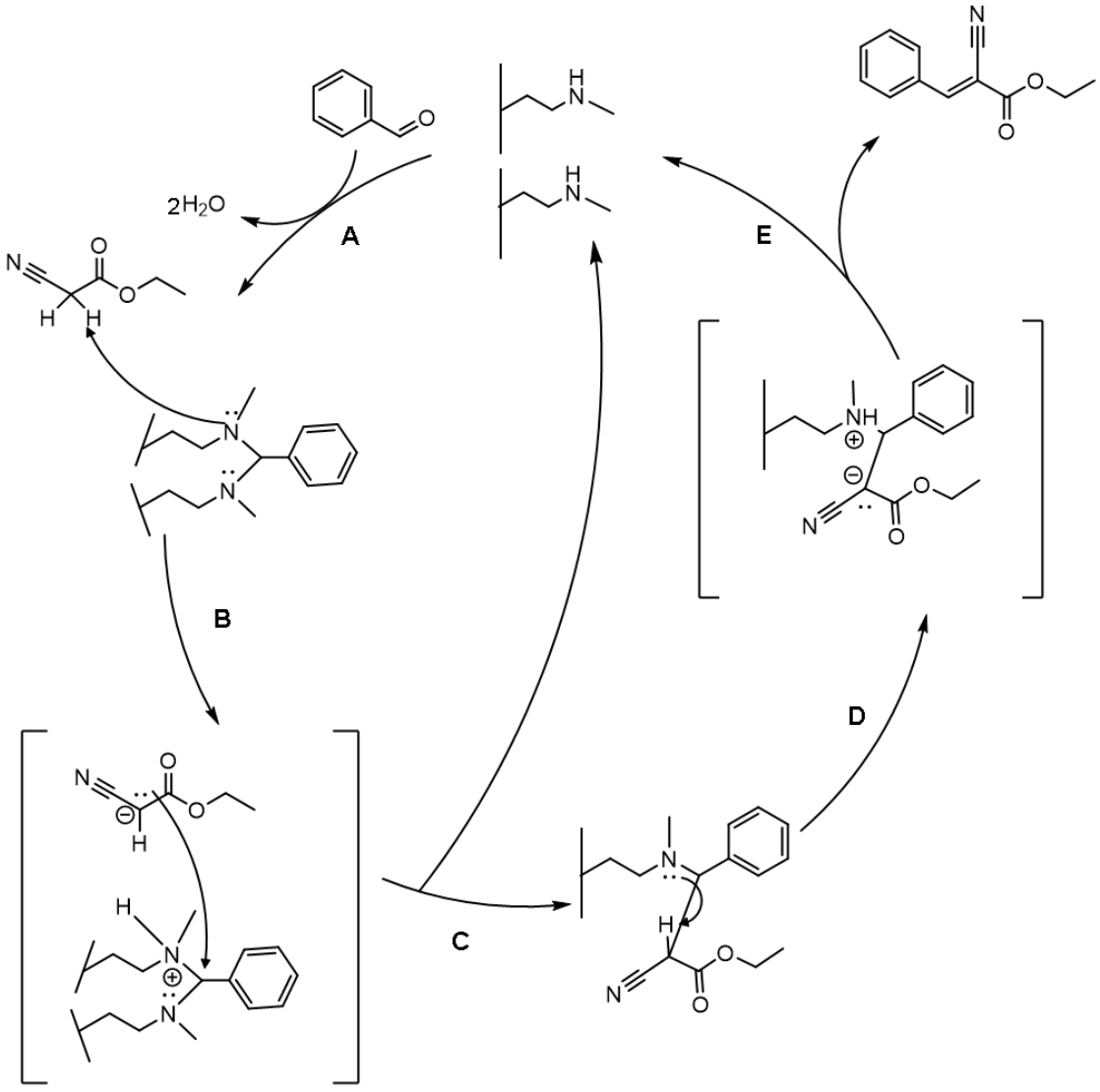

Figure 4-7 Proposed mechanism of the reaction between benzaldehyde and ethyl cyanoacetate catalyzed by MAP-SBA-15 (secondary amine).

Figure 4-8 shows the reaction mechanism of Knoevenagel condensation using DMAP-SBA-15 which was drawn based on previous reports.[14, 15] First, the basic nitrogen extracts the proton from the active methylene compound to form the carbanion (step A). Next, the carbanion and benzaldehyde react (step B). The third step consists of a proton shift, giving an arrangement to a hydroxyl group (step C). Finally, the water and products are desorbed, and the catalyst returns to its original state (step D). In general, it is described that there are no intermediates in the Knoevenagel condensation using tertiary amines.[15] And because of the differences in the intermediates in each reaction, it is assumed that the catalytic activity differs depending on the class of amine.

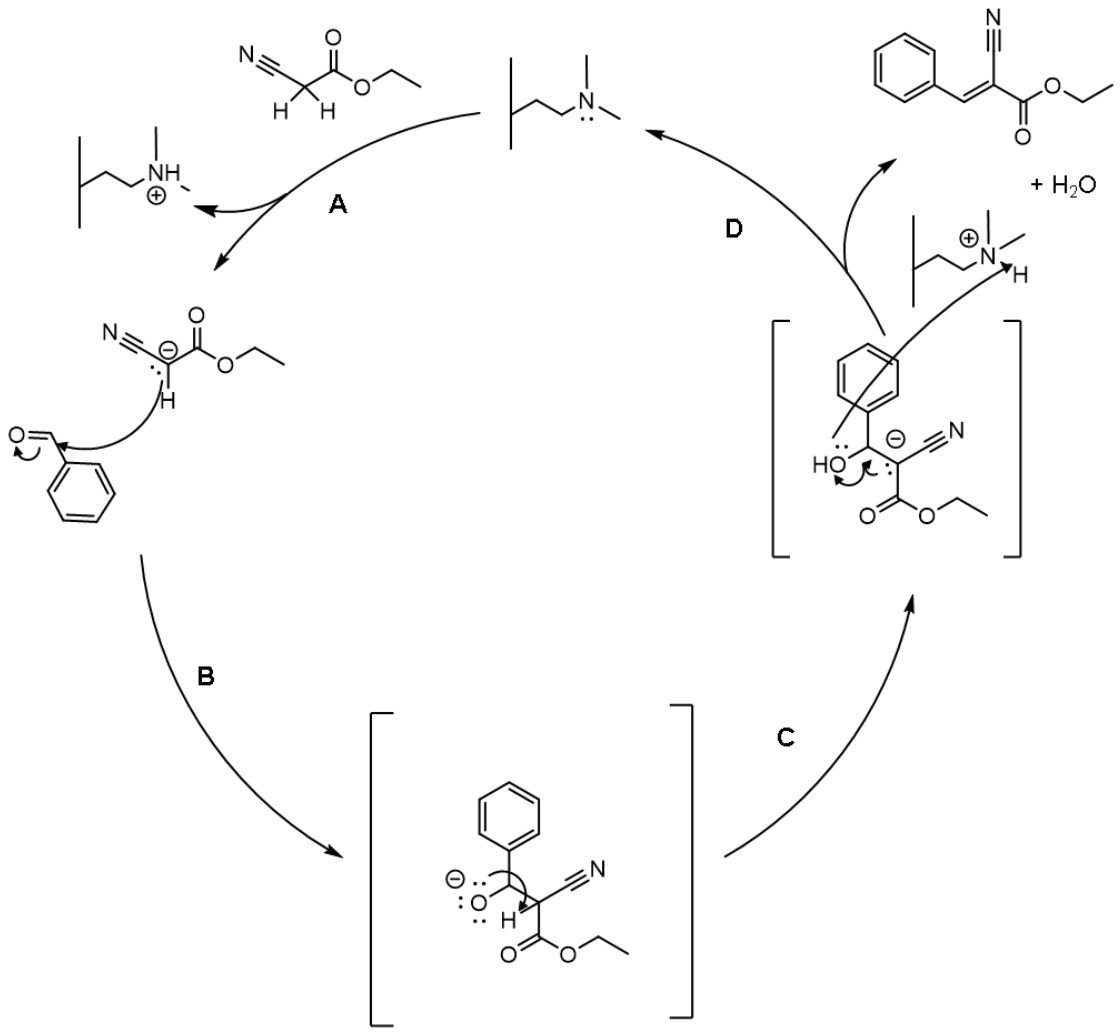

Figure 4-8 Proposed mechanism of the reaction between benzaldehyde and ethyl cyanoacetate catalyzed by DMAP-SBA-15 (tertiary amine).

In order to compare the catalytic properties of SBA-15, nitrided SBA-15 (NSBA-15), amine-functionalized SBA-15, and methylated nitrided SBA-15 (MeNSBA-15), Knoevenagel condensation of benzaldehyde and diethyl malonate was performed (Table 4-3). In previous report, SBA-15 and nitrided SBA-15 cannot catalyze the reaction. On the other hand, MeNSBA-15, AP-SBA-15, and MAP-SBA-15 catalyzed the reaction. Therefore, the secondary amine connected to carbon atoms (the C-NH-C species) is more active than the secondary amine connected to silicon atoms (the Si-NH-Si species) for Knoevenagel condensation.

Table 4-3 The relationship between the yield at 24 hours after the start of the reaction and the amount of active sites of the catalysts in Knoevenagel condensation between benzaldehyde and diethyl malonate.

Catalyst	Amount of active sites / mmol·g^{-1}	Yield / %
SBA-15, NSBA-15[17]	0.0*1	0.0
MeNSBA-15[17]	3.2*1	14.7
AP-SBA-15	1.2*2	16.9
MAP-SBA-15	1.4*2	10.2
DMAP-SBA-15	1.4*2	0.36

*1 amount of methylated nitrogen sites (Si-N(-CH_3)-Si) measured by elemental analysis

*2 amount of functionalized amine measured by elemental analysis

The percentage of nitrogen remaining before and after the reaction was compared. The used catalysts were collected by filtration of reaction liquid after catalytic reaction, washed by ethanol, and dried at 373 K. The nitrogen contents of catalysts before and after catalytic reaction are showed in Figure 4-9. Almost all nitrogen atoms remained after the reaction test in AP-SBA-15, but only two-thirds nitrogen atoms remained in NSBA-15-973. Si-N bond is easily hydrolyzed. So, Si-N bond in NSBA-15 was hydrolyzed by water formed by Knoevenagel condensation. Therefore, NSBA-15 showed lower catalytic stability than AP-SBA-15. The reuse tests have not been conducted yet. However, the catalytic stability of aminopropyl modified MCM-41 was reported.[3] The conversion kept 95% within three repeated runs of Knoevenagel condensation between benzaldehyde and diethyl malonate. Therefore, AP-SBA-15 is considered to be a reusable catalyst.

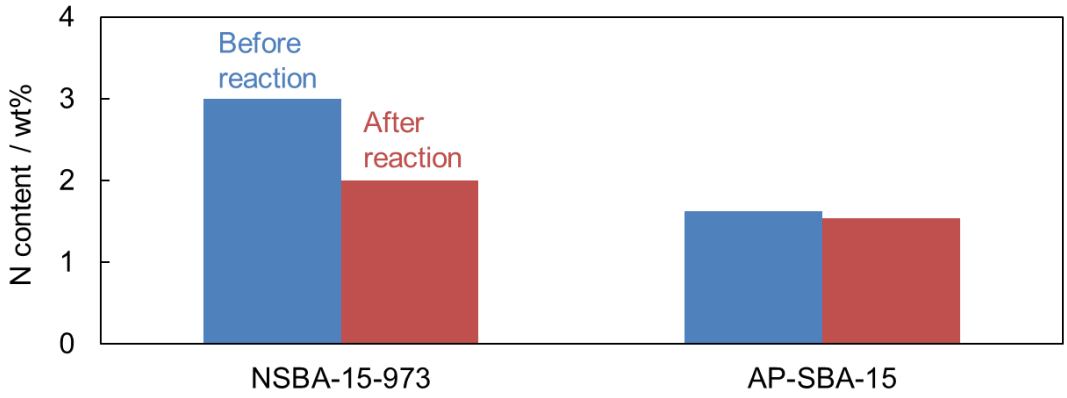

Figure 4-9 Nitrogen content of NSBA-15-973 and AP-SBA-15 before and after the reaction test.

4.4 Conclusions

AP-SBA-15, MAP-SBA-15, DMAP-SBA-15 and PAP-SBA-15 were prepared by functionalizing SBA-15 with aminopropyl, methyl aminopropyl, dimethyl aminopropyl and phenyl aminopropyl groups using silane coupling agents. Elemental analysis and FT-IR measurement revealed that the desired amine groups were functionalized. Amine-functionalized SBA-15 showed high selectivity and stability for Knoevenagel condensation. Aliphatic amine functionalized SBA-15 (AP-SBA-15, MAP-SBA-15, and DMAP-SBA-15) showed higher catalytic activity than aromatic amine functionalized SBA-15 (PAP-SBA-15) for Knoevenagel condensation probably because of the electron-donating groups. The order of catalytic activities of aliphatic amine functionalized SBA-15 catalysts for the reactions of benzaldehyde and malononitrile or ethyl cyanoacetate was AP-SBA-15 > MAP-SBA-15 > DMAP-SBA-15. Comparison between amine-functionalized SBA-15 and nitrided SBA-15 revealed that alkyl amines are more active and durable than silanamines.

References

[1] Y. Ono, H. Hattori, Solid Base Catalysis, Springer Berlin Heidelberg, 2012.

[2] T. Yokoi, Y. Kubota, T. Tatsumi, Amino-functionalized mesoporous silica as base catalyst and adsorbent, Applied Catalysis a-General, 421 (2012) 14-37.

[3] K.M. Parida, D. Rath, Amine functionalized MCM-41: An active and reusable catalyst for Knoevenagel condensation reaction, Journal of Molecular Catalysis a-Chemical, 310 (2009) 93-100.

[4] D.J. Macquarrie, R. Maggi, A. Mazzacani, G. Sartori, R. Sartorio, Understanding the influence of the immobilization procedure on the catalytic activity of aminopropylsilicas in C-C forming reactions, Applied Catalysis a-General, 246 (2003) 183-188.

[5] M. Geszke-Moritz, M. Moritz, APTES-modified mesoporous silicas as the carriers for poorly water-soluble drug. Modeling of diflunisal adsorption and release, Applied Surface Science, 368 (2016) 348-359.

[6] X.F. Zhang, E.S.M. Lai, R. Martin-Aranda, K.L. Yeung, An investigation of Knoevenagel condensation reaction in microreactors using a new zeolite catalyst, Applied Catalysis a-General, 261 (2004) 109-118.

[7] L.N. Zhang, H. Wang, W.Z. Shen, Z.F. Qin, J.G. Wang, W.B. Fan, Controlled synthesis of graphitic carbon nitride and its catalytic properties in Knoevenagel condensations, Journal of Catalysis, 344 (2016) 293-302.

[8] H. Liu, H. Yu, P. Jin, M. Jiang, G. Zhu, Y. Duan, Z. Yang, H. Qiu, Preparation of mesoporous silica materials functionalized with various amino-ligands and investigation of adsorption performances on aromatic acids, Chemical Engineering Journal, 379 (2020).

[9] Y.D. Xia, R. Mokaya, Highly ordered mesoporous silicon oxynitride materials as base catalysts, Angewandte Chemie-International Edition, 42 (2003) 2639-2644.

[10] J.M. Celedonio, J.H. Park, Y.S. Ko, FT-IR study on CO_2 adsorbed species of CO_2 sorbents, Research on Chemical Intermediates, 42 (2016) 141-154.
[11] S.L. Hruby, B.H. Shanks, Acid-base cooperativity in condensation reactions with functionalized mesoporous silica catalysts, Journal of Catalysis, 263 (2009) 181-188.
[12] X.C. Wang, J. Li, G.J. Chen, Z.J. Guo, Y. Zhou, J. Wang, Hydrophobic Mesoporous Poly(ionic liquid)s towards Highly Efficient and Contamination-Resistant Solid-Base Catalysts, Chemcatchem, 7 (2015) 993-1003.
[13] Y. Kubota, Y. Nishizaki, H. Ikeya, M. Saeki, T. Hida, S. Kawazu, M. Yoshida, H. Fujii, Y. Sugi, Organic-silicate hybrid catalysts based on various defined structures for Knoevenagel condensation, Microporous and Mesoporous Materials, 70 (2004) 135-149.
[14] G. Sartori, F. Bigi, R. Maggi, R. Sartorio, D.J. Macquarrie, M. Lenarda, L. Storaro, S. Coluccia, G. Martra, Catalytic activity of aminopropyl xerogels in the selective synthesis of (E)-nitrostyrenes from nitroalkanes and aromatic aldehydes, Journal of Catalysis, 222 (2004) 410-418.
[15] K. van Beurden, S. de Koning, D. Molendijk, J. van Schijndel, The Knoevenagel reaction: a review of the unfinished treasure map to forming carbon-carbon bonds, Green Chemistry Letters and Reviews, 13 (2020) 85-100.
[16] A. Lee, A. Michrowska, S. Sulzer-Mosse, B. List, The Catalytic Asymmetric Knoevenagel Condensation, Angewandte Chemie-International Edition, 50 (2011) 1707-1710.
[17] K. Sugino, N. Oya, N. Yoshie, M. Ogura, A Simple Modification Creates a Great Difference: New Solid-Base Catalyst Using Methylated N-Substituted SBA-15, Journal of the American Chemical Society, 133 (2011) 20030-20032.

Chapter 5. Evaluation of basicity by CO_2 adsorption

5.1 Introduction

Adsorption of acidic molecules such as CO_2, benzoic acid and phenol is one of the typical tools for evaluating basicity.[1] Since the CO_2 molecule is smaller than the substrates used in the catalytic reactions, the basicity of the sample can be evaluated without being affected by steric hindrance.

In this section, the catalysts prepared in previous chapters were evaluated by CO_2 probe FT-IR at ambient temperature. Comparing the results of the CO_2 probe FT-IR with those of the catalytic reaction, the results agreed that the silica with aliphatic amines had stronger basicity.

5.2 Experimental

The FT-IR spectra of the products were collected by a 4100 FT-IR spectrometer (JASCO).

15 mg of samples (SBA-15 and NSBA-15-973-2 prepared in Chapter 2 and amine-functionalized SBA-15 prepared in Chapter 4) were pressed into a self-supporting disk of 20 mm diameter and placed in a quartz IR cell. In the case of PCN-600 (prepared in Chapter 3), 0.30 mg of samples and 30 mg of binder fumed silica (Aldrich, pre-treated with deionized water and agglomerated by drying overnight at 393 K in the air) [2] was mixed. The mixture was pressed into a self-supporting disk of 20 mm diameter and placed in a quartz IR cell.

The sample was pretreated by evacuation at 423 K for 1.5 h and the spectra were recorded at room temperature under vacuum condition with a resolution of 4.0 cm^{-1}. Highly pure CO_2 gas (99.995%, Taiyo Nippon Sanso Corp.) was introduced into the cell. The introduce pressure of CO_2 was 6.0 torr. After more than 10 minutes from the introduction of CO_2 gas, the cell was evacuated.

5.3 Results and Discussion

Figure 5-1 shows time-resolved FT-IR difference spectra of SBA-15 for CO_2 adsorption. After the introduction of CO_2 gas, a peak at 2345 cm^{-1} was observed (Figure 5-1(a)). The peak was derived from linear CO_2 molecules hydrogen bonded to silanol groups in SBA-15 (Figure 5-2).[1, 3-6] A peak around 1625 cm^{-1} was also observed after the introduction of CO_2 gas. The peak was derived from adsorbed water. After the evacuation, the peak at 2345 cm^{-1} decreased with time (Figure 5-1(b)).

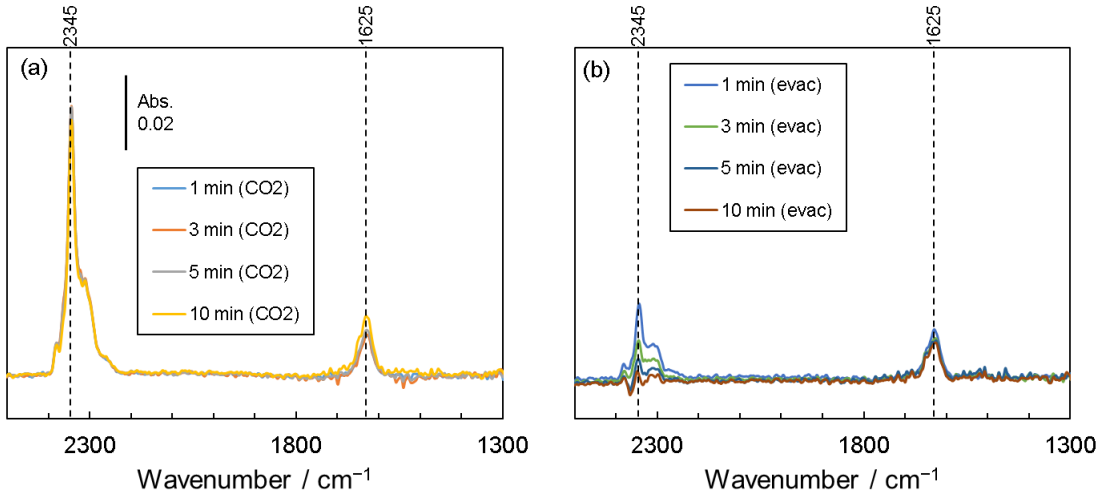

Figure 5-1 Time-resolved CO_2 probe FT-IR difference spectra of SBA-15 measured at ambient temperature. 6.0 torr CO_2 was introduced. Spectra at 1 min, 3 min, 5 min, and 10 min are shown (a) after CO_2 introduction and (b) after evacuation.

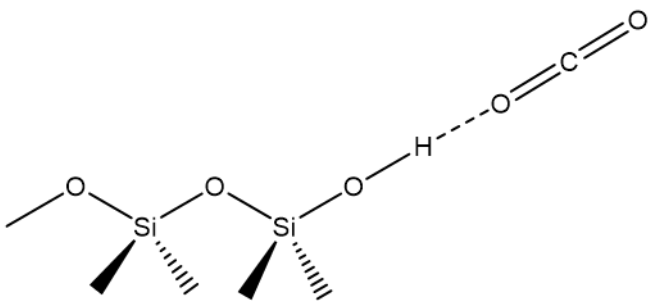

Figure 5-2 Schematic diagram of CO_2 adsorption on SBA-15.

Figure 5-3 shows time-resolved FT-IR difference spectra of NSBA-15-973-2 for CO_2 adsorption. After the introduction of CO_2 gas, a peak at 2345 cm^{-1} was observed (Figure 5-3(a)). The peak was derived from hydrogen bonds between CO_2 molecules and silanol groups or silanamine groups in NSBA-15 (Figure 5-4).[1] A peak around 1622 cm^{-1} was also observed after the introduction of CO_2 gas. The peak was derived from adsorbed water. After the evacuation, the peak at 2345 cm^{-1} decreased with time (Figure 5-3 (b)). A negative spectrum at 1622 cm^{-1} was observed after the evacuation. It is assumed that water was still adsorbed on this sample after pretreatment and that the adsorbed water was desorbed by the evacuation.

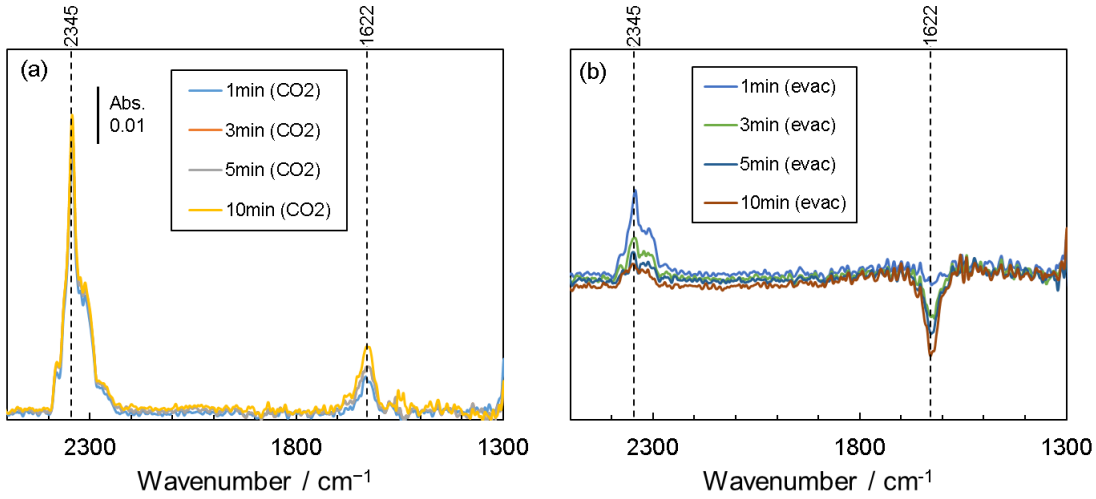

Figure 5-3 Time-resolved CO_2 probe FT-IR difference spectra of NSBA-15-973-2 measured at ambient temperature. 6.0 torr CO_2 was introduced. Spectra at 1 min, 3 min, 5 min, and 10 min are shown (a) after CO_2 introduction and (b) after evacuation.

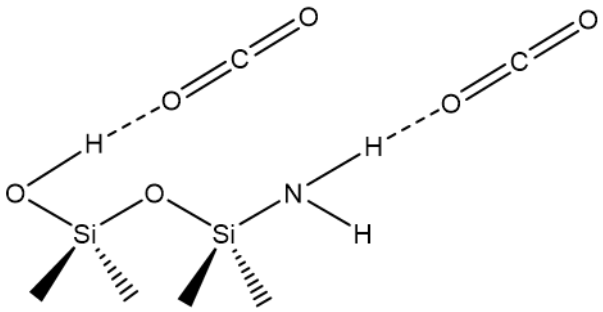

Figure 5-4 Schematic diagram of CO_2 adsorption on NSBA-15.

Figure 5-5 shows typical FT-IR difference spectra of SiO_2 used as a binder for PCN. Almost no hydrogen bonds were formed between this material and CO_2. Therefore, SiO_2 as the binder does not seem to affect the CO_2 probe FT-IR measurement of PCN.

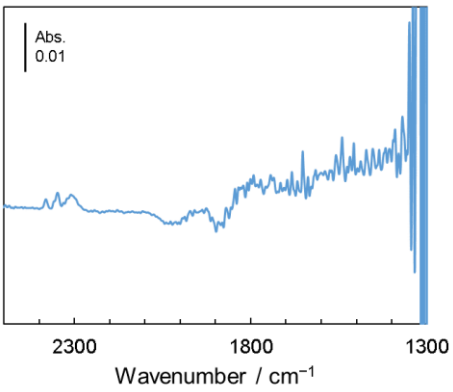

Figure 5-5 CO_2 probe FT-IR difference spectra of SiO_2 measured at ambient temperature. 6.0 torr CO_2 was introduced.

Figure 5-6 shows time-resolved FT-IR difference spectra of PCN-600 for CO_2 adsorption. After the introduction of CO_2 gas, a peak at 2345 cm^{-1} was observed (Figure 5-6(a)). The peak might be derived from hydrogen bonds between CO_2 molecules and amine groups in PCN. No peak derived from adsorbed water was observed suggesting that the surface of PCN is hydrophobic. After the evacuation, the peak at 2345 cm^{-1} decreased with time (Figure 5-6(b)).

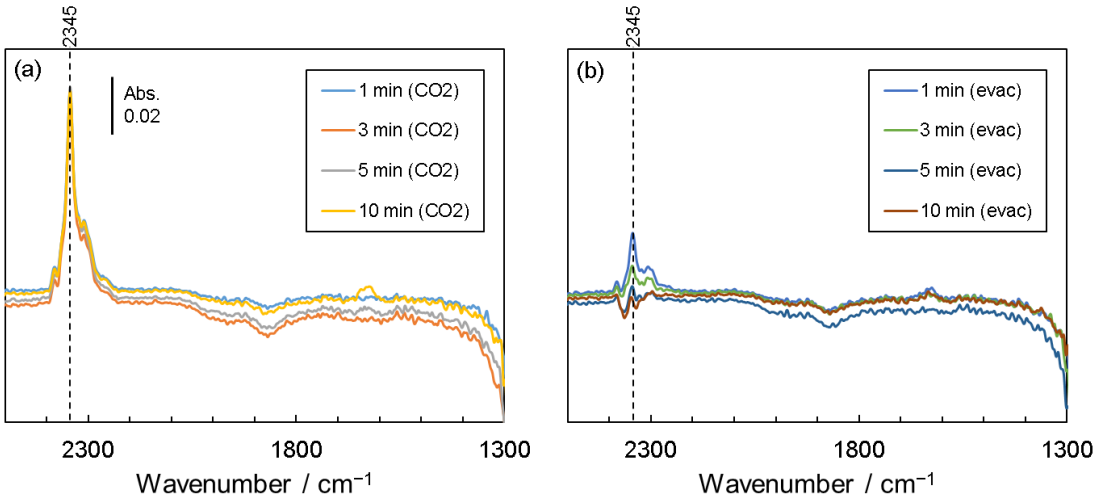

Figure 5-6 Time-resolved CO_2 probe FT-IR difference spectra of PCN-600 measured at ambient temperature. 6.0 torr CO_2 was introduced. Spectra at 1 min, 3 min, 5 min, and 10 min are shown (a) after CO_2 introduction and (b) after evacuation.

Figure 5-7 shows FT-IR difference spectra of each amine functionalized SBA-15 for CO_2 adsorption. A broad peak was observed at around 2345 cm^{-1} in all samples. The peak was derived from hydrogen bonds between CO_2 molecules and silanol groups or amine groups in

amine-functionalized SBA-15.[1] Figure 5-8 shows FT-IR difference spectra above 2500 cm^{-1}. In the case of AP-SBA-15 (Figure 5-8(a)), the bands at 3370, 2935, and 2870 cm^{-1} were observed. The bands could be assigned to ν_a(NH) of aliphatic primary amine (C-NH_2), ν_a(CH), and ν_s(CH) of methylene groups, respectively.[7] In the case of MAP-SBA-15, (Figure 5-8(b)), the band at 3320 cm^{-1} was observed. The band could be assigned to ν(NH) of aliphatic secondary amine (C-NH-C). The bands at 2940, 2860 and 2810 cm^{-1} were derived from ν(CH) of methylene groups. Therefore, it is thought that CO_2 molecules are hydrogen-bonded to the amine and alkyl groups (Figure 5-9). Furthermore, in the case of AP-SBA-15 and MAP-SBA-15, five bands were observed in the range of 1380-1620 cm^{-1}. The bands at 1620, 1430-1440, 1385-1390 cm^{-1} could be assigned to δ(NH) of NH_3^+ species.[8] The bands at 1540-1560 and 1490-1495 cm^{-1} could be assigned to ν_a(CO) and ν_s(CO) of CO_2^- species.[8] Therefore, carbamate species (Figure 5-10) would be formed on the surface of AP-SBA-15 and MAP-SBA-15 (Figure 5-9). It indicates that strong bond between amine sites and CO_2 molecules formed in AP-SBA-15 and MAP-SBA-15. This result indicates that AP-SBA-15 and MAP-SBA-15 possess a stronger basicity than NSBA-15, PCN, tertiary alkyl amine sites and aromatic amine sites. The result is consistent with the results of the Knoevenagel condensation between benzaldehyde and diethyl malonate in Chapter 3 and 4. In PAP-SBA-15, peaks at 1602 cm^{-1} and 1510 cm^{-1} were observed. The peaks might be derived from interaction of phenyl groups with CO_2.

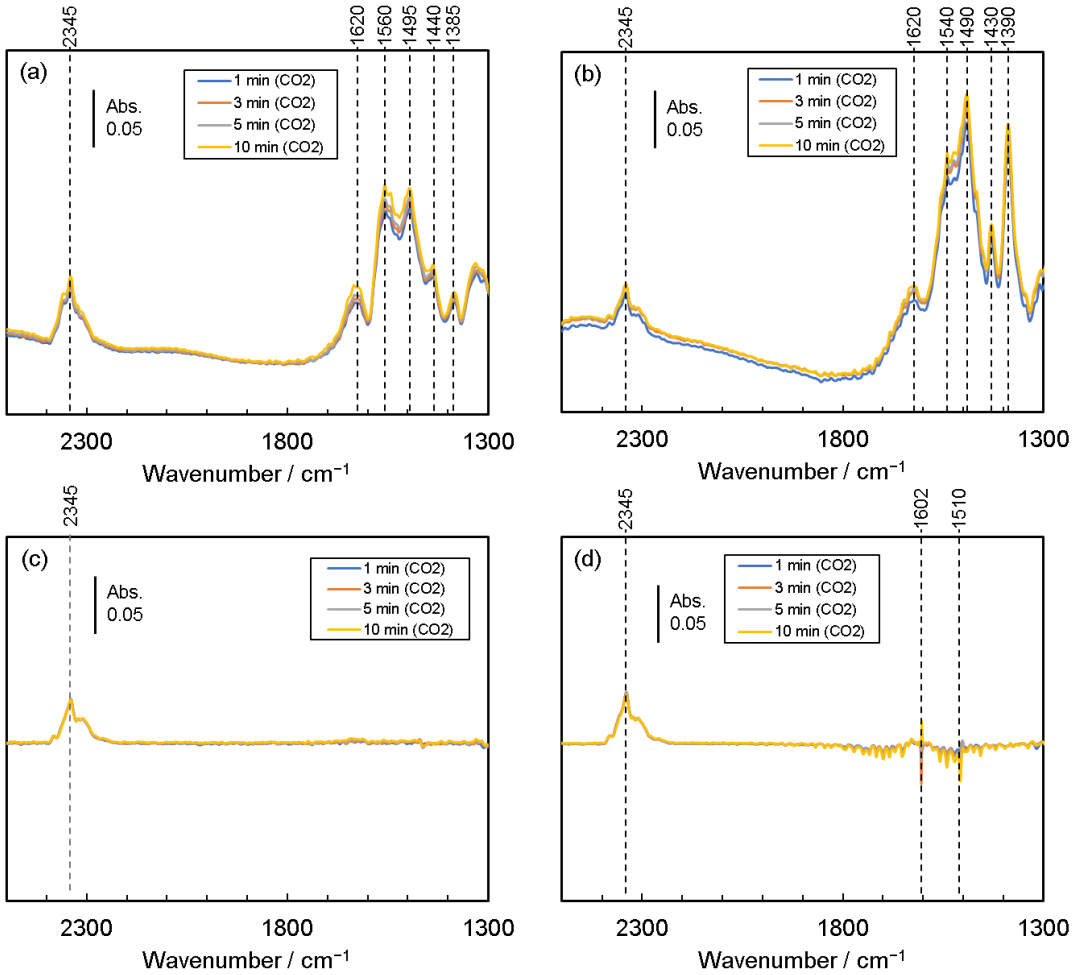

Figure 5-7 Time-resolved CO_2 probe FT-IR difference spectra of (a) AP-SBA-15, (b) MAP-SBA-15, (c) DMAP-SBA-15, and (d) PAP-SBA-15 measured at ambient temperature. 6.0 torr CO_2 was introduced. Spectra at 1 min, 3 min, 5 min, and 10 min are shown after CO_2 introduction.

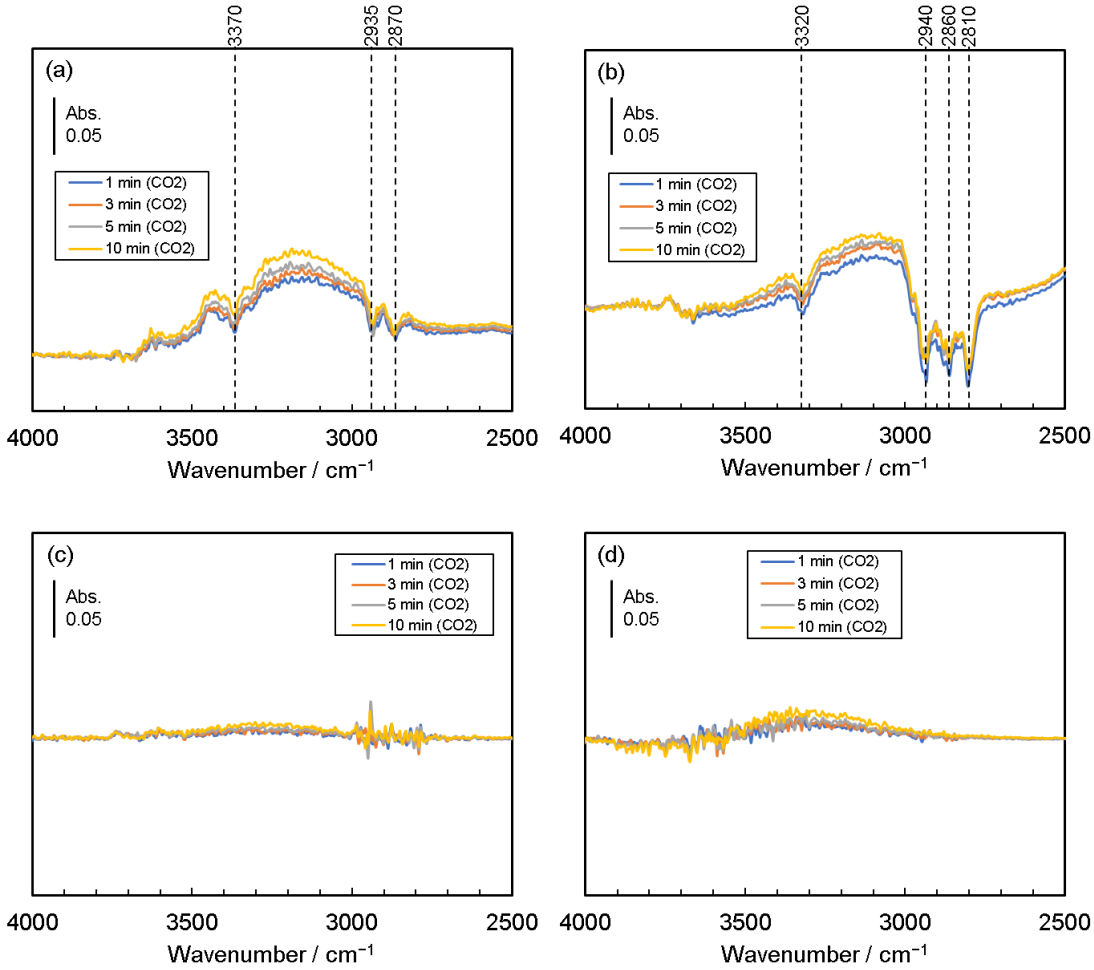

Figure 5-8 Time-resolved CO_2 probe FT-IR difference spectra (higher wavenumber) of (a) AP-SBA-15, (b) MAP-SBA-15, (c) DMAP-SBA-15, and (d) PAP-SBA-15 measured at ambient temperature. 6.0 torr CO_2 was introduced. Spectra at 1 min, 3 min, 5 min, and 10 min are shown after CO_2 introduction.

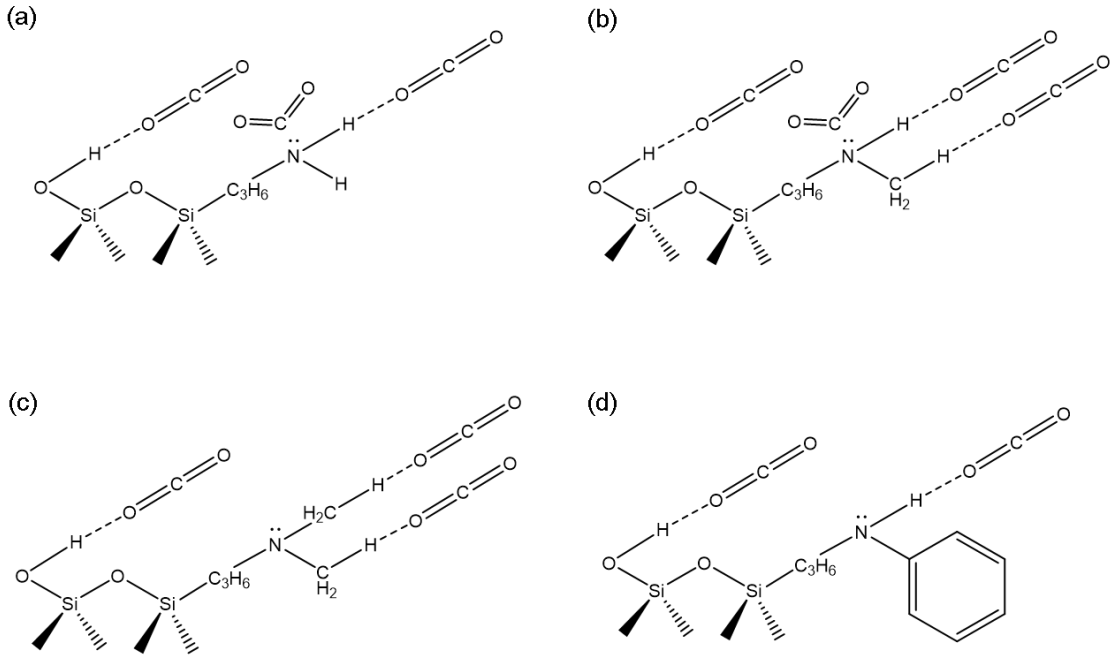

Figure 5-9 Schematic diagram of CO_2 adsorption on (a) AP-SBA-15, (b) MAP-SBA-15, (c) DMAP-SBA-15 and (d) PAP-SBA-15.

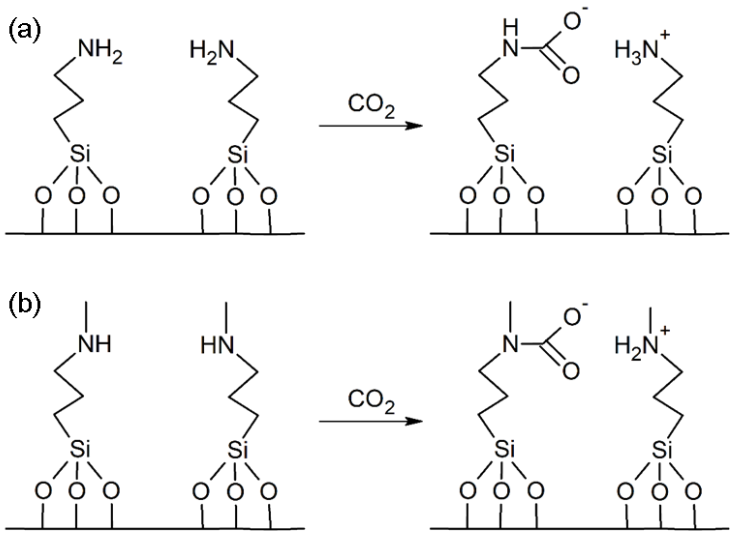

Figure 5-10 Structure of carbamate species on (a) AP-SBA-15 and (b) MAP-SBA-15.

Figure 5-11 shows FT-IR difference spectra of each amine functionalized SBA-15 for CO_2 adsorption after the evacuation. It was observed that the peaks derived from CO_2 decreased with time.

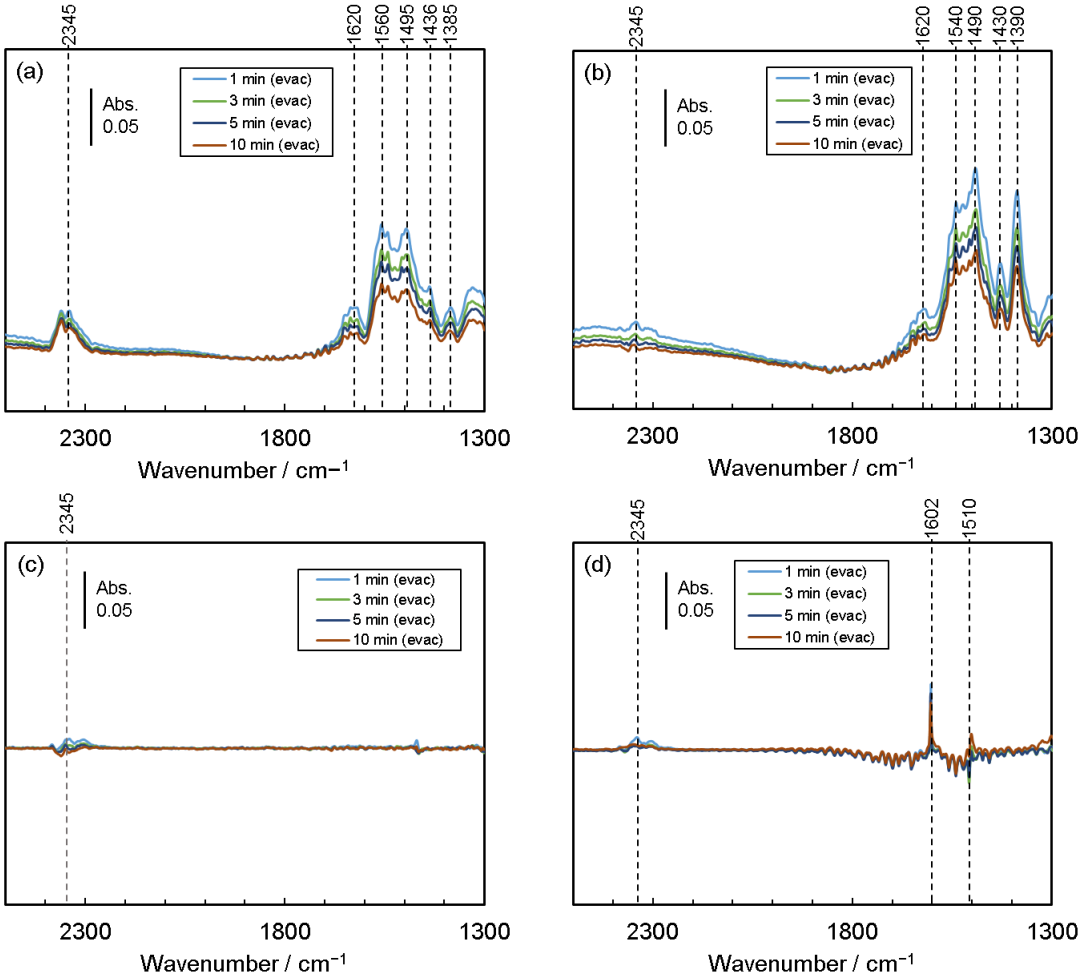

Figure 5-11 Time-resolved CO_2 probe FT-IR difference spectra of (a) AP-SBA-15, (b) MAP-SBA-15, (c) DMAP-SBA-15, and (d) PAP-SBA-15 measured at ambient temperature. 6.0 torr CO2 was introduced. Spectra at 1 min, 3 min, 5 min, and 10 min are shown after evacuation.

To evaluate the basicity of each sample, the rate of adsorption and desorption of CO_2 was investigated. Figure 5-12 shows the change in the intensity of the peak at 2345 cm^{-1}. In Figure 5-12 (b), the value for 10 minutes after the introduction is used as the value for 5 seconds after the evacuation. Assuming that adsorption of CO_2 is a first-order reaction, the rate constant k was calculated (Table 5-1). Figure 5-13 shows the relationship between CO_2 adsorption and catalytic activity investigated in Chapter 2, 3, and 4. A proportional relationship between CO_2 adsorption and catalytic activity was observed.

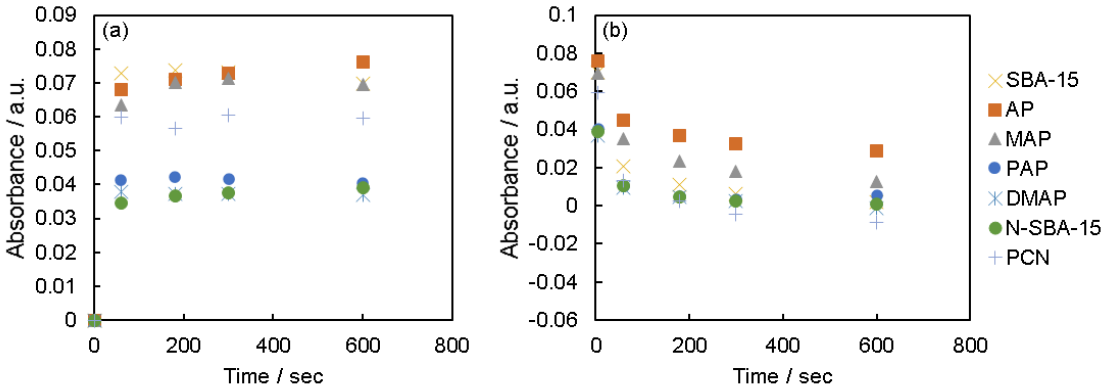

Figure 5-12 Change in the intensity of the peak at 2345cm^{-1} (a) after CO_2 introduction and (b) after evacuation.

Table 5-1 Rate constants and equilibrium constants of CO_2 adsorption on SBA-15, nitrided SBA-15, PCN, and amine-functionalized SBA-15.

Samples	k / s^{-1} *1	k' / s^{-1} *2	$K = k/k'$
SBA-15	2.51×10^{-5}	2.20×10^{-2}	1.14×10^{-3}
NSBA-15	3.29×10^{-4}	2.35×10^{-2}	1.40×10^{-2}
PCN	3.49×10^{-5}	2.43×10^{-2}	1.43×10^{-3}
AP-SBA-15	4.80×10^{-4}	9.67×10^{-3}	4.96×10^{-2}
MAP-SBA-15	5.97×10^{-4}	1.25×10^{-2}	2.37×10^{-2}
DMAP-SBA-15	0	2.44×10^{-2}	0
PAP-SBA-15	1.67×10^{-4}	2.47×10^{-2}	6.76×10^{-3}

*1 Calculated in the range of 60–300 s

*2 Calculated in the range of 5–60 s

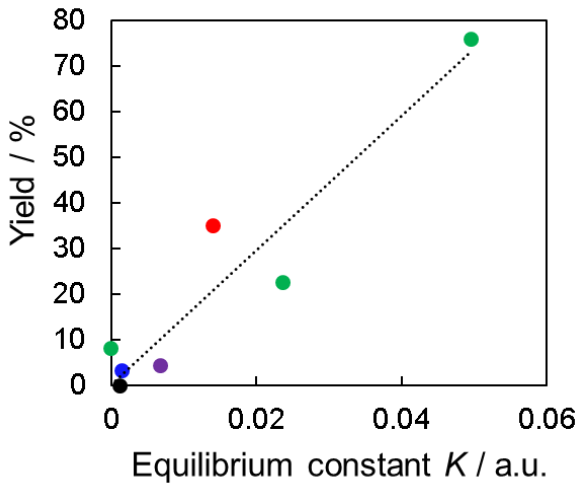

Figure 5-13 The relationship between the yields at three hours after the start of the reaction in Knoevenagel condensation between benzaldehyde and ethyl cyanoacetate and equilibrium constant *K* of CO_2 adsorption. Black point, red point, blue point, green points and purple point show the result of SBA-15, NSBA-15, PCN, aliphatic amine functionalized SBA-15, and aromatic amine functionalized SBA-15, respectively. The dashed lines joining the points are approximation curves.

First, comparing aliphatic and aromatic amines, the aliphatic amine showed larger values in both measurements. This is probably due to the electron-donating properties of the functional groups. Then, comparing AP-SBA-15 and NSBA-15, AP-SBA-15 showed larger values in CO_2 adsorption without the influence of surface silanol groups or steric hindrance. Therefore, the higer catalytic activity of AP-SBA-15 than NSBA-15 could be attributed to hydrophobicity. Comparing AP-SBA-15 and MAP-SBA-15, AP-SBA-15 showed a larger value of *K*, similar to the catalytic reaction, suggesting that AP-SBA-15 is stronger basic than MAP-SBA-15 since there is no effect of intermediates on CO_2 adsorption. In addition to the equilibrium constants compared in this study, primary amines have been reported to adsorb CO_2 more readily than secondary amines by comparing amine efficiency[9, 10] and heat of adsorption.[11] This tendency is thought to be due to the steric hindrance caused by the functional groups attached to the nitrogen atoms. From the viewpoint of computational chemistry, I discussed the effect of functional groups. The activation energies of CO_2 adsorption with propylamine (a primary amine) and methylpropylamine (a secondary amine) were calculated by DFT calculation (Figure 5-14). The activation energy for the secondary amine was larger than that for the primary amine. In general, it is thought that the base strength of secondary amines is larger and the activation energy is smaller due to the electron donation of the methyl group. This reverse trend is thought to be due to steric hindrance.

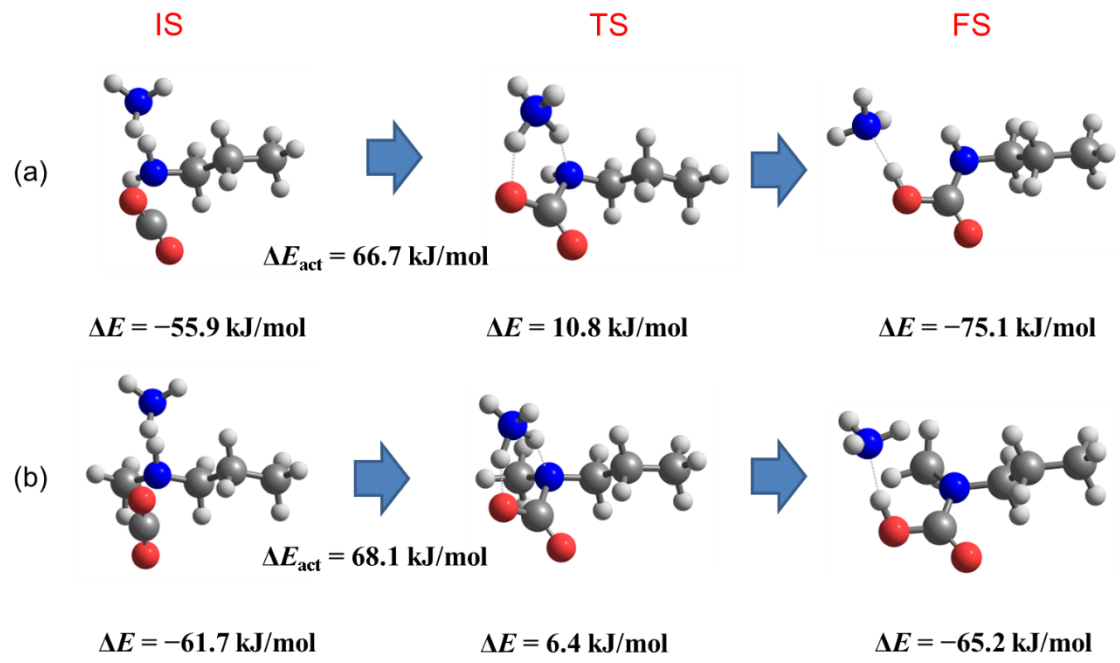

Figure 5-14 Initial state, transition state, and final state of CO_2 adsorption with (a) propylamine or (b) methylpropylamine. $\Delta E = E_{total} - E(C_3H_7NH_2) - E(CO_2) - E(NH_3)$. The ammonia molecules are receptors for protons.

5.4 Conclusions

The nitrogen-containing materials prepared in Chapter 2, 3, and 4 was evaluated by CO_2 probe FT-IR at ambient temperature. The peaks derived from carbamate species were observed in AP-SBA-15 and MAP-SBA-15. Therefore, AP-SBA-15 and MAP-SBA-15 are considered to be highly basic than other catalysts, and this result is consistent with the catalytic reaction in Chapter 4. A proportional relationship between CO_2 adsorption and catalytic activity was observed. It suggests that higher activity of C-NH_2 than that of Si-NH_2 probably due to hydrophobicity and that higher activity of primary amine than that of secondary amine probably due to not only intermediate but also steric hinderance.

References

[1] M. Ogura, S. Fukuzawa, S. Fukunaga, H. Yamazaki, J.N. Kondo, M. Morimoto, R. Guillet-Nicolas, M. Thommes, Identification of the Basic Sites on Nitrogen-Substituted Microporous and Mesoporous Silicate Frameworks Using CO_2 as a Probe Molecule, Langmuir, 34 (2018) 1376-1385.

[2] R.A. Iloy, K. Jalama, Effect of Operating Temperature, Pressure and Potassium Loading on the Performance of Silica-Supported Cobalt Catalyst in CO_2 Hydrogenation to Hydrocarbon Fuel, Catalysts, 9 (2019).

[3] G. Ramis, G. Busca, V. Lorenzelli, LOW-TEMPERATURE CO_2 ADSORPTION ON METAL-OXIDES - SPECTROSCOPIC CHARACTERIZATION OF SOME WEAKLY ADSORBED SPECIES, Materials Chemistry and Physics, 29 (1991) 425-435.

[4] G.D. Pirngruber, P. Raybaud, Y. Belmabkhout, J. Cejka, A. Zukal, The role of the extra-framework cations in the adsorption of CO_2 on faujasite Y, Physical Chemistry Chemical Physics, 12 (2010) 13534-13546.

[5] Z. Bacsik, R. Atluri, A.E. Garcia-Bennett, N. Hedin, Temperature-Induced Uptake of CO_2 and Formation of Carbamates in Mesocaged Silica Modified with n-Propylamines, Langmuir, 26 (2010) 10013-10024.

[6] R. Roque-Malherbe, O.N.C. Uwakweh, C. Lozano, R. Polanco, A. Hernandez-Maldonado, P. Fierro, F. Lugo, J.N. Primera-Pedrozo, Structural Effects and Interactions of Carbon Dioxide Molecules Adsorbed on Ni, Zn, and Cd Nitroprussides, Journal of Physical Chemistry C, 115 (2011) 15555-15569.

[7] J.M. Celedonio, J.H. Park, Y.S. Ko, FT-IR study on CO_2 adsorbed species of CO_2 sorbents, Research on Chemical Intermediates, 42 (2016) 141-154.

[8] A. Danon, P.C. Stair, E. Weitz, FTIR Study of CO_2 Adsorption on Amine-Grafted SBA-15: Elucidation of Adsorbed Species, Journal of Physical Chemistry C, 115 (2011) 11540-11549.

[9] N. Hiyoshi, K. Yogo, T. Yashima, Adsorption characteristics of carbon dioxide on organically functionalized SBA-15, Microporous and Mesoporous Materials, 84 (2005) 357-365.

[10] V. Zelenak, D. Halamova, L. Gaberova, E. Bloch, P. Llewellyn, Amine-modified SBA-12 mesoporous silica for carbon dioxide capture: Effect of amine basicity on sorption properties, Microporous and Mesoporous Materials, 116 (2008) 358-364.

[11] S. Satyapal, T. Filburn, J. Trela, J. Strange, Performance and properties of a solid amine sorbent for carbon dioxide removal in space life support applications, Energy & Fuels, 15 (2001) 250-255.

Chapter 6. General Conclusions and Future Perspectives

6.1. General Conclusions

In this dissertation, three different nitrogen-containing solid base catalysts, nitrided porous silica, porous carbon nitride, and amine-functionalized porous silica, were prepared and their properties were compared. The catalytic properties of catalysts were evaluated by Knoevenagel condensation, and the basicity was evaluated by CO_2 probe FT-IR.

In Chapter 2, a proportional relationship between the initial rate and the external surface area was observed and the nitrogen content on the external surface showed less linear correlation with the formation rate. It is because the increase of the external surface area brings the increase of structurally unique Si–OH and eventually Si–NH_2, which is more active than Si–NH–Si or Si–NH_2···Al on the same surface. Therefore, delamination of lamellar zeolite precursor is an effective approach to increase the base catalytic activity of nitrided zeolites for a reaction involving larger molecules. The primary silanamine species were the most active site for Knoevenagel condensation in NSBA-15.

In Chapter 3, it was not possible to identify the most dominant nitrogen site for the reaction in PCN. NSBA-15 showed higher catalytic activity than PCN for Knoevenagel condensation between benzaldehyde and ethyl cyanoacetate probably because of their higher pK_a. PCN showed higher catalytic stability than NSBA-15 because of the lack of unstable Si-N bond. Based on the above results, a catalyst with aliphatic amines and no Si-N bond is considered to have both high activity and high stability.

In Chapter 4, amine-functionalized SBA-15 showed high selectivity and stability for Knoevenagel condensation. AP-SBA-15 and MAP-SBA-15 showed higher catalytic activity than PAP-SBA-15 for Knoevenagel condensation between benzaldehyde and ethyl cyanoacetate probably because of the electron-donating groups (aminopropyl group and methyl aminopropyl group). The order of catalytic activities of aliphatic amine functionalized SBA-15 catalysts for the reactions of benzaldehyde and malononitrile or ethyl cyanoacetate was AP-SBA-15 > MAP-SBA-15 > DMAP-SBA-15 probably due to the reaction mechanism. Alkyl amines are more active and durable than silanamines.

In Chapter 5, the basicity of catalysts (prepared in Chapter 2, 3 and 4) was evaluated by CO_2 probe FT-IR. A proportional relationship between CO_2 adsorption and catalytic activity was observed. It suggests that higher activity of C-NH_2 than that of Si-NH_2 probably due to hydrophobicity and that higher activity of primary amine than that of secondary amine probably due to not only intermediate but also steric hinderance.

I focused on the following five properties of solid base catalysts: **activities, durabilities, selectivities, accessibilities and safeties of the synthesis method**. Through the studies in the dissertation, the relationship between the type of nitrogen site and the catalytic properties was

clarified (Table 6–1). All of the nitrogen sites investigated in this study are highly selectivity for Knoevenagel condensation. Nitrogen sites bonded to an electron-donating group (such as an alkyl group), i.e., nitrogen sites with a high pK_a, can proceed with reactions using substrates with low reactivity. In addition, a catalyst with high hydrophobicity can make the reaction proceed faster. Nitrogen sites bonded to silicon atoms are not durable because they are easily decomposed by water vapor in the air or water produced in catalytic reactions. These results indicate that the base catalytic properties are determined by the hydrophobicity and electron-donating properties of the functional groups around the nitrogen atoms.

Table 6-1 The relationship between the type of nitrogen site and the catalytic properties

	Nitrided silica	Carbon nitride	Aliphatic amine functionalized silica (primary, secondary)
Type of nitrogen sites	Si-NH_2 Si-NH-Si N-$(Si)_3$	C=N-C, N-$(C)_3$, C-NH-C, C-NH_2	C-NH_2 C-NH-C
Activity	$13 < pK_a < 16$	$11 < pK_a \leq 13$	$16 < pK_a$
Durability (percentage of N remaining after reaction)	67.9%	100%	96.3%
Selectivity	> 99%	> 99%	> 99%
Accessibility	Mesoporous, delaminated	Porous	Mesoporous
Safety of the synthesis method	NH_3 treatment		

6.2. Future Perspectives

As described in the conclusions, the type of nitrogen site in the catalyst determines the catalytic properties. Therefore, it is important to select the most appropriate nitrogen site for the reaction to be used. Applications of nitrogen-containing solid base catalysts are summarized in Table 6-2.

- Nitrogen containing solid base catalysts show high selectivities (> 99%).
- Aliphatic amine functionalized silica can be used as a catalyst even when substrates with high pK_a are used. The primary amine-functionalized silica is the most active catalyst for Knoevenagel condensation. The base sites in amine functionalized silica are controllable.
- Nitrided silica can catalyze reactions using substrates with pK_a less than 16. It was reported that alkylation of N sites in nitrided silica can be used to improve hydrophobicity and catalytic

properties.

- Cabon nitride can catalyze reactions using substrates with pK_a less than 13. This catalyst can be prepared at low cost.
- Water-sensitive catalysts such as nitrided silica should be used for reactions without water generation, such as Morita-Baylis-Hillman reaction, Henry reaction, Michael addition. These reactions are used in various industries such as synthesis of fiber and pharmaceuticals.
- Water-tolerant catalysts such as carbon nitride and amine-functionalized silica can be used for reactions with water generation, such as Knoevenagel condensation, ketonization, Claisen-Schmidt condensation, Aldol condensation. These reactions are widely used in various industries such as synthesis of pharmaceuticals and fragrances.

In this way, an appropriate catalyst can be selected based on the results of this study. I strongly hope that in the future, these catalysts will be utilized in appropriate reactions and play an active role in the synthesis of fine chemicals.

Table 6-2 Applications of nitrogen-containing solid base catalysts

	Nitrided silica	Carbon nitride	Amine functionalized silica
Reaction substrate	pK_a < 16	pK_a ≤ 13	16 < pK_a (aliphatic primary or secondary amine)
Utility	Reaction without water generation	Reaction with water generation	
Example of product	Synthetic fibers, pharmaceuticals	Pharmaceuticals, fragrances	
Feature	Methylation ↓ Improving activity and durability	Low cost	Controllable base sites

List of achievements

Publications

1. Aisa Kawano (1.0), Takahiko Moteki, Masaru Ogura, Effect of delamination on active base site formation over nitrided MWW-type zeolite for Knoevenagel condensation, Microporous and Mesoporous Materials, 2020, 299, 110104.
2. Aisa Kawano (1.0), Takahiko Moteki, Masaru Ogura, Differences in catalytic activity and durability of nitrogen sites on nitrided SBA-15 or porous carbon nitride, Journal of the Japan Petroleum Institute, accepted.

International Conference Presentations

1. Aisa Kawano, Takahiko Moteki, Masaru Ogura, Nitridation of Delaminated MWW-type Zeolite and Its Base Catalytic Property in Knoevenagel Condensation, 4th Euro Asia Zeolite Congress, Taormina, Italy, January 2019. (Oral)
2. Aisa Kawano, Takahiko Moteki, Masaru Ogura, Preparation and Catalytic Property of Methylamine Modified ZSM-5, International Symposium on Porous Materials 2019, Tokyo, Japan, November 2019. (Poster)
3. Aisa Kawano, Takahiko Moteki, Masaru Ogura, Knoevenagel condensation catalyzed by nitrided mesoporous silica or porous carbon nitride, The 18th Japan-Korea Symposium on Catalysis, virtual, November 2021. (Oral)

国内学会発表

1. 河野愛紗，茂木堯彦，小倉　賢，窒素置換高比表面積ゼオライトの合成とその塩基触媒特性，第 6 回 JACI／GSC シンポジウム，東京国際フォーラム，東京都， 2017 年 7 月．（ポスター）
2. 河野愛紗，茂木堯彦，小倉　賢，MWW 型ゼオライトの修飾・窒化とその塩基触媒特性，第 120 回触媒討論会，愛媛大学，愛媛県，2017 年 9 月．（口頭）
3. 河野愛紗，茂木堯彦，小倉　賢，窒化 ITQ-2 ゼオライトを用いた Knoevenagel 縮合，第 48 回石油・石油化学討論会，船堀タワーホール，東京都，2018 年 10 月．（口頭）
4. 河野愛紗，茂木堯彦，小倉　賢，窒化メソポーラスシリカあるいは多孔質カーボンナイトライドを触媒とした Knoevenagel 縮合，第 36 回ゼオライト研究発表会，オンライン，2020 年 11 月．（口頭）

Awards

Aisa Kawano, The IIS PhD Student Live 2019, Encouragement Award（生産技術研究所内博士課程学生の研究発表コンペにおいて，最優秀発表賞を受賞）

Acknowledgements

At first, I would like to express deep respect and gratitude to my supervisor, Professor Masaru Ogura. He always supported me throughout the thesis and the life in doctoral course. There were many times when I needed his help, but he was always willing to guide me. I learned not only knowledges of solid base catalyst but also how to be a good researcher through his guidance and mentorship. This dissertation would not have been possible without his heartfelt and enthusiastic instruction.

I would like to express appreciation to Assistant Professor Takahiko Moteki, for all the support in my experiment, valuable comments, and fruitful discussions in thesis.

I would like to express appreciation Professor Toru Wakihara, Professor Yoshiko Tsuji, Associate Professor Ryuji Kikuchi, and Professor Kazuya Yamaguchi for their insightful comments and advice as members of the thesis defense committee.

I sincerely appreciate to Professor Teruyasu Mizoguchi, for his support in the TEM measurement (Chapter 2). I am sincerely grateful to Assistant Professor Masao Kamiko, for his support and instructions in XPS measurements (Chapter 2 and 3). I deeply appreciate to Associate Professor Takeshi Yoshikawa and Mr. Atsushi Fukuda, for his support and instructions in the research of hydrofluoric acid treatment (Chapter 3). I would like to express appreciation to Professor Akira Nakayama, for his support in DFT calculation (Chapter 5).

I would like to express my gratitude for kind support from all the members in Ogura laboratory. In particular, I would like to thank Ms. Ayumi Sato, for her experiment such as CO_2 probe FT-IR measurements in Chapter 5. Through my instruction to her, I was able to grow as well. I would like to appreciate to Assistant Professor Yuki Nakamura for her support in the silane coupling experiments in Chapter 4 and valuable advice for English writing and life as a woman researcher. I sincerely thanks to Mrs. Junko Tori for the continuous assistance and support in the official work. I thank to Dr. Takeshi Ohnishi for maintenance of laboratory equipment. I appreciate to the former technical staffs, Ms. Yumiko Shimada and Ms. Naoko Ito for their guidance for the experiments and maintenance of the equipment. I deeply thanks to Dr. Kiyoyuki Yamazaki, Dr. Choi Jihye, and Dr. Yusuke Ohata, who were my senior as the Ph. D students in the laboratory, to give some viewpoints on how to behave in doctoral course. I would like to thank Mr. Shohei Harada for his support and advice in CO_2 probe FT-IR (Chapter 5). Also, I would like to thank past and present members of Ogura laboratory: Ms. Subramaniam Vishnupriya, Dr. Sibel Sogukkanli, Mr. Ken Watanabe, Mr.

Yuuki Koga, Mr. Kai Hidaka, Mr. Tatsuya Muramatsu, Ms. Yanling Gan, Mr. Tomohiro Imaseki, Mr. Naoto Tominaga, Mr. Tomohiro Sei, Ms. Jing Ma, Mr. Jiachen Ge, Mr. Leo Takahashi, Mr. Takahiro Kimura, Mr. Shunsuke Hayashi, and Ms. Chuang Liu.

I would like to acknowledge financial support from Chemistry Personnel Cultivation Program (Japan Chemical Industry Association).

Finally, I would like to express my deepest gratitude to my husband and parents, who always supported me. They made me what I am today.

Aisa Kawano